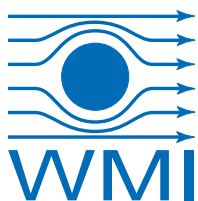
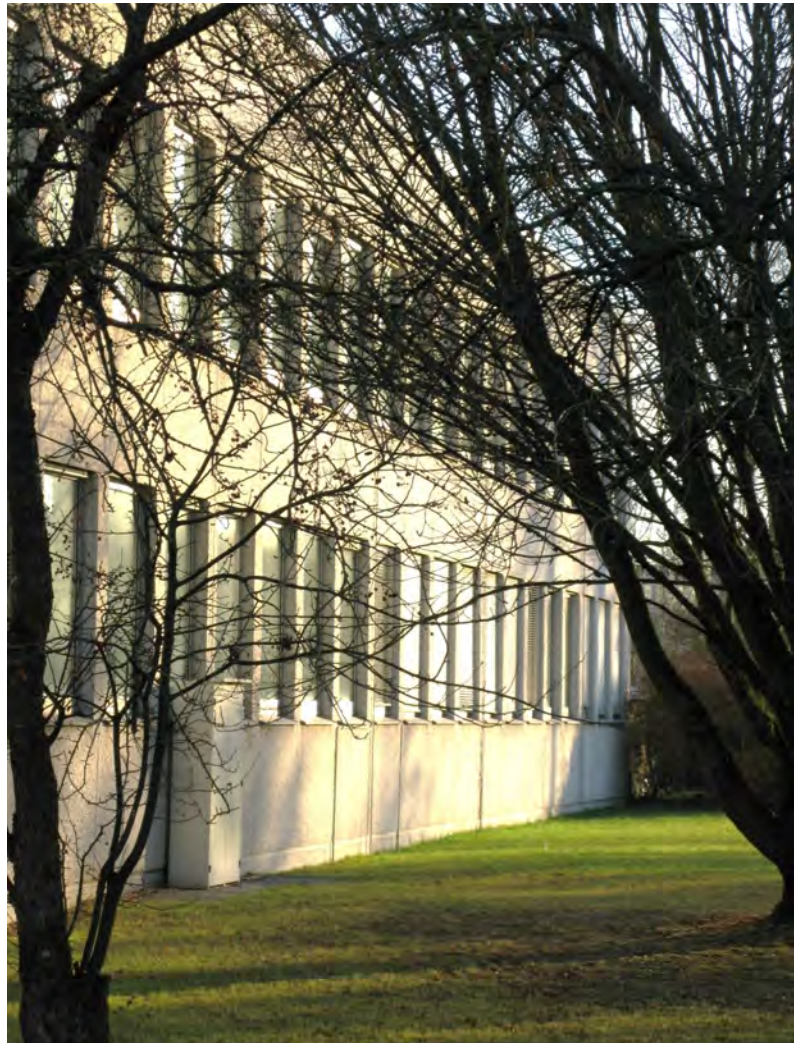


# Annual Report Jahresbericht

# 2016



**Walther-Meißner-Institut**  
für Tieftemperaturforschung  
Bayerische Akademie der Wissenschaften





**Contact:**

**Prof. Dr. Rudolf Gross**

Walther–Meißner–Institut für Tieftemperaturforschung  
Bayerische Akademie der Wissenschaften  
and  
Lehrstuhl für Technische Physik – E23  
Technische Universität München

**Address:**

Walther–Meißner–Str. 8	Phone: +49 – (0)89 289 14201
D - 85748 Garching	Fax: +49 – (0)89 289 14206
GERMANY	e-mail: Rudolf.Gross@wmi.badw.de
	www: <a href="http://www.wmi.badw.de">http://www.wmi.badw.de</a>

**Secretary's Office and Administration:**

**Emel Dönertas**

Phone: +49 – (0)89 289 14202  
Fax: +49 – (0)89 289 14206  
e-mail: Emel.Doenertas@wmi.badw.de  
Sekretariat@wmi.badw.de

**Ludwig Ossiander**

Phone: +49 – (0)89 289 14205  
Fax: +49 – (0)89 289 14206  
e-mail: Ludwig.Ossiander@wmi.badw.de  
Verwaltung@wmi.badw.de





## Preface

Dear colleagues, friends, partners, and alumni of the Walther-Meißner-Institute for Low Temperature Research (WMI) of the Bavarian Academy of Sciences and Humanities (BAW)!

It almost goes without saying that 2016 was a successful and dynamic year for WMI, because that has developed into being the norm over the past years. Our successful research resulted in a large number of high level publications (see page 85), new extramural funding (see page 97), the participation in many coordinated research projects and graduate schools on the European and national level (see page 97), as well as fruitful collaborations with international research institutions and industry (see page 105). The high international impact of our research work is documented by more than 1800 citations of WMI publications in 2016 and a large number of invited conference presentations, colloquium and seminar talks (see page 109). In 2016, WMI also organized several symposia, workshops and international conferences, and contributed to public outreach events (see page 101). Our *Annual Report 2016* gives you an overview of our last year's activities. It also provides some statistical data and recent developments in infrastructure and experimental facilities.

The year 2016 was already considerably influenced by the development of cluster initiatives for the next round of the *German Excellence Strategy*, aiming at strengthening Germany's position as an outstanding place for research and further improving its international competitiveness. As WMI is a very active player in the present Excellence Cluster *Nanosystems Initiative Munich (NIM)*, it is strongly involved in the planning of successor clusters. Actually, the present cluster NIM was so successful and became so big and broad that the NIM Executive Board decided not to apply for a follow-up cluster. Instead, three new cluster initiatives were created out of NIM Research Area 1, 3 and 4, focusing on quantum science & technology, energy conversion, and synthetic biology, respectively. All three cluster initiatives created out of NIM were considered promising by the university boards of the two Munich universities and letters of intent have been submitted to the German Research Foundation in November 2016. WMI will play a key role in the cluster focusing on quantum science & technology. Already now, WMI is an active player in several quantum science related projects. This includes the *Munich Quantum Center (MQC)*, the International Ph.D. School of Excellence (IDK) entitled *Exploring Quantum Matter (ExQM)* within the *Elite-Netzwerk Bayern*, and the International Max Planck Research School *Quantum Science and Technology (IMPRS-QST)* (see page 14–18). IMPRS-QST just started early in 2016. ExQM passed a very positive intermediate evaluation in 2016 and was extended until May 2022. Late in 2016, we got granted a new EU Collaborative Project (H2020-FETOPEN-1-2016-2017) with partners from Vienna, Innsbruck and Barcelona. This projects aims at the development of *Magnetomechanical Platforms for Quantum Experiments and Quantum Enabled Sensing Technologies (MaQSens)*. Finally, WMI contributes to the structuring of the planned BMBF program *“Quantentechnologie: Grundlagen und Anwendungen” (QUTEGA)* with Rudolf Gross of WMI being member of the QUTEGA committee. QUTEGA will go hand in hand with the *EU Quantum Technology Flagship* which is presently in its ramp-up phase.

In general, the WMI research program is strongly dependent on third party funding. Beyond the quantum science related projects mentioned above, these research projects include the *Transregional Collaborative Research Center TRR 80* “From Electronic Correlations to Functionality” (second funding period: 01/2014 – 12/2017), the *Priority Program SPP 1458* “High  $T_c$  Superconductivity in Iron Pnictides” (second funding period: 04/2013 – 03/2016), the *Priority Program SPP 1538* “Spin Caloritronic Transport” (second funding period: 07/2014 – 06/2017), and the *Priority Program SPP 1601* “New Frontiers in Sensitivity for EPR Spectroscopy” (second funding period: 07/2015 – 06/2018).

Keeping the technological infrastructure on a state-of-the-art level is a key prerequisite for successful experimental research. To this end, the year 2016 was highly successful. First, our application for a new UHV sputtering system for superconducting and magnetic materials within the DFG Major Research Instrumentation Program was successful. The new sputtering system will be delivered in February 2017 and will considerably extend the WMI capabilities for the deposition of superconducting and magnetic heterostructures. Second, supported by the BMBF research network *Quantum Communication (Q.com)* we could order a critical point dryer and a state-of-the-art laser writer, considerably extending our facilities for micro- and nano-patterning. Third, the Bavarian Ministry for Science and Arts granted more than 5 Mio. Euro to WMI for redevelopment measures regarding the technical infrastructure, safety requirements and energy efficiency. The planning stage of this building project is completed and the construction work will start early in 2017.

Our success in research is only possible by the strong commitment of our scientific, technical and administrative staff. Together with our guests and the large number of talented and dedicated students they make our ambitious research possible by their hard work and persistence. In 2016, 4 bachelor, 13 master and 4 Ph.D. theses, as well as 1 habilitation thesis were completed, while 13 master, 17 Ph.D. students and two habilitation candidates are still ongoing with their work (see page 91). Of equal importance is the continuous support by various funding agencies. In this context we gratefully acknowledge financial support from the BAdW, the DFG, the Bavarian Ministry for Science and Arts, the BMBF and the EU. A further key to our success in research is the recruitment of outstanding, scientifically independent group leaders with complementary research interests and technical expertise, a process which is supported and monitored by the scientific advisory board of WMI. We are strongly committed to support and promote young scientists in their career. In this context, we are particularly happy that one of our junior group leaders, Sebastian Gönnerwein, got a W3 professorship at the Institute of Solid State Physics of TU Dresden and also became a member of the new *Center for Transport and Devices of Emergent Materials (CTD)* at Dresden.

I hope that our Annual Report 2016 inspires your interest in WMI. I take this opportunity to thank all the colleagues, guests, students, postdocs and cooperating partners, who contributed to our research and teaching activities within the last year, and last but not least all our friends and sponsors for their interest, trust and continuous support.



Rudolf Gross

Garching, December 2016

# Contents

Preface . . . . .	1
The Walther–Meißner–Institute . . . . .	5
<b>Scientific Reports:</b>	<b>9</b>
<b>Joint Research Projects</b>	<b>9</b>
The Cluster of Excellence “Nanosystems Initiative Munich” (NIM) . . . . .	11
Coordinated Projects in Quantum Science and Technology . . . . .	14
A very productive period of research: The DFG Priority Program “Fe-based superconductors” (SPP 1458) ended in 2016. . . . .	19
<b>Basic Research</b>	<b>21</b>
Spin Hall Magnetoresistance in a Canted Ferrimagnet . . . . .	23
Universal two-magnon line shape in spin $\frac{1}{2}$ antiferromagnets? . . . . .	25
Finite-Time Correlations of Propagating Squeezed Microwave States . . . . .	27
Second-Order Decoherence Mechanisms of a Transmon Qubit Probed with Thermal Microwave States . . . . .	29
Photon Statistics of Propagating Thermal Microwaves . . . . .	31
Electronic Correlations in the Organic Metal $\kappa$ -(BETS) <sub>2</sub> Mn[N(CN) <sub>2</sub> ] <sub>3</sub> Probed by Magnetic Quantum Oscillations . . . . .	33
Interlayer Coupling and Magnetoresistance in $\kappa$ -(BETS) <sub>2</sub> FeCl <sub>4</sub> . . . . .	35
Anisotropic Superconductivity under Hydrostatic Pressure in $\alpha$ -(BEDT-TTF) <sub>2</sub> KHg(SCN) <sub>4</sub> . . . . .	37
Absence of Static Magnetic Proximity Effects in the Pt/Y <sub>3</sub> Fe <sub>5</sub> O <sub>12</sub> System . . . . .	39
<b>Application–Oriented Research</b>	<b>43</b>
Flux-driven Non-degenerate Josephson Parametric Amplifiers: Hysteretic Flux Response and Gain Measurements . . . . .	45
Characterization of Tunable Resonators for Quantum Simulation . . . . .	47
On-chip Environments Characterized with a Superconducting Qubit . . . . .	49
A Scalable 3D Quantum Memory . . . . .	51
Circuit Electromechanics with Aluminium Nanobeams . . . . .	53
A Combined Circuit Qed Circuit Nanomechanical System . . . . .	55

<b>Materials, Thin Film and Nanotechnology, Experimental Techniques</b>	<b>57</b>
Magnetoresistance of the Electron Underdoped Cuprate Superconductor $\text{Nd}_{2-x}\text{Ce}_x\text{CuO}_4$ . . . . .	59
Pure Spin Current Transport in Gallium-Doped Zinc Oxide . . . . .	61
Combined Brillouin Light Scattering and Microwave Absorption Study of Magnon- Photon Coupling in a Split-Ring Resonator/Yig Film System . . . . .	63
Pulsed Electron Spin Resonance of Phosphorus Donors at Millikelvin Temperatures .	65
<b>Experimental Facilities:</b>	<b>67</b>
<b>Overview of Key Experimental Facilities and Infrastructure</b> . . . . .	69
<b>Statistics:</b>	<b>83</b>
<b>Publications</b> . . . . .	85
<b>Bachelor, Master, Doctoral and Habilitation Theses</b> . . . . .	91
<b>Research Projects</b> . . . . .	97
<b>Conferences, Workshops, Public Outreach, Collaborations, Stays abroad etc.</b> . . . .	101
<b>Invited Conference Talks and Seminar Lectures</b> . . . . .	109
<b>Appointments, Honors and Awards, Membership in Advisory Boards, etc.</b> . . . . .	113
<b>Teaching:</b>	<b>115</b>
<b>Lectures, Courses and other Teaching Activities</b> . . . . .	117
<b>Seminars and Colloquia</b> . . . . .	121
<b>Staff:</b>	<b>127</b>
<b>Staff of the Walther-Meißner-Institute</b> . . . . .	129
<b>Guest Researchers</b> . . . . .	131
<b>Scientific Advisory Board and Executive Committee:</b>	<b>133</b>
<b>Scientific Advisory Board</b> . . . . .	133
<b>Executive Committee</b> . . . . .	134

## The Walther–Meißner–Institute

### General Information

The *Walther-Meißner-Institute for Low Temperature Research (WMI)* was originally operated by the Commission for Low Temperature Research of the *Bavarian Academy of Sciences and Humanities (BAdW)*. Between 2013 and 2015, the Bavarian Academy of Sciences and Humanities with its more than 300 employees was reorganized. With the passing of the new statutes in October 2015, the 36 Commissions (Research Groups) of the Academy — they were originally set up in order to carry out long-term projects, which are too ambitious for the lifetime or capacity of any single researcher, or which require the collaboration of specialists in various disciplines — were abolished. The research program of BAdW is now implemented in Academy Institutes (such as the Walther-Meißner-Institute or the Leibniz Supercomputing Center) and Academy Projects. The Academy Institutes and Projects are managed by the Institute and Project Committees and supervised by the Institute and Project Advisory Boards, respectively. In this way a clear separation between the managing bodies of the institutes/projects (responsible for the implementation of the research programs) and the corresponding supervisory bodies (responsible for the quality control) was established. To this end, also the Commission for Low Temperature Research was dissolved and replaced by the WMI Committee and the WMI Advisory Board in 2015.

The historical roots of WMI go back to Walther Meißner. He founded the Commission for Low Temperature Research in 1946 when he was president of BAdW (1946 – 1950). The first research activities then were started in 1946 in the Herrsching barracks. After the retirement of Walther Meißner in 1952, Heinz Maier-Leibnitz, who followed Walther Meißner on the Chair for Technical Physics of the Technische Universität München, became the new head of the Commission for Low Temperature Research. In 1967, the commission moved to the Garching research campus after the construction of the new “Zentralinstitut für Tieftemperaturforschung (ZTTF)” was completed (director: Prof. Heinz Maier-Leibnitz, technical director: Prof. Franz Xaver Eder). Until 1972, the theory group of the Institute Laue Langevin was hosted at the ZTTF with prominent members such as Peter Gulde. In 1980, Prof. Dr. Klaus Andres became the new director of the ZTTF again associated with the Chair for Technical Physics (E23) at the Technische Universität München, followed by Prof. Dr. Rudolf Gross in 2000. In 1982, the ZTTF was renamed into Walther-Meißner-Institute for Low Temperature Research (WMI) on the occasion of Walther Meißner’s 100. birthday.

Starting from 2000, the so far unused basement of the WMI building was made available for technical infrastructure (airconditioning, particulate airfilters, pure water system etc. for clean room) and additional laboratory space. Fortunately, in 2008 WMI succeeded in getting extra money from the state government within the so-called “Konjunkturpaket II”. This money has been used to establish the new “WMI Quantum Science Laboratory” in the basement of the building, providing about 150 m<sup>2</sup> additional laboratory space particularly suited for low temperature facilities and ultra-sensitive studies on solid state quantum systems. The WMI Quantum Science Laboratory was fully operational early in 2011 and meanwhile hosts three new mK systems and sophisticated experimental techniques for the study of solid state based quantum systems and circuits.

As already mentioned, it is a long tradition that WMI hosts the Chair for Technical Physics (E 23) of the Technische Universität München (TUM) with the director of the WMI being a full professor at the Faculty of Physics of TUM. However, there are also close ties with the Ludwig-Maximilians-Universität (LMU). Between 2004 and 2010, WMI hosted a scanning probe division with the head of this division being a professor at the Ludwig-Maximilians-Universität (LMU). In this way a tight collaboration has been established between WMI and

research groups of both Munich universities, joining technological and human resources in the fields of experimental and theoretical solid-state and condensed matter physics, low temperature techniques, materials science as well as thin film and nanotechnology. Noteworthy, the WMI supplies liquid helium to more than 25 research groups at both Munich universities and provides the technological basis for low temperature research. In 2016, the Bavarian Ministry for Science and Arts granted more than 5 Mio. Euro for redevelopment measures regarding the technical infrastructure, safety requirements and energy efficiency. An important part of the building project is the reconstruction of the entrance area, providing then direct access to the new WMI Quantum Laboratories in the basement of the WMI building and additional meeting rooms. Moreover, it includes the replacement of all windows, the upgrade of the technical infrastructure for cooling water, air conditioning, liquid nitrogen and helium storage, as well as various safety measures.

## Research Activities

The research activities of the Walther-Meißner-Institute are focused on low temperature condensed matter physics (see reports below). The research program is devoted to both **fundamental** and **applied research** and also addresses **materials science, thin film and nanotechnology** aspects. With respect to **basic research** the main focus of the WMI is on

- superconductivity and superfluidity,
- magnetism, spin transport, spin mechanics and spin caloritronics,
- quantum phenomena and quantum coherence in mesoscopic systems and solid state nanostructures,
- circuit quantum electrodynamics and circuit electro-nanomechanics,
- ordering and emergent phenomena in correlated electron systems,
- and the general properties of metallic systems at low and very low temperatures.

The WMI also conducts **applied research** in the fields of

- solid-state quantum information processing systems,
- superconducting and spintronic devices,
- oxide electronics,
- multi-functional and multiferroic materials,
- and the development of low and ultra-low temperature systems and techniques.

With respect to **materials science, thin film and nanotechnology** the research program is focused on

- the synthesis of superconducting and magnetic materials,
- the single crystal growth of oxide materials,
- the thin film technology of complex superconducting and magnetic heterostructures, including multi-functional and multi-ferroic material systems,
- and the fabrication of superconducting, magnetic and hybrid nanostructures.

The WMI also develops and operates systems and techniques for low and ultra-low temperature experiments. A successful development have been dry mK-systems that can be operated without liquid helium by using a pulse-tube refrigerator for precooling. In the early 2000s, these systems have been successfully commercialized by the company VeriCold Technologies GmbH at Ismaning, Germany, which was taken over by Oxford Instruments in 2007. As a further typical example we mention very flexible dilution refrigerator inserts for temperatures down to about 20 mK fitting into a 2 inch bore. These systems have been engineered and fabricated at WMI. Within the last years, several dilution refrigerators have been provided to other research groups for various low temperature experiments. WMI also operates a helium

liquifier with an annual capacity of above 180.000 liters and supplies both Munich universities with liquid helium. To optimize the transfer of liquid helium into transport containers, WMI has developed a pumping system for liquid helium that is commercialized in collaboration with a company.

To a large extent the research activities of WMI are integrated into national and international research projects such as Clusters of Excellence, Collaborative Research Centers, Research Units, or EU projects. The individual research groups of WMI offer a wide range of attractive research opportunities for bachelor and master students, Ph.D. students and postdoctoral fellows.

## Experimental Facilities and Resources

The WMI is equipped with state of the art facilities for the preparation and characterization of superconducting and magnetic materials as well as for various low and ultra-low temperature experiments. The main experimental and technological resources of WMI are listed in the following.

### Materials Preparation and Fabrication of Nanostructures

- Laser Molecular Beam Epitaxy (L-MBE) system for oxide heterostructures (equipped with in-situ RHEED, Omicron AFM/STM system, atomic oxygen/nitrogen source, infrared-laser heating system, metallization)
- molecular beam epitaxy (MBE) system for metals
- UHV magnetron sputtering systems for metals (e.g. Nb, Al, NiPd, ... )
- magnetron sputtering system for oxide heteroepitaxy (equipped with four sputtering guns and an oxygen ion gun)
- reactive ion etching (RIE) system, Plasmalab 80 Plus with ICP plasma source, Oxford Instruments Plasma Technology
- ion beam etching (IBE) system equipped with a LN<sub>2</sub> cooled sample holder
- automated critical point dryer Leica EM CPD 300
- polishing machine for substrate preparation
- ultrasonic bonding machine
- 50 m<sup>2</sup> class 1000 clean room facility
- optical lithography (Süss maskaligner MJB 3 and projection lithography)
- 100 kV nB5 Electron Beam Lithography System by NanoBeam Limited, UK, with 6 inch laser stage
- four-mirror image furnace for crystal growth

### Characterization

- 2-circle x-ray diffractometer (Bruker D8 Advance, sample temperature up to 1 600°C)
- high resolution 4-circle x-ray diffractometer with Göbel mirror and Ge monochromator (Bruker D8 Discover)
- Philips XL 30 SFEG scanning electron microscope with EDX analysis
- UHV room temperature AFM/STM system
- two Raman spectroscopy systems (1.5 to 300 K, in-situ sample preparation)
- tip-enhanced Raman spectroscopy (TERS) system
- SQUID magnetometer (Quantum Design, 1.5 to 700 K, up to 7 T)
- several high field magnet systems (up to 17 T Tesla) with variable temperature inserts
- 7 T split coil magnet systems with optical access and variable temperature insert

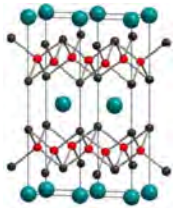
- 3D vector magnet (2/2/6 Tesla) with variable temperature inserts
- experimental set-ups for the measurement of noise including low noise SQUID amplifiers and signal analyzers
- high-frequency network analyzers (up to 40 GHz) and various microwave components (sources, mixers, circulators, attenuators) for the determination of high frequency parameters
- ultra-sensitive microwave receiver for state tomography of quantum microwaves (dual path method with FPGA signal processing)
- high-frequency cryogenic probing station (up to 20 GHz,  $T > 4$  K)
- magneto-optical Kerr effect (MOKE) system
- broadband ferromagnetic resonance (FMR) system

### Low temperature systems and techniques

- several  $^3\text{He}/^4\text{He}$  dilution refrigerator inserts for temperatures down to 10 mK
- “dry” mK-cooler based on a dilution refrigerator with pulse-tube precooling and equipped with a large number of microwave lines and cold electronics (e.g. amplifiers, circulators, attenuators, directional couplers) for ultra-sensitive experiments on solid state quantum systems
- “dry” dilution refrigerator with a base temperature of about 10 mK equipped with a 3D vector magnet (1/1/6 Tesla)
- “wet” mK-cooler based on a dilution refrigerator liquid helium precooling and equipped with a large number of microwave lines and cold electronics (e.g. amplifiers, circulators, attenuators, beam splitters) for time-domain microwave experiments on solid state quantum systems
- experimental set-ups for the measurement of specific heat, magnetization, thermal expansion as well as electrical and thermal transport properties as a function of temperature, magnetic field and pressure



# Joint Research Projects



SPP 1458



SPP 1601



SPP 1538



## The Cluster of Excellence “Nanosystems Initiative Munich” (NIM)

*Rudolf Gross, Frank Deppe, Kirill Fedorov, Sebastian T.B. Gönnenwein, Hans Hübl, Achim Marx<sup>1</sup>*



The Walther-Meißner-Institute (WMI) is a founding member of the excellence cluster *Nanosystems Initiative Munich (NIM)* which was established in 2006. After a successful first funding period (2006 – 2012), a second five-year funding period (2012 – 2017) was granted. Recently, this second funding period has been extended until December 2018 to guarantee a smooth transition to the next round of the *German Excellence Strategy* starting from 2019. WMI contributes to the research areas on *Quantum Nanophysics* (RA I) and *Hybrid Nanosystems* (RA II) of NIM's in total five research areas. Research area I is coordinated by R. Gross of WMI. Several WMI scientists (Deppe, Fedorov, Gönnenwein, Gross, Hübl, Marx) actively contribute to the ambitious research program of NIM.

### Preparing for the German Excellence Strategy 2019

The past two years were considerably influenced by the discussion of cluster initiatives for the next round of the *German Excellence Strategy*, which aims to strengthen Germany's position as an outstanding place for research and to further improve its international competitiveness. Regarding the present Excellence Cluster *Nanosystems Initiative Munich (NIM)* there have been two possible options for the upcoming next round of the German Excellence Strategy: (i) applying for a third funding period of NIM with an updated research strategy or (ii) applying for new excellence clusters with new research directions having strong overlap with particular research areas of NIM. As WMI is a very active player in NIM, it is strongly involved in the planning of successor clusters. On the one hand, NIM was and still is highly successful making the application for a third funding period a promising option. However, on the other hand NIM became so big and so broad that the NIM Executive Board decided not to apply for a follow-up cluster. Instead, it was decided to support the creation of three new and much more focussed cluster initiatives out of the NIM Research Area 1, 3 and 4, focusing on quantum science & technology, energy conversion, and synthetic biology, respectively. As the coordinator of the NIM Research Area I on *Quantum Nanophysics*, Rudolf Gross submitted an extended proposal for a new excellence cluster on *Quantum Science, Technology & Matter* to the university board of TUM already in August 2015. Finally, after a lengthy selection procedure all three cluster initiatives created out of NIM were considered promising by the university boards of both Munich universities and letters of intent for joint initiatives have been submitted to the German Research Foundation in November 2016.

WMI contributes to the cluster initiative finally named *Munich Center for Quantum Science & Technology*. It was submitted to the German Research Foundation as a joint proposal of LMU Munich and TUM and is coordinated by the three spokesmen Immanuel Bloch (LMU Munich and MPQ), Ignacio Cirac (MPQ and TUM) and Rudolf Gross (TUM and BAAdW). A key goal of this cluster initiative is to establish an internationally leading center for quantum science & technology in Munich. Based on its experience, scientific and technological excellence as well as the interdisciplinary knowledge available, the Munich area is in a unique position to achieve this goal.

<sup>1</sup>This work is supported by the German Excellence Initiative via the Nanosystems Initiative Munich (NIM).

The rationale for a cluster initiative focussing on quantum science and technology is straightforward. Although quantum information science was first developed to describe the working principles of future quantum computers, it meanwhile emerged into a powerful description of our physical world, with wide ranging relevance for fields such as quantum materials, quantum chemistry or even quantum cosmology. At the core of this description is the notion of entanglement. In fact, understanding and controlling entanglement on different length and time scales is a key objective of the new cluster initiative and is considered a key prerequisite for numerous technological revolutions. The *Munich Center for Quantum Science & Technology* intends to combine multidisciplinary research across physics, mathematics, computer science, materials science, chemistry, and cosmology. This promises extraordinary applications ranging from inherently secure communications and processing of information, to ultrasensitive sensors and transducers for precision metrology, as well as providing new insights into the behavior of quantum many-body systems and quantum phases of matter and allowing the design of novel materials.

### Proposal for New Collaborative Research Center UNIFy

Although the nanoscience oriented excellence cluster *Nanosystems Initiative Munich (NIM)* will be discontinued at the end of 2018, there is still strong interest in nanoscience and nanotechnology in the Munich area. Therefore, several principal investigators of NIM contributed to prepare a preliminary proposal for a new Collaborative Research Center named *Unified Nanoscale Integration and Functionality (UNIFy) – Integrated Nanosystems Approaching the Atomic Limit*. It has been submitted to the German Research Foundation by TUM with Jonathan Finley being the spokesman.

The long-term vision of UNIFy will be to build and explore new classes of functional nanosystems in which one nanometer scale systems are site-selectively positioned, orientated and linked to form integrated devices and circuits with macroscopic functionality. UNIFy will explore and control interactions mediated by photons as well as magnetic and electrical forces, to achieve feedforward functionalities in which a stimulus provided by one atomically precise sub-system induces a well-defined, conditional response in another. This will open the way to building new classes of functional nano-devices and circuits that combine various functionalities. WMI will contribute to UNIFy with the project *Magneto-optoelectronics at Nanoscopic Interfaces* (Hübl, Gross).

### NIM Seed Funding

Apart from planning for the future, WMI continued its successful research program within NIM. Also in 2016, WMI succeeded in attracting NIM seed funding for several projects, which are reviewed by the NIM Scientific Advisory Board. Within the project *Superconducting Flux Qubit Quantum Processor for Embedding and Banded Quantum Simulations* (Gross, Deppe) we develop a superconducting flux-qubit platform for quantum simulations. Flux qubits combine reasonable coherence times (better than  $1 \mu\text{s}$ ) with a very large (GHz) anharmonicity. They, hence, allow for hard and short control pulses without exciting higher levels and provide access not only to strong, but also to ultra-strong and deep strong coupling. Furthermore, in a specific gradiometric version recently studied at WMI, flux qubits are frequency-tunable while remaining at their “sweet spot” with optimal phase coherence.

Within the seed funding project *Nano-electromechanical Systems with Inductive Coupling – an Avenue to the Single Phonon-Single Photon Strong Coupling Regime* (Hübl, Gross) we aim at accessing the true non-linear nature of the opto-mechanical interaction Hamiltonian which has

not been experimentally demonstrated so far. Recent theoretical proposals indicate that the complementary approach using a displacement sensitive inductive element in form of a superconductive interference device (SQUID) might fill this gap and allow to reach the single photon-single phonon strong coupling regime. Conceptually, the SQUID represents a flux tunable inductor, which is integrated into the superconducting resonator. As the flux threading the SQUID loop is given by the product of the applied magnetic flux density and the loop area, a modulation in either of both quantities results in a change of the SQUID's inductance and thus a shift of the resonance frequency of the microwave resonator. For opto-mechanics we are interested in the vibrational state of the freely suspended nanobeam, which modulates the resonance frequency of the microwave resonator via the SQUID loop area. Realizing this approach represents a major step towards reaching the single photon single phonon strong coupling limit.

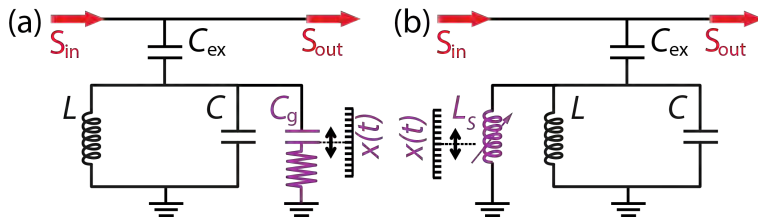


**Figure 1:** Coupling schemes in nano-electromechanical circuits. The conventional capacitive coupling method displayed in (a) vs. the inductive coupling approach envisaged for the NIM seed funding project shown in (b).

## NIM Conferences

Following the recommendation of the NIM Scientific Advisory Board, we started the NIM Research Conferences in 2015. The NIM Conferences aim to bring together leading international experts to discuss and explore emerging new fields, as well as to bridge different communities to share, pursue and diffuse the benefits of collaborations. The topic of the first NIM Conference in 2015 was *Resonator Quantum Electrodynamics (Resonator QED 2015)*. It was organized by Rudolf Gross (WMI) jointly with Jonathan Finley (WSI) and Gerhard Rempe (MPQ). Achim Marx and Frank Deppe of WMI were members of the local organisation team and many Ph.D students of WMI contributed to the success of the conference. Due to the huge success of this first NIM Conference, the NIM Executive Board decided to provide funding for the next Resonator QED Conference in 2017. It will take place at the Kardinal Wendel Haus in Munich from 28 August to 1 September 2017 and again will be organized by Rudolf Gross (WMI), Jonathan Finley (WSI) and Gerhard Rempe (MPQ).

## Research Activities

As in previous years, also in 2016 the WMI research activities strongly profited from NIM. Some of our recent results are presented in several contribution to this Annual Report. They range from the field of superconducting quantum circuits, hybrid quantum systems, electro-nanomechanical systems, to spin dynamics, spin caloritronics and the study of physics related to pure spin currents.

## Coordinated Projects in Quantum Science and Technology

*Rudolf Gross, Frank Deppe, Kirill Fedorov, Hans Hübl, Achim Marx*

Since many years, Walther-Meißner-Institute (WMI) is participating in several coordinated research projects in the field of Quantum Science and Technology (QST). One is the excellence cluster *Nanosystems Initiative Munich (NIM)* which will end in 2018 (see page 11 to 13). The other is the highly successful Collaborative Research Center 631 on *Solid State Quantum Information Processing* which already ended in 2015. Since WMI is interested to continue its ambitious research program in QST with competent partners in coordinated projects on a long-term basis, in the past few years several new projects have already been started or plans for their implementation have been developed. The focus of these projects and their present status is briefly summarized below.

### The Munich Quantum Center (MQC)



The *Munich Quantum Center (MQC)* was founded in 2014. It gathers more than 20 research groups belonging to different institutions, including the Ludwig-Maximilians University Munich (LMU), the Technical University of Munich (TUM), the Max Planck Institute of Quantum Optics (MPQ) and the Walther-Meißner-Institute (WMI).



Joint Workshop of the IMPRS for Quantum Science and Technology  
and the Munich Quantum Center  
October 27-28, 2016

**INVITED SPEAKERS**

- Mete Atatüre
- Michel Brune
- Philippe Corboz
- Nilanjana Datta
- Frank Deppe
- Jens Eisert
- Nathan Goldman
- Achim Marx
- Renato Renner
- Achim Rosch

 + 

**LOCATION**  
Research Campus Garching  
<http://www.munich-quantum-center.de>  
<http://www.imprs-quantum.mpg.de>



MQC serves as a unique platform to communicate advances and developments achieved in the field of QST between the large number of Munich research groups working in this field. In this way it reflects and stresses the coherence and common points and directions existing behind our research activity. Furthermore, MQC aims at improving the outside visibility of the Munich research activities in the field of QST. Since decades, the Munich area is hosting a large number of institutions and researchers playing a leading role in the study of quantum physics.

The MQC member institutions cover a large variety of topics ranging from mathematical foundations, quantum information, computational methods, quantum nanosystems, quantum optics, and quantum many-body physics to superconducting devices. In MQC, mathematicians and theoretical and experimental physicists analyze physical systems exhibiting intriguing quantum mechanical properties. They also design

new methods for leveraging and controlling such systems, thus paving the way for the development of quantum technologies.



MQC is very successful in organizing workshops and schools as well as in stimulating new coordinated research projects. WMI was organizing a Joint Workshop of the International Max Planck Research School for Quantum Science and Technology (IMPRS-QST) and the Munich Quantum Center (MQC). The workshop was taking place on the Research Campus Garching on 27 and 28 October 2016. The poster session on 28 October with more than 80 participants was hosted by Walther-Meißner-Institute.

### The Ph.D. School of Excellence “Exploring Quantum Matter” (ExQM)

The International Ph.D. School of Excellence (IDK) entitled *Exploring Quantum Matter (ExQM)* was founded within the *Elite-Netzwerk Bayern* in June 2014. Its key goal is to unite the unique competence in quantum physics in Munich and to integrate it into an international excellence network of doctoral training centres with partners at the Austrian Academy of Sciences in Vienna and Innsbruck, at ETH Zurich, ICFO Barcelona, Imperial College London, Caltech, and Harvard. The participating institutions are the Technical University of Munich (TUM, spokesman: Stefan Glaser), the Ludwig-Maximilians University Munich (LMU), the Max Planck Institute of Quantum Optics (MPQ), and the Walther-Meißner-Institute of BAAdW. The research topics of ExQM include (i) quantum simulation of many-body systems, (ii) quantum phase transitions, (iii) open quantum systems, (iv) cavity an circuit QED, and (v) numerical and tensor methods. The training of Ph.D. students is supported by the development of new-media tools tailored to research requirements (e.g. visualization, outreach, interaction with partners). The graduate programm ExQM passed a very positive intermediate evaluation in November 2016 and was extended until May 2022.



One of the WMI Ph.D. students, Michael Fischer, gets a scholarship from ExQM. He works on *Scalable Networks of Solid-state Quantum Circuits*. This topic is becoming increasingly attractive for quantum simulations. For example, networks of nonlinear superconducting transmission line resonators or optical nanocavities can be used as scalable quantum simulators for the Bose-Hubbard Hamiltonian. The resonators are made nonlinear by a controllable coupling to superconducting or semiconductor quantum bits, thereby forming harmonic oscillators with tunable Kerr nonlinearity. Networks of these entities would be particularly well suited for accessing the strongly correlated regime and for investigating quantum many-body dynamics of interacting particles under the influence of driving and dissipation. Solid-state quantum circuits with multiple drives are another attracting system (e.g. superconducting quantum bits strongly coupled to a resonator field mode and subjected to multiple classical drives can be used for quantum simulations of relativistic quantum physics such as the dynamics of the Dirac equation).

### The International Max Planck Research School “Quantum Science and Technology” (IMPRS-QST)

The International Max Planck Research School *Quantum Science and Technology (IMPRS-QST)*



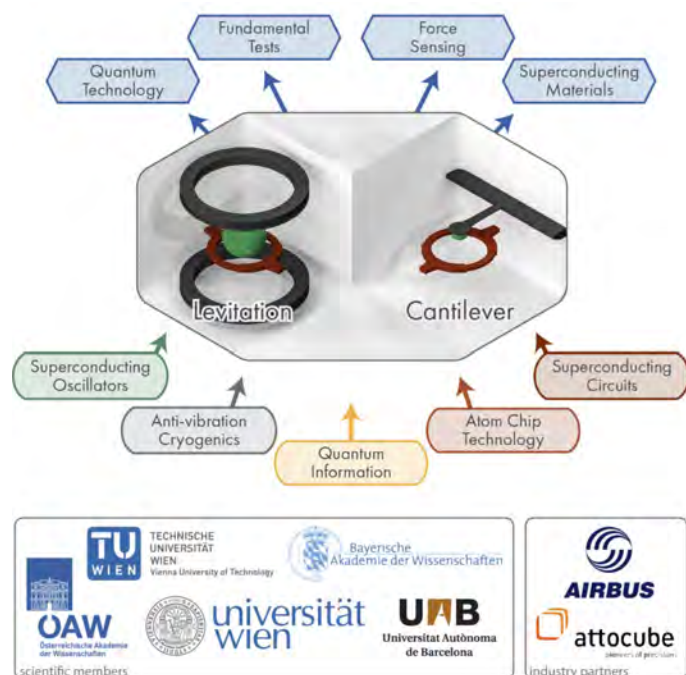
was approved in December 2015 and started early in 2016. The spokesman of IMPRS-QST is Ignacio Cirac of MPQ. The IMPRS-QST provides the opportunity of a common research and teaching platform to unite the competences of leading research groups in

Munich in an interdisciplinary, professional and coherent manner. The IMPRS-QST particularly exploits the synergies between MPQ, WMI and the Munich universities of excellence LMU and TUM. The latter include the Walter Schottky Institute (WSI) and the Center for Nanoscience and Nanomaterials (CNN) of TUM as well as the Center for NanoScience (CeNS) of LMU.

With over twenty experimental and theoretical research groups, Munich is one of the leading research centers in the field of QST. This multidisciplinary research field spans the entire spectrum of experimental and theoretical physics, mathematics, computer science and material science. It also promises extraordinary applications, ranging from communication and processing of information, to sensor and metrological device design, the understanding of quantum many-body systems, up to quantum phases and material science. At the same time, it has its roots in fundamental science, as it investigates and exploits the phenomena based on the fundamental principles of quantum mechanics. The unique combination and quality of activities in the Munich area places it in a particularly strong position to reach the very forefront of research on QST worldwide. The Ph.D. students of IMPRS-QST therefore profit from an exceptionally broad, yet focussed, international training at the highest level that combines theoretical, experimental and communication skills in a vibrant field pertinent to new technologies.

### The EU Collaborative Project “Magnetomechanical Platforms for Quantum Experiments and Quantum Enabled Sensing Technologies” (MaQSens)

Late in 2016, WMI get granted a new EU Collaborative Project (H2020-FETOPEN-1-2016-2017) with partners from the University of Vienna (coordinator: Markus Aspelmeyer), the Technical University of Vienna, the Austrian Academy of Sciences, and the Universitat Autònoma de Barcelona as well as the industry partner Airbus DS GmbH and attocube systems AG. This projects aims at the development of *Magnetomechanical Platforms for Quantum Experiments and Quantum Enabled Sensing Technologies (MaQSens)*. It will start early in 2017.



MaQSens seeks to establish a radically new technology platform for experiments in macroscopic quantum physics and for quantum enabled sensing. It exploits magnetic coupling between superconducting quantum circuits and superconducting mechanical resonators – both levitated and suspended – to enter a hitherto inaccessible parameter regime of both unprecedented force sensitivity and full quantum control of massive, macroscopic objects. The approach followed by MaQSens combines, in a new way, techniques from different research areas (magnetic levitation, superconducting circuits, atom-chip technology, cavity opto-mechanics and quantum optics) and is set up as a joint collaborative effort between expert European teams from academia and industry. The technology developed in MaQSens will enable quantum



experiments of otherwise unachievable coherence times and masses, which has immediate implications for testing fundamental physical questions, for performing hybrid quantum information processing and, on the applied side, for ultrasensitive force sensing applications.

### The BMBF Project “Quantentechnologie – Grundlagen und Anwendungen” (QUTEGA)

The Federal Ministry of Education and Research (BMBF) has decided to set up a national initiative *Quantentechnologie – Grundlagen und Anwendungen (QUTEGA)* to promote quantum technologies in Germany and to prepare for the EU Quantum Technology Flagship. Following a suggestion from the scientific community, Gerd Leuchs (Max Planck Institute for the Science of Light, Erlangen) has been assigned the coordination of QUTEGA. He is supported by the *QUTEGA Committee*. Rudolf Gross of WMI is member of this expert committee which is working out the research strategy and funding structure for QUTEGA.



By the beginning of 2017, a concept paper will be completed by the QUTEGA Committee which describes the different research topics to be addressed by the national QUTEGA initiative. It also will contain recommendations for the funding structure of the QUTEGA program. Furthermore, the BMBF decided to launch the first pilot projects already in 2017, providing an early boost for QUTEGA. Proposals have been accepted until 13 November 2016. More than 20 proposals were submitted and three of them were selected as pilot projects.

### The EU Quantum Technology Flagship

The European Commission announced a *EU Quantum Technology Flagship* which is presently in its ramp-up phase. The Euro 1 billion initiative will provide an ambitious, coordinated and long-term strategy needed to support joint science, engineering and application oriented research & development in the field of quantum science and technology, including IPR, standardization, market development, training and public procurement.

Following a series of dialogues initiated by the European Commission with industry and other stakeholders, a *Quantum Manifesto* has been published with the support of more than 3 000 representatives from academia, industry and governmental and funding institutions. The roadmap presented in the Quantum Manifesto calls for an ambitious strategy to set the bases of a world-class quantum industry in Europe that will unlock the full potential of quantum technologies and bring commercial products to public and private markets, combining education, science, engineering and entrepreneurship.



The Quantum Technology Flagship will be managed as part of the *Future and Emerging Technologies (FET)* program. It is expected to be a large-scale initiative similar in size, timescale and ambition to the two ongoing FET flagships, the Graphene Flagship and the Human Brain Project. The flagship will be partly financed from H2020 and from different other sources at EU and national level. The additional sources for its financial support, its leadership and governance will be defined as part of the flagship preparation process.

## A very productive period of research: The DFG Priority Program “Fe-based superconductors” (SPP 1458) ended in 2016.

R. Hackl, T. Böhm, A. Baum, D. Jost<sup>1</sup>  
B. Büchner, D. Johrendt<sup>2,3</sup>

Superconductivity at high transition temperatures  $T_c$  in Fe-based compounds (FeSCs) came as a big surprise in 2008 [1], although materials of the same family were known for a while [2] and even found to be superconducting [3]. Similarly as in the cuprates, magnetism and superconductivity are in close proximity, and the electron-phonon coupling is considered to be too weak to support  $T_c$  values in the 50 K range [4]. Hence, FeSCs constitute another class of materials in addition to the heavy fermions and the cuprates in which Cooper pairing is likely to originate in interactions other than phonons [5] making them very attractive for fundamental studies including the search for new materials.

Motivated not only by the perspective for basic research but also by potential applications, the German Research Foundation (DFG) funded the Priority Program “High Temperature Superconductivity in Iron Pnictides” (SPP 1458) in the period 2010-2016. Approximately 50 groups from all parts of Germany were supported and were very productive in the last 6 years. According to the ISI Web of Knowledge approximately 300 publications acknowledged support via the SPP 1458. In addition, the results were also shared with an international audience in four smaller and two bigger meetings in Augsburg, Dresden and Munich.

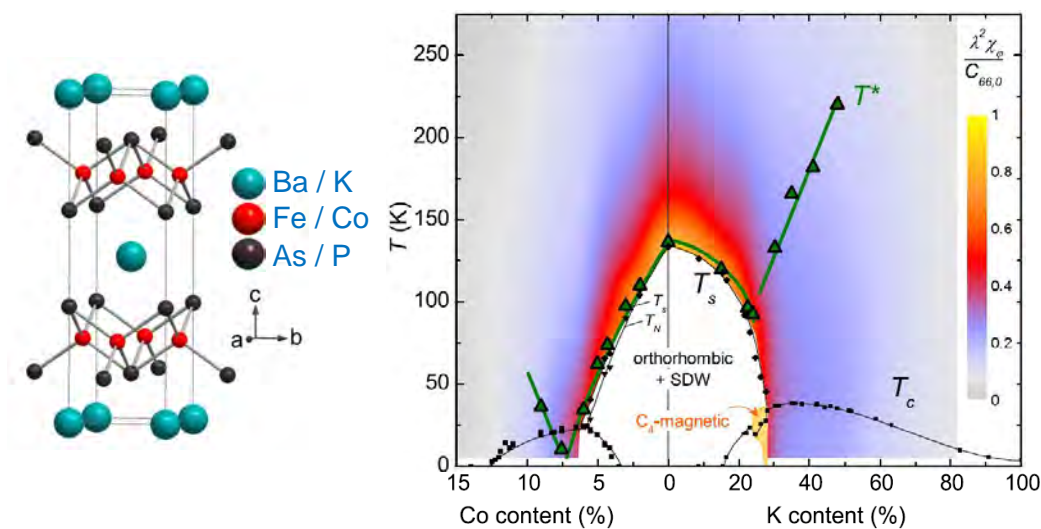


**Figure 1:** Crystal structure and phase diagram [6] of  $\text{BaFe}_2\text{As}_2$ -based compounds. Ba, Fe and As can be substituted by K, Co, and P, respectively, in wide ranges. The maximal  $T_c$  is obtained for 40% K substitution [7]. The parent compound develops a stripe-like spin density wave below  $T_{\text{SDW}} = 138\text{ K}$ . For all types of substitution  $T_{\text{SDW}}$  decreases and superconductivity appears. Above  $T_{\text{SDW}}$  there is a wide range of fluctuations accompanied by a decrease of the shear modulus  $c_{66}$ .

Studies of the FeSCs started from the early recognition of the influence of the band and orbital structure [8]. Soon the materials were found to be a laboratory for studying the interrelation of magnetism, fluctuations, frustration, and superconductivity with band structure and Fermi surface properties (Fig. 1), since the filling can be tuned by either substitution or pressure. Although the mechanism for Cooper pairing remains elusive, there are indications that fluc-

<sup>1</sup>The project was funded by the German Research Foundation (DFG) via the Priority Program SPP 1458 (grant-No. HA 2071/7-2) and partially via the Transregional Collaborative Research Center TRR 80.

<sup>2</sup>IFW Dresden, Helmholtzstr. 20, 01069 Dresden, Germany.

<sup>3</sup>Department Chemie und Biochemie, Ludwig-Maximilians-Universität München, Butenandtstrasse 5-13, 81377 München, Germany.

tuations of either spin or orbital order are intertwined with superconductivity [9, 10]. At least qualitatively, both the spin density wave (SDW) type of ordering in the parent compounds and superconductivity can be explained on this basis. Very soon new states of matter were found in addition to SDW order and superconductivity. The most prominent one is nematicity which formally means that the rotational  $C_4$  is broken, whereas the translational symmetry survives. Physically, nematicity results from either the ordering of the  $d_{xz}$  and  $d_{yz}$  orbitals or from an imbalance of the magnetization along the  $x$  and  $y$ . In both cases the lattice follows the electronic order and becomes orthorhombic. In  $\text{Ba}(\text{Fe}_{1-x}\text{Co}_x)_2\text{As}_2$  the lattice distortion precedes the magnetic order, in  $\text{Ba}_{1-x}\text{K}_x\text{Fe}_2\text{As}_2$  the two transitions coincide, FeSe has only a structural phase transition but does not develop long range order down to the lowest temperatures [11]. As shown theoretically the persistent fluctuations may result from magnetic frustration and the proximity of various types of possible magnetic states [12].

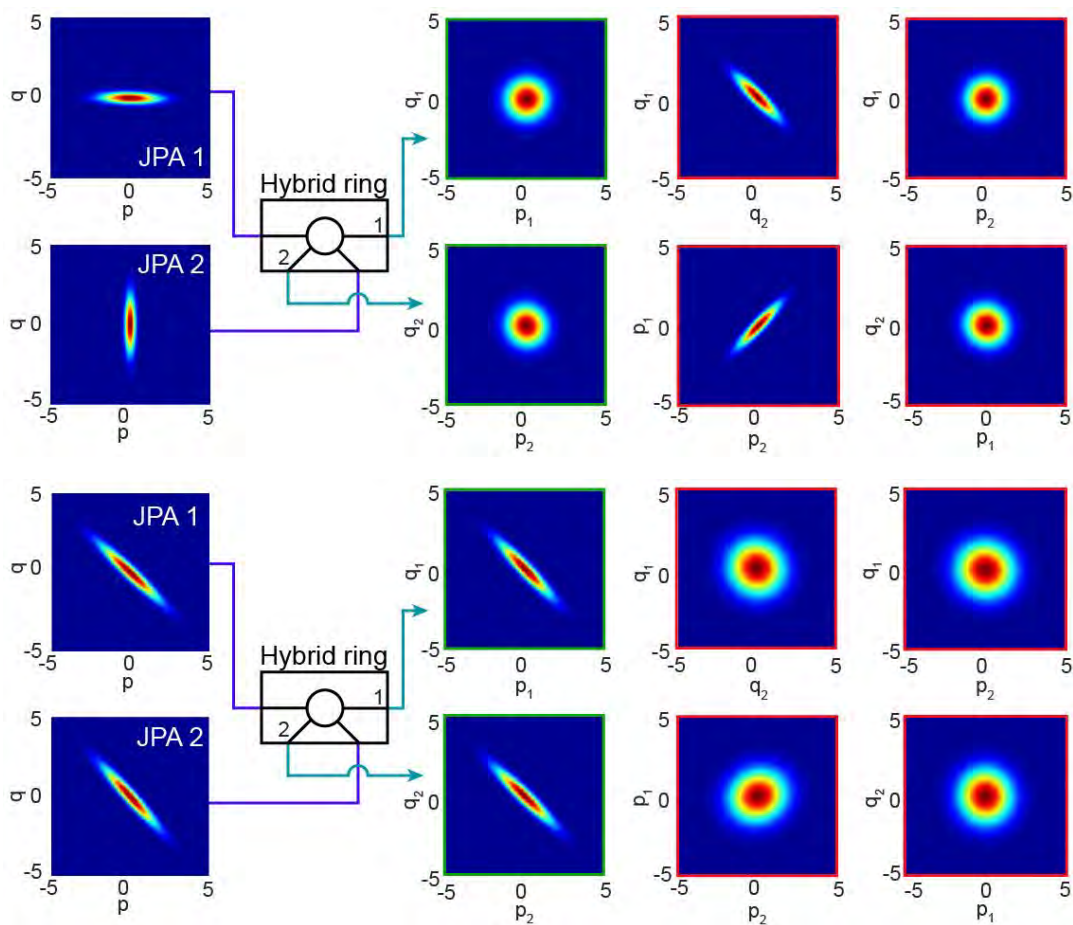
At the WMI fluctuations in the normal state and superconductivity were studied by light scattering. Above the SDW fluctuations could be observed in the Raman spectra. The response from fluctuations vanishes abruptly at the magnetic ordering temperature arguing for spin rather than charge fluctuations [13, 14]. Below  $T_c$  the work focused on the structure of the ground state. It could be demonstrated that there are two almost equally strong channels for Cooper pairing in  $\text{Ba}_{1-x}\text{K}_x\text{Fe}_2\text{As}_2$  [15–18]. The ground and the subleading state have  $s$ - and, respectively,  $d$ -wave symmetry. This combination favors spin fluctuations to be at the origin of superconductivity.

What kind of new directions looks promising? Although superconductivity at 203 K in  $\text{H}_2\text{S}$  at 190 GPa is a spectacular discovery [19] it is not clear (yet) how conventional devices can be realized on this basis. The perspective of exploiting or improving the properties of FeSe thin films [20], having  $T_c$  values in the 100 K range, or of intercalated FeSe [21] seems more promising at the moment. Certainly, FeSe itself offers lots of intriguing new physics to be discovered, and possible applications [22] are propelling a field in general. However, the hope for the advent of a new material class remains the best motivation for continuously improving our understanding - and tickle the creativity of the materials scientists.

## References

- [1] Y. Kamihara, T. Watanabe, M. Hirano, and H. Hosono, *J. Am. Chem. Soc.* **130**, 3296 (2008).
- [2] B. I. Zimmer, W. Jeitschko, J. H. Albering, R. Glaum, and M. Reehuis, *J. Alloys Compd.* **229**, 238 (1995).
- [3] B. I. Zimmer. *Darstellung und Charakterisierung ternärer Phosphide und quarternärer Phosphid-Oxide der Selten-erdelemente und des Thoriums mit Übergangsmetallen*. Ph.D. thesis, Wilhelms-Universität Münster (1996) (Westfälische 1996).
- [4] L. Boeri, O. V. Dolgov, and A. A. Golubov, *Phys. Rev. Lett.* **101**, 026403 (2008).
- [5] D. J. Scalapino, *Rev. Mod. Phys.* **84**, 1383–1417 (2012).
- [6] A. E. Böhmer, and C. Meingast, *C. R. Physique* **17**, 90 – 112 (2016).
- [7] M. Rotter, M. Tegel, and D. Johrendt, *Phys. Rev. Lett.* **101**, 107006 (2008).
- [8] I. I. Mazin, D. J. Singh, M. D. Johannes, and M. H. Du, *Phys. Rev. Lett.* **101**, 057003 (2008).
- [9] E. Fradkin, S. A. Kivelson, and J. M. Tranquada, *Rev. Mod. Phys.* **87**, 457–482 (2015).
- [10] S. Lederer, Y. Schattner, E. Berg, and S. A. Kivelson, *Phys. Rev. Lett.* **114**, 097001 (2015).
- [11] S.-H. Baek *et al.*, *Nature Mater.* **14**, 210–214 (2014).
- [12] J. K. Glasbrenner *et al.*, *Nature Phys.* **11**, 953–958 (2015).
- [13] R. Hackl *et al.*, *Annual Report WMI 2015* 25–28 (2015).
- [14] F. Kretzschmar *et al.*, *Nature Phys.* **12**, 560–563 (2016).
- [15] F. Kretzschmar *et al.*, *Annual Report WMI 2012*, 53–57 (2012).
- [16] T. Böhm *et al.*, *Annual Report WMI 2013*, 39–40 (2013).
- [17] F. Kretzschmar *et al.*, *Phys. Rev. Lett.* **110**, 187002 (2013).
- [18] T. Böhm *et al.*, *Phys. Rev. X* **4**, 041046 (2014).
- [19] A. P. Drozdov, M. I. Erements, I. A. Troyan, V. Ksenofontov, and S. I. Shylin, *Nature* **525**, 73–76 (2015).
- [20] J.-F. Ge, Z.-L. Liu, C. Liu, C.-L. Gao, D. Qian, Q.-K. Xue, Y. Liu, and J.-F. Jia, *Nature Mater.* **14**, 285–289 (2015).
- [21] M. Burrard-Lucas *et al.*, *Nature Mater.* **12**, 15–19 (2013).
- [22] C. Tarantini *et al.*, *Phys. Rev. B* **86**, 214504 (2012).

# Basic Research



Marginal distributions of the Wigner function characterizing experimental two-mode squeezing results. Two orthogonally squeezed vacuum states impinge on the hybrid ring. Squeezing levels of 7.968 dB for JPA 1 and 8.089 dB for JPA 2 and a JPA frequency of  $f_0 = 5.323$  GHz are used. Tomography of the output states shows thermal Wigner functions in the self-correlated subspaces (green borders) and two-mode squeezing in the cross-correlated subspaces (red borders).





## Spin Hall Magnetoresistance in a Canted Ferrimagnet

M. Althammer, K. Ganzhorn, R. Schlitz, S. Geprägs, M. Opel, R. Gross, H. Huebl <sup>1</sup>  
J. Barker, G.E.W. Bauer <sup>2</sup> B.A. Piot <sup>3</sup> S.T.B. Gönnenwein <sup>4</sup>

In past 4 years, we intensely investigated novel pure spin current effects in ferromagnetic insulator normal metal hybrid structures (see Annual Reports of 2013, 2014, and 2015). Among these effects is the spin Hall magnetoresistance (SMR), which allows one to sense the magnetization direction in a ferromagnetic insulator using an all electrical detection scheme. After establishing a fundamental understanding of the SMR in collinear ferromagnets, a next logical step is the study of the SMR in materials with more complex spin structure. This allows to address the important question whether the SMR response reflects the direction of the individual sublattice magnetizations or just the total net-magnetization of the system. To this end, we analyzed the SMR of the rare earth iron garnets (ReIGs) yttrium iron garnet (YIG) and yttrium doped gadolinium iron garnet (InYGdIG)/Pt hybrids. In particular, the InYGdIG is of interest, as this material allows to prepare a non-collinear sublattice magnetization configuration or canted phase which is ideally suited to test the established hypotheses.

Here we focus on experiments carried out on two different ReIG/Pt bilayers: One 40 nm thick yttrium iron garnet ( $\text{Y}_3\text{Fe}_5\text{O}_{12}$ , YIG) film with a 4 nm thin Pt on top and one indium and a 61.5 nm thin yttrium doped gadolinium iron garnet ( $\text{Y}_1\text{Gd}_2\text{Fe}_4\text{In}_1\text{O}_{12}$ , InYGdIG) film covered with 3.6 nm of Pt. For both samples the ReIGs have been deposited via pulsed laser deposition, while the Pt was deposited in-situ, without breaking the vacuum, via electron beam evaporation at WMI. The InYGdIG sample exhibits a magnetic compensation temperature  $T_{\text{comp}} = 85$  K, where we expect the development of a non-collinear (spin canted) phase via the application of an external magnetic field.

Figure 1(a-c) shows a typical set of magnetoresistance measurements for the YIG/Pt bilayer, taken at fixed temperatures of  $T = 10$  K, 85 K, 300 K and an external magnetic field of 7 T. The magnetoresistance behavior is fully consistent with previous measurements [1, 2]. The SMR amplitude

$$\text{SMR} = \frac{\rho(\alpha_H = 0^\circ) - \rho(\alpha_H = 90^\circ)}{\rho(\alpha_H = 0^\circ)} \quad (1)$$

<sup>1</sup>We gratefully acknowledge financial support via DFG Priority Programme 1538 "Spin-Caloric Transport" (GO 944/4, BA 2954/2).

<sup>2</sup>Institute for Materials Research, Tohoku University, Sendai, Miyagi 980-8577, Japan

<sup>3</sup>Laboratoire National des Champs Magnétiques Intenses, LNCMI-CNRS-UGA-UPS-INSA-EMFL, F-38042 Grenoble, France

<sup>4</sup>Institut für Festkörperphysik, Technische Universität Dresden, D-01062 Dresden, Germany

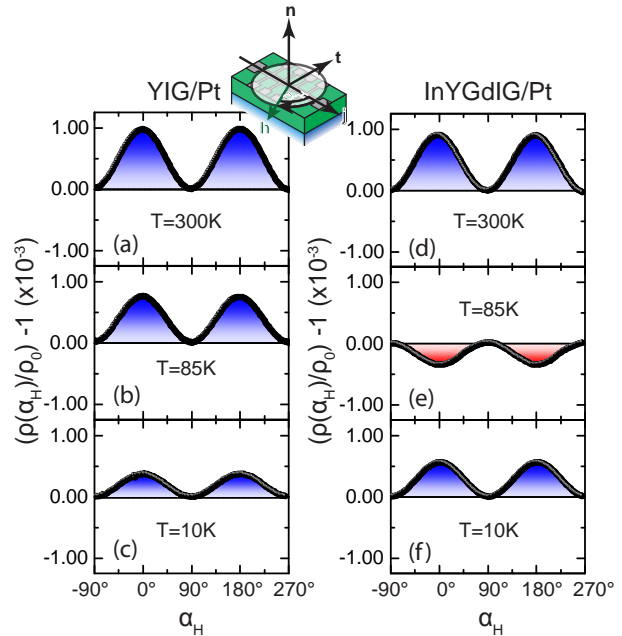


**Figure 1:** Evolution of the magnetoresistance in YIG/Pt (panels a-c) and InYGdIG/Pt (panels d-f). The data were recorded at  $T = 10$  K, 85 K and 300 K as a function of the angle  $\alpha_H$  between the current direction  $\mathbf{J}_c$  and the orientation of the external, in-plane magnetic field  $\mu_0 H = 7$  T, respectively. The SMR in InYGdIG/Pt inverts sign around the magnetization compensation temperature  $T_{\text{comp}} \approx 85$  K (panel e), but the extrema stay at the same  $\alpha_H$  for all temperatures.

is positive at all temperatures, and decreases with decreasing  $T$  by about a factor of 2 as also reported in the literature [2]. A similar set of magnetoresistance measurements for the InYGdIG/Pt sample is shown in Fig. 1(d-f), again for  $T = 10$  K, 85 K and 300 K. The measurements at  $T = 10$  K and  $T = 300$  K (panels (d) and (f)) show the same positive SMR as for YIG/Pt. However, at  $T = 85$  K  $\approx T_{\text{comp}}$  (panel (e)), the SMR has negative sign, and comparatively small amplitude. This is surprising and cannot be accounted for by the standard SMR theory [3, 4].

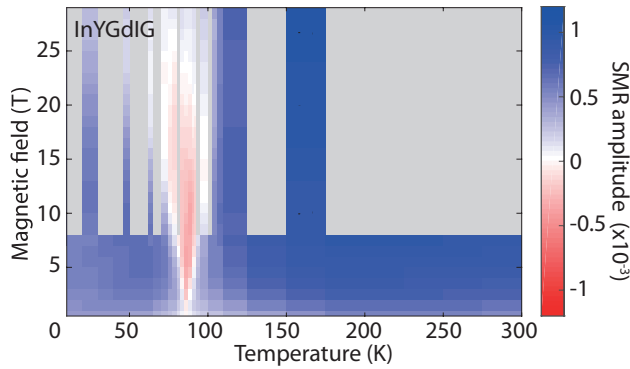


**Figure 2:** SMR amplitude as a function of temperature and magnetic field, as measured for InYGdIG. In the blue regions the SMR is positive. The red regions indicate negative SMR (as in Fig. 1(e)). No data has been taken in the regions shaded in grey.

To substantiate the SMR sign change, we studied the evolution of the SMR amplitude (Eq. (1)) with magnetic field strength and temperature in the YIG/Pt and InYGdIG/Pt samples. In YIG/Pt, the SMR amplitude monotonically increases with  $T$ , as reported previously [2]. In InYGdIG/Pt, the behaviour is much richer. Figure 2 shows corresponding data obtained for  $\mu_0 H \leq 7$  T (measured at WMI), as well as  $\mu_0 H \leq 29$  T at the high field magnet laboratory in Grenoble, in a false color plot. The SMR sign change in InYGdIG/Pt is clearly evident as a red pocket around  $T_{\text{comp}}(\text{InYGdIG}) = 85$  K.

The observed behavior clearly indicates that the macrospin picture of the SMR breaks down for non-collinear magnets. Note that the spin current transport across the magnetic insulator/normal metal interface is relevant for SMR. As this corresponds to an additional (transverse) dissipation channel for charge transport, the SMR cannot change sign with temperature [1, 3]. Furthermore, the applied magnetic field well exceeds the demagnetization or anisotropy fields, such that the orientation of  $\mu_0 H$  corresponds to that of the net magnetization. Thus, if the net magnetization indeed would govern the SMR, the SMR amplitude needs to be positive for all temperatures and magnetic fields. The InYGdIG/Pt sample clearly violates this conjecture, showing that the SMR is a powerful method to characterize even complex spin textures.

Our results demonstrate that simple transport experiments can identify non-collinear magnetic phases in highly resistive magnets contacted by heavy metals. The SMR thus might prove useful also for the investigation of topological spin textures, e.g. skyrmion phases, in thin films and nanostructures. More details on this work can be found in Ref. [5].

## References

- [1] M. Althammer, S. Meyer, H. Nakayama, M. Schreier, S. Altmannshofer, M. Weiler, H. Huebl, S. Geprags, M. Opel, R. Gross, D. Meier, C. Klewe, T. Kuschel, J.-M. Schmalhorst, G. Reiss, L. Shen, A. Gupta, Y.-T. Chen, G. E. W. Bauer, E. Saitoh, and S. T. B. Goennenwein, *Phys. Rev. B* **87**, 224401 (2013).
- [2] S. Meyer, M. Althammer, S. Geprags, M. Opel, R. Gross, and S. T. B. Goennenwein, *Appl. Phys. Lett.* **104**, 242411 (2014).
- [3] Y.-T. Chen, S. Takahashi, H. Nakayama, M. Althammer, S. T. B. Goennenwein, E. Saitoh, and G. E. W. Bauer, *Phys. Rev. B* **87**, 144411 (2013).
- [4] Y.-T. Chen, S. Takahashi, H. Nakayama, M. Althammer, S. T. B. Goennenwein, E. Saitoh, and G. E. W. Bauer, *J. Phys.: Condens. Matter* **28**, 103004 (2016).
- [5] K. Ganzhorn, J. Barker, R. Schlitz, B. A. Piot, K. Ollefs, F. Guillou, F. Wilhelm, A. Rogalev, M. Opel, M. Althammer, S. Geprags, H. Huebl, R. Gross, G. E. W. Bauer, and S. T. B. Goennenwein, *Phys. Rev. B* **94**, 094401 (2016).



## Universal two-magnon line shape in spin $\frac{1}{2}$ antiferromagnets?

N. Chelwani, T. Böhm, A. Baum, M. Opel, A. Erb, R. Hackl <sup>1</sup>

Light scattering is a widely used technique for the study of antiferromagnets [1] which experienced a renaissance with the discovery of the cuprates [2]. It was realized from the beginning that useful information could be extracted if the understanding of the entire spectra could be improved. From an experimental point of view there were reliable results on  $\text{Gd}_2\text{CuO}_4$  already in 1991 [3]. The data were presented as a function scattering symmetry and proved to be robust until now at least in the strongest scattering channel, the  $B_{1g}$  ( $x^2 - y^2$ ) symmetry which essentially probes the simultaneous flip of two neighboring spins [Fig. 1 (a)]. In spin wave theory the energy required is  $NSJ = 3J$  with  $N = 6$  and  $S = 1/2$  and  $J$  being the exchange coupling of nearest neighbor spins. Multi-magnon processes reduce the energy from  $3J$  to  $2.7J$  [4]. In addition, excitations were observed in the antisymmetric  $A_{2g}$  ( $xy - yx$ ) channel which were interpreted in terms of the chiral spin operator  $\hat{C} = \mathbf{S}_i \cdot (\mathbf{S}_j \times \mathbf{S}_k)$  [5]. Yet the discussion is not settled even by now for both theoretical [6, 7] and experimental reasons: The  $A_{2g}$  spectra have too much intensity and depend strongly on the material class [8].

Upon a closer look, there are also various open questions concerning the  $B_{1g}$  as well as the  $A_{1g}$  ( $x^2 + y^2$ ) and  $B_{2g}$  ( $xy$ ) spectra: (i) Are the line shapes universal? (ii) Is there a satisfactory description? (iii) Which parameters can be extracted reliably? (iv) Can the spectra at symmetries other than  $B_{1g}$  be explained? In a first step we focused on questions (i)-(iii) and reexamined and supplemented the data of  $\text{YBa}_2\text{Cu}_3\text{O}_{6.05}$  (Y123),  $\text{La}_2\text{CuO}_4$  (LCO), and  $\text{Bi}_2\text{Sr}_2\text{YCu}_2\text{O}_{8+\delta}$  (Bi2212). The  $B_{1g}$  spectra of the three materials will be discussed here.

Fig. 1 (b) shows a superposition of the spectra of Y123, LCO, and Bi2212. Both the intensity and the energy scales are normalized. The spectra of Y123 and LCO are multiplied by factors of 1.11 and 2.27, respectively, to match the peak intensity of Bi2212. The peak maxima in the raw data of Y123, LCO, and Bi2212 are observed to be at 2735 (339.3), 3300 (409.4), and 2890 (358.6)  $\text{cm}^{-1}$  (meV), respectively. The energies are divided

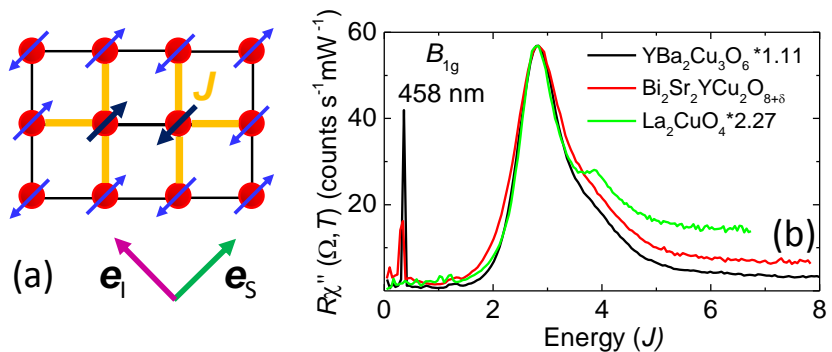


**Figure 1:** Light scattering in an antiferromagnet. (a) Scattering process. The polarized photons flip two spins (black) and break six bonds. The polarizations indicated project  $B_{1g} + A_{2g}$  symmetry. (b)  $B_{1g}$  spectra ( $A_{2g}$  subtracted) of  $\text{YBa}_2\text{Cu}_3\text{O}_{6.05}$  (black),  $\text{La}_2\text{CuO}_4$  (green), and  $\text{Bi}_2\text{Sr}_2\text{YCu}_2\text{O}_{8+\delta}$  (red). The intensities are scaled by factors as indicated. The energy axis is given in units of the exchange coupling  $J$ . The normalized position of the peak maxima matches the theoretically predicted energy of  $2.84 J$  [9].

by appropriate factors to collapse the peaks on the canonical value of  $2.84 J$  derived recently [9]. From the peak positions alone one obtains 119, 144, and 126 meV, respectively, for  $J$ . For Y123 and LCO the full theoretical analysis yields 126 and 149 meV fairly close to the values of 120 and 143 meV, respectively, found by neutron scattering [10, 11].

Close to the maximum between 2.5 and  $3.2 J$  the line shapes of the peaks are rather similar. At low energies the lines of Y123 and LCO coincide down to  $2.3 J$ . Below  $2.3 J$ , LCO has a

<sup>1</sup>The project was funded by the German Research Foundation (DFG) via the Transregional Collaborative Research Center TRR 80.

higher intensity from resonantly enhanced phonon contributions. Above  $3.2 J$ , LCO exhibits a secondary maximum whereas  $Y_{123}$  has only an almost linear tail before the intensity saturates at a value lower than that in all other materials. The two-magnon maximum of  $Bi_{2212}$  is generally wider than those of LCO and  $Y_{123}$ . The substantially off-stoichiometric composition of  $Bi_{2212}$  suggests that the line is inhomogeneously broadened. The most dramatic differences are found above  $4.4 J$ , where the saturation values of the intensities differ by more than a factor of three. We do not believe that this part of the spectra results from differences in the spin excitations. Rather, contributions from luminescence should be considered a possible (extrinsic) origin.

Concerning the overall (intrinsic) line shape a satisfactory description was achieved only recently using field-theoretic methods [9] after various studies on the basis of spin wave theory [4, 12–14]. The progress became possible through the inclusion of multi-magnon processes and amplitude (“Higgs”) fluctuations of the staggered magnetization on equal footing as suggested first by Podolsky and coworkers [15] who, then, neglected the effect of the form factors. As a result the  $\Omega^3$  variation of the low-energy response and the linear part between  $3.2$  and  $4.4 J$  in  $Y_{123}$  and  $Bi_{2212}$  found an almost quantitative explanation. In addition, the differences to LCO can be traced back to a variation of the coupling constant of the Higgs mode.

Similar line shapes of the two-magnon lines were also observed in some iridates [16] suggesting a universal behavior. However, the spectra in the other symmetries and in metallic materials such as doped cuprates or Fe-based compounds remain widely unexplained and can probably only be reproduced using numerical methods [17–19].

## References

- [1] P. A. Fleury, and R. Loudon, *Phys. Rev.* **166**, 514 (1968).
- [2] T. P. Devereaux, and R. Hackl, *Rev. Mod. Phys.* **79**, 175 (2007).
- [3] P. E. Sulewski, P. A. Fleury, K. B. Lyons, and S.-W. Cheong, *Phys. Rev. Lett.* **67**, 3864 (1991).
- [4] C. M. Canali, and S. M. Girvin, *Phys. Rev. B* **45**, 7127–7160 (1992).
- [5] B. S. Shastry, and B. I. Shraiman, *Phys. Rev. Lett.* **65**, 1068 (1990).
- [6] W.-H. Ko, Z.-X. Liu, T.-K. Ng, and P. A. Lee, *Phys. Rev. B* **81**, 024414 (2010).
- [7] F. Michaud, F. Vernay, and F. Mila, *Phys. Rev. B* **84**, 184424 (2011).
- [8] F. Venturini. *Raman Scattering Study of Electronic Correlations in Cuprates: Observation of an Unconventional Metal-Insulator Transition*. Ph.D. thesis, TU-München (2003).
- [9] S. A. Weidinger, and W. Zwirger, *Eur. Phys. J. B* **88**, 237 (2015).
- [10] D. Reznik, P. Bourges, H. F. Fong, L. P. Regnault, J. Bossy, C. Vettier, D. L. Milius, I. A. Aksay, and B. Keimer, *Phys. Rev. B* **53**, R14741–R14744 (1996).
- [11] N. S. Headings, S. M. Hayden, R. Coldea, and T. G. Perring, *Phys. Rev. Lett.* **105**, 247001 (2010).
- [12] P. Knoll, C. Thomsen, M. Cardona, and P. Murugaraj, *Phys. Rev. B* **42**, 4842–4845 (1990).
- [13] M. Rübhausen, N. Dieckmann, A. Bock, and U. Merkt, *Phys. Rev. B* **54**, 14967–14970 (1996).
- [14] M. Rübhausen *et al.*, *Phys. Rev. B* **56**, 14797–14808 (1997).
- [15] D. Podolsky, A. Auerbach, and D. P. Arovas, *Phys. Rev. B* **84**, 174522 (2011).
- [16] H. Gretarsson *et al.*, *Phys. Rev. Lett.* **116**, 136401 (2016).
- [17] B. Moritz, S. Johnston, T. P. Devereaux, B. Muschler, W. Prestel, R. Hackl, M. Lambacher, A. Erb, S. Komiya, and Y. Ando, *Phys. Rev. B* **84**, 235114 (2011).
- [18] C.-C. Chen, C. J. Jia, A. F. Kemper, R. R. P. Singh, and T. P. Devereaux, *Phys. Rev. Lett.* **106**, 067002 (2011).
- [19] C. J. Jia, E. A. Nowadnick, K. Wohlfeld, Y. F. Kung, C.-C. Chen, S. Johnston, T. Tohyama, B. Moritz, and T. P. Devereaux, *Nature Commun.* **5**, 3314 (2014).

## Finite-Time Correlations of Propagating Squeezed Microwave States

*K. G. Fedorov, S. Pogorzalek, P. Yard, P. Eder, M. Fischer, J. Goetz, F. Wulschner, E. Xie, F. Deppe, A. Marx, R. Gross*<sup>1</sup>

Propagating quantum microwave signals in the form of squeezed states are natural candidates for quantum communication and quantum information processing with continuous variables. This assessment stems from the fact that they belong to the same frequency range and are generated using the same material technology as information processing platforms based on superconducting quantum circuits. In this way, one can potentially achieve a seamless connection between distant superconducting quantum computers and the realization of hybrid computation schemes with continuous variables [1, 2]. Nonclassical finite-time correlations of microwave squeezed states can be captured using a well-established normalized second order correlation function  $g^{(2)}(\tau) = \langle \hat{a}^\dagger(0)\hat{a}^\dagger(\tau)\hat{a}(\tau)\hat{a}(0) \rangle / \langle \hat{a}^\dagger(0)\hat{a}(0) \rangle^2$ , where  $\hat{a}^\dagger(\tau)$  and  $\hat{a}(\tau)$  are the creation and annihilation operators of the signal mode at the time moment of  $\tau$ . It allows one to observe how the nonclassical properties of travelling states of light dephase in time and relate an autocorrelation time to this process. The latter quantity is important in quantum communication protocols as it sets the maximal amount of acceptable phase delays between different channels.

To measure the  $g^{(2)}(\tau)$  function of propagating squeezed microwaves we employ the experimental setup shown in Fig. 1. We use a flux-driven Josephson parametric amplifier (JPA) for generation of squeezed microwave states. The JPA consists of a  $\lambda/4$  coplanar resonator shunted to ground by a dc-SQUID. A strong pump tone allows to modulate the Josephson inductance of the dc-SQUID at twice the JPA frequency,  $f_{\text{pump}} = 2f_{\text{JPA}}$  [3, 4]. The JPA is placed in a magnetically shielded sample holder inside a custom-made dry dilution refrigerator. During all experiments the JPA temperature is stabilized at 50 mK. The task of the JPA is to perform a squeezing operation on an incident vacuum state  $\hat{S}(\xi)|0\rangle$ , where  $\hat{S}(\xi) = \exp(\frac{1}{2}\xi^* \hat{a}^2 - \frac{1}{2}\xi (\hat{a}^\dagger)^2)$ , and  $\xi = re^{i\phi}$  is a complex squeezing amplitude. Here, the phase  $\phi$  determines the squeezed quadrature direction in phase space, while the squeezing factor  $r$  parameterises the amount of squeezing.

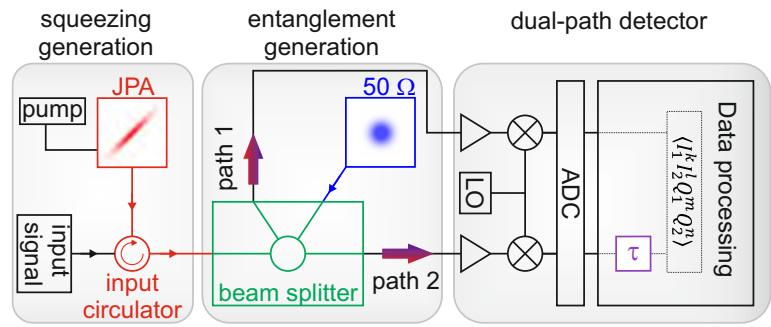


**Figure 1:** Schematic layout for finite-time correlation measurements of propagating squeezed microwave states.

In order to reconstruct the squeezed vacuum states, we apply a modified dual-path reconstruction scheme [3]. It consists in splitting our signal into two paths with a hybrid ring, then amplifying the signal with a chain of cryogenic and room temperature rf amplifiers, and finally, performing cross-correlation measurements. In this way, we can retrieve all the moments of the annihilation and creation operators,  $\langle (\hat{a}^\dagger)^n \hat{a}^m \rangle$ , of the signal mode. An important modification here is the introduction of a digital time-delay inside one of the dual-path arms (see Fig. 1). This allows us to delay the chosen channel by a certain time  $\tau$  in order to acquire  $\tau$ -dependent signal moments and use them for the  $g^{(2)}(\tau)$  function calculation.

<sup>1</sup>We acknowledge support from DFG through FE 1564/1-1, the doctorate program ExQM of the Elite Network of Bavaria, the IMPRS ‘Quantum Science and Technology’, and the German Excellence Initiative via the ‘Nanosystems Initiative Munich’ (NIM). We also acknowledge the productive collaboration with the groups of Y. Nakamura (Tokyo) and E. Solano (Bilbao).

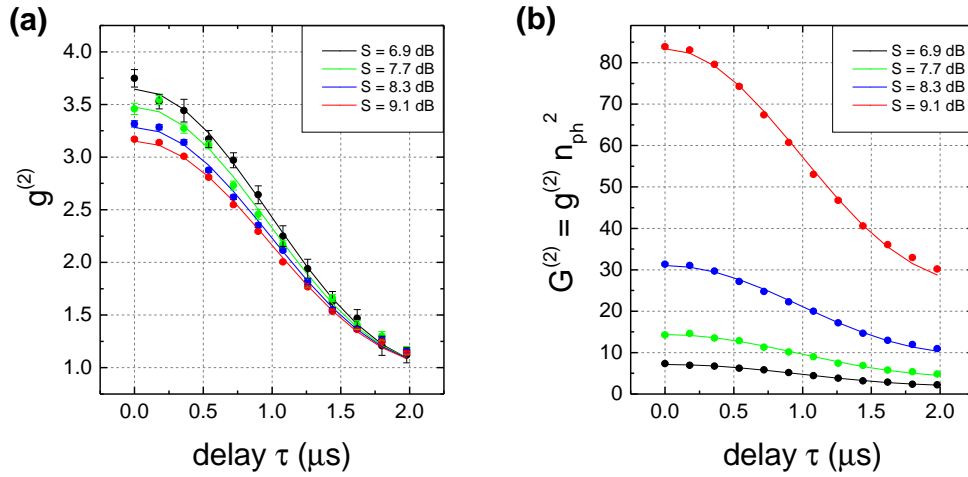


**Figure 2:** Finite-time second order correlations of a microwave squeezed state. Dots depict experimental data, lines show corresponding theory fits using Eq. 1,  $S$  denotes a squeezing level generated by the JPA. (a) depicts the  $g^{(2)}$  function results, (b) shows the same experimental results for the unnormalized representation  $G^{(2)} = g^{(2)} n_{ph}^2$ .

Figure 2 shows the experimental results of respective  $g^{(2)}(\tau)$  measurements. As expected from theory, one can see the super-Poissonian character of squeezed microwave states as  $g^{(2)}(0) > 1$ . We observe a smooth decay of  $g^{(2)}(\tau)$  to the coherent limit  $g^{(2)}(\tau) = 1$  on the time scale of  $\tau \sim 2 \mu s$ . In order to describe our results, we use a variant of the input-output theory [5] developed in collaboration with the group of E. Solano (Bilbao)

$$g^{(2)}(\tau) = 1 + \text{sinc}^2(\Omega\tau) \frac{1 + 2\sigma_x^2(\sigma_x^2 - 1) + 2\sigma_p^2(\sigma_p^2 - 1)}{(1 - \sigma_x^2 - \sigma_p^2)^2}, \quad (1)$$

where  $\Omega$  is a measurement filter bandwidth,  $\sigma_x$  and  $\sigma_p$  are orthogonal quadrature variances of the squeezed state. Fitting Eq. (1) to the experimental data (see Fig. 2) allows us to extract the experimental filter bandwidth  $\Omega \simeq 420$  kHz which agrees very well with the bandwidth of the digital FIR filter used in our measurement protocol,  $\Omega_{\text{FIR}} = 430$  kHz.

In conclusion, we have successfully measured finite-time second order correlations of propagating squeezed microwave states by the means of the  $g^{(2)}(\tau)$  function. We have confirmed the super-Poissonian character of squeezed states. By developing a theory model, we have determined that the autocorrelation time of quantum correlations is exclusively dependent on a minimum filter bandwidth in the measurement setup (in our case, it was limited by the bandwidth of the digital FIR filter). Our results are an important milestone towards fundamental understanding of propagating quantum microwaves and their respective applications in the areas of quantum communication and computation.

## References

- [1] U. L. Andersen, J. S. Neergaard-Nielsen, P. van Loock, and A. Furusawa, *Nat. Phys.* **11**, 713–719 (2015).
- [2] K. G. Fedorov, L. Zhong, S. Pogorzalek, P. Eder, M. Fischer, J. Goetz, E. Xie, F. Wulschner, K. Inomata, T. Yamamoto, Y. Nakamura, R. Di Candia, U. Las Heras, M. Sanz, E. Solano, E. P. Menzel, F. Deppe, A. Marx, and R. Gross, *Phys. Rev. Lett.* **117**, 020502 (2016).
- [3] E. P. Menzel, R. Di Candia, F. Deppe, P. Eder, L. Zhong, M. Ihmig, M. Haeberlein, A. Baust, E. Hoffmann, D. Ballester, K. Inomata, T. Yamamoto, Y. Nakamura, E. Solano, A. Marx, and R. Gross, *Phys. Rev. Lett.* **109**, 250502 (2012).
- [4] L. Zhong, E. P. Menzel, R. D. Candia, P. Eder, M. Ihmig, A. Baust, M. Haeberlein, E. Hoffmann, K. Inomata, T. Yamamoto, Y. Nakamura, E. Solano, F. Deppe, A. Marx, and R. Gross, *New Journal of Physics* **15**, 125013 (2013).
- [5] N. B. Grosse, T. Symul, M. Stobińska, T. C. Ralph, and P. K. Lam, *Phys. Rev. Lett.* **98**, 153603 (2007).

## Second-Order Decoherence Mechanisms of a Transmon Qubit Probed with Thermal Microwave States

*J. Goetz, F. Deppe, P. Eder, M. Fischer, S. Pogorzalek, F. Wulschner, E. Xie, K. G. Fedorov, A. Marx, and R. Gross*<sup>1</sup>

Thermal microwave states are omnipresent noise sources in superconducting quantum circuits covering all relevant frequency regimes. Hence they can be a strong source for decoherence in these circuits [1]. To optimize the coherence properties of superconducting qubits, several strategies to decouple them from the environmental noise have been developed. In the first place, the most convenient way to suppress noise over a broad frequency range is to place the qubit inside a superconducting resonator. This concept is efficient when the qubit transition frequency is far detuned from the resonator frequency by an amount  $\delta$  much larger than their coupling strength  $g$ . Nevertheless, even in this case, noise still couples to the qubit in second-order with strength  $g^2/\delta$ . In the second place, fluctuations that modify the qubit transition frequency  $\omega_q$  can be noticeably suppressed by tuning the qubit to an operation point where the derivative of  $\omega_q$  with respect to the fluctuating quantity vanishes. Again, even at such a sweet spot, second-order coupling of environmental fluctuations can be a source for decoherence. In addition to these decoherence processes,

intrinsic qubit parameters such as its relaxation rate can be fluctuating in time. One prominent source for these fluctuations are two-level states (TLSs) mediating low-frequency noise to the qubit. The three second-order decoherence mechanisms mentioned above can be reliably studied with propagating thermal fields because their power spectral density  $S(\omega)$  can be adjusted with a high accuracy by controlling the temperature of a black-body radiator. Furthermore,  $S(\omega)$  is white for low frequencies and sufficiently smooth at the qubit transition frequency, which allows for a quantitative analysis of second-order decoherence mechanisms. Besides the fact that thermal fields are an accurate control knob to study second-order effects of noise, their omnipresence in superconducting circuits naturally results in a strong demand to investigate their second-order influence on the coherence properties of superconducting quantum circuits.

We systematically study the effect of the second-order coupling between thermal fields generated by a black-body radiator and a superconducting transmon qubit placed in a super-

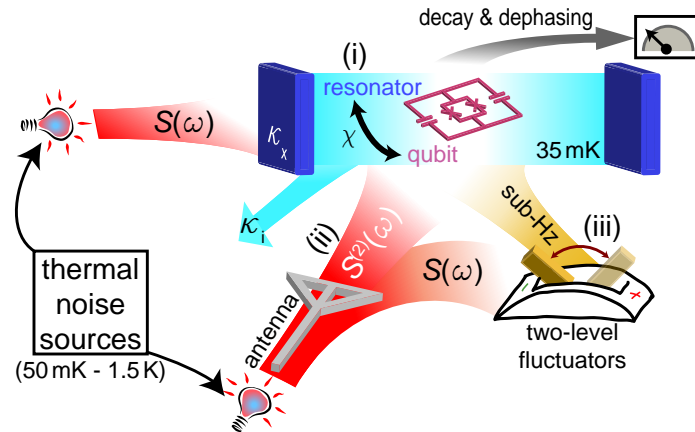


**Figure 1:** Sketch of the experimental idea. We characterize the second-order coupling between a thermal noise source (black-body radiator of variable temperature) and a superconducting qubit by measuring the qubit decay and dephasing rate. The second-order coupling to the thermal noise field becomes relevant in the following situations: (i) When the qubit is dispersively coupled to a resonator acting as a filter for the noise field with spectral density  $S(\omega)$ . (ii) When the qubit is directly irradiated by a noise field using a near-field antenna, but operated at a sweet spot making the second-order spectral density  $S^{(2)}(\omega)$  the leading contribution. (iii) When one or multiple two-level fluctuators change the noise spectral density in the sub-Hz regime.

<sup>1</sup>We acknowledge support from DFG through FE 1564/1-1, the doctorate program ExQM of the Elite Network of Bavaria, the IMPRS ‘Quantum Science and Technology’, and the German Excellence Initiative via the ‘Nanosystems Initiative Munich’ (NIM).



conducting resonator [2]. We analyze the three individual decoherence mechanisms depicted in Fig. 1. The novel aspect of our experiments is that we can either irradiate the qubit directly or via the resonator filter function with thermal noise of controllable power spectral density while keeping the qubit at the base temperature of a dilution refrigerator. In this way, we can quantify the impact of thermal noise without suffering from parasitic effects such as quasiparticle generation in the superconducting circuits.

We first analyze the decoherence mechanism labeled with (i) in Fig. 1, which is the relaxation rate  $\gamma_1$  of the qubit due to dispersively coupled thermal noise (see Fig. 2). In the dispersive Jaynes-Cummings regime, noise at the resonator frequency couples in second-order. In our experiments, we find a coupling to broadband fields, which is enhanced as compared to that expected from the Purcell filter effect of the resonator. Furthermore, using coherent states and narrow-band shot noise, we demonstrate the counter-intuitive effect that the qubit relaxation rate is decreasing for increasing field strengths. We also characterize thermal noise fields which are directly irradiated onto the qubit via a near-field antenna without the cavity filter (labeled with (ii) in Fig. 1). At the flux sweet spot, this direct irradiation reveals the influence of second-order-coupled noise on the qubit dephasing rate. In particular, we observe the expected  $T^3$  temperature dependence of the qubit dephasing rate (data shown in Ref. [2]). Finally, we show that low-frequency fluctuations of the qubit relaxation rate (labeled with (iii) in Fig. 1) are related to the temperature of the black-body radiator if the field is not Purcell filtered. In particular, we experimentally confirm the  $T^2$ -dependence of the fluctuation spectrum expected for noninteracting two-level states (data shown in Ref. [2]). The presence of these two-level fluctuators in the spatial vicinity of the qubit change the effective noise spectral density leading to fluctuations of the relaxation rate.

Our work establishes thermal fields as an important tool to probe the coherence properties of superconducting quantum circuits. In this way, we gain important insight into second-order decoherence mechanisms of superconducting qubits. Furthermore, our quantitative analysis of the decoherence rates is crucial to optimize the performance of superconducting qubits, which is necessary for many quantum computation and communication protocols.

## References

- [1] J. Goetz, S. Pogorzalek, F. Deppe, K. G. Fedorov, P. Eder, M. Fischer, F. Wulschner, E. Xie, A. Marx, and R. Gross, ArXiv e-prints (2016). [arXiv:1609.07353](https://arxiv.org/abs/1609.07353) [quant-ph].
- [2] J. Goetz, F. Deppe, P. Eder, M. Fischer, M. Müting, J. Puertas Martínez, S. Pogorzalek, F. Wulschner, E. Xie, K. G. Fedorov, A. Marx, and R. Gross, ArXiv e-prints (2016). [arXiv:1609.07351](https://arxiv.org/abs/1609.07351) [quant-ph].

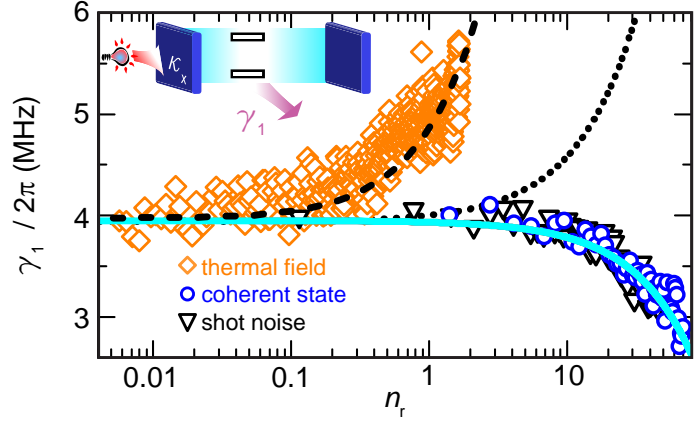


**Figure 2:** Qubit relaxation rate  $\gamma_1$  for microwave fields coupling the qubit through the resonator (see inset for setup sketch) plotted versus the average photon number  $n_r$ . The solid line is a numerical linear fit. The dotted line is based on calculations presented in Ref. [2] modeling the expected increase due to thermal fields. For the dashed line we use a numerical calculation, where the enhanced relaxation rate is modeled as a free parameter.

## Photon Statistics of Propagating Thermal Microwaves

J. Goetz, F. Deppe, P. Eder, M. Fischer, S. Pogorzalek, F. Wulschner, E. Xie, K. G. Fedorov, A. Marx, and R. Gross <sup>1</sup>

As propagating electromagnetic fields in general, propagating microwaves with photon numbers on the order of unity are essential for quantum computation, communication, and illumination protocols. Because of their omnipresence in experimental setups, the investigation of propagating thermal states is a fundamental task. Specifically in the microwave regime, sophisticated experimental techniques for their generation, manipulation, and detection have been developed in recent years. In this context, an important technique established at the WMI is the generation of propagating thermal microwaves using black-body emitters. These emitters can be spatially separated from the setup components used for manipulation and detection, which allows one to individually control the emitter and the setup temperature. Due to the low energy of microwave photons, the detection of these fields typically requires the use of near-quantum-limited amplifiers, cross-correlation detectors, or superconducting qubits.

The unique nature of propagating fields is reflected in their photon statistics, which is described by a probability distribution either in terms of the number states or in terms of moments. The former were studied by coupling the field to an atom or qubit and measuring the coherent dynamics or by spectroscopic analysis. The moment-based approach, in practice, requires knowledge on the average photon

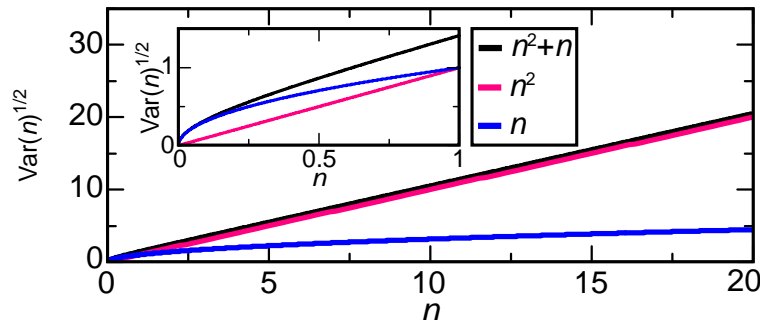


**Figure 1:** Photon number correlations.  $[Var(n)]^{1/2}$  plotted versus photon number for thermal fields (black), their classical limit (red), and coherent states (blue). The inset shows the regime that we capture in our experiments.

number  $n$  and its variance  $Var(n)$  to distinguish many states of interest. To this end, the second-order correlation function  $g^{(2)}(\tau)$  has been measured to analyze the photon statistics of thermal or quantum emitters ever since the ground-breaking experiments of Hanbury Brown and Twiss. While these experiments use the time delay  $\tau$  as control parameter, at microwave frequencies the photon number  $n$  can be controlled conveniently. In the specific case of a thermal field at frequency  $\omega$ , the Bose-Einstein distribution yields  $n(T) = [\exp(\hbar\omega/k_B T) - 1]^{-1}$  and  $Var(n) = n^2 + n$ , which can be controlled by the temperature  $T$  of the emitter. In practice, one wants to distinguish this relation from both the classical limit  $Var(n) = n^2$  and the Poissonian behavior  $Var(n) = n$  characteristic for coherent states or shot noise. Hence, as shown in Fig. 1, the most relevant regime for experiments is  $0.05 \lesssim n \lesssim 1$ , which translates into emitter temperatures between 100 mK and 1 K at approximately 6 GHz [1].

We experimentally confirm the theoretically expected photon number variance  $Var(n)$  of thermal microwave fields for  $0.05 \lesssim n \lesssim 1.5$  using two fundamentally distinct experimental setups [2]. To this end, we first use a superconducting transmon qubit interacting with the propagating fields via a dispersively coupled microwave resonator (setup shown in Fig. 1 of the contribution “Second-order decoherence mechanisms of a transmon qubit probed with

<sup>1</sup>We acknowledge support from DFG through FE 1564/1-1, the doctorate program ExQM of the Elite Network of Bavaria, the IMPRS ‘Quantum Science and Technology’, and the German Excellence Initiative via the ‘Nanosystems Initiative Munich’ (NIM).

thermal microwave states”). Differently to approaches relying on the coherent dynamics, where decoherence is detrimental, the additional qubit dephasing rate induced by the field directly reflects the photon number variance in our experiments. A systematic temperature sweep reveals the additional dephasing rate  $\gamma_\varphi(n_r) \propto n_r^2 + n_r$  as displayed in Fig. 2. We furthermore can distinguish between fields of equal photon number variance if the resonator has a different decay constant for them. In particular, we find the expected factor of two between the dephasing rates caused by coherent states and shot noise.

In a second step, we use an alternative setup to extract the super-Poissonian photon statistics of propagating thermal microwaves from direct correlation measurements and from measurements using a near-quantum-limited Josephson parametric amplifier (JPA) as preamplifier (data shown in Ref. [2]). The results show that the noise added by the JPA inevitably alters the photon statistics of the amplified field. Our results provide a quantitative picture of propagating thermal microwaves, which is especially relevant for the characterization of more advanced quantum states in the presence of unavoidable thermal background fields.

Our results demonstrate that the three types of propagating microwave states we investigate can be reliably distinguished below the single photon level in an experiment by their photon statistics. We demonstrate that superconducting qubits and direct correlation measurements are complementary tools to explore decoherence mechanisms possibly limiting high-performance superconducting qubits and the properties of more advanced quantum microwave states. With respect to superconducting qubits, we gain systematic insight into a dephasing mechanism which may become relevant for state-of-the-art devices with long coherence times.

## References

- [1] J. Goetz, F. Deppe, P. Eder, M. Fischer, M. Müting, J. Puertas Martínez, S. Pogorzalek, F. Wulschner, E. Xie, K. G. Fedorov, A. Marx, and R. Gross, ArXiv e-prints (2016). [arXiv:1609.07351](https://arxiv.org/abs/1609.07351) [quant-ph].
- [2] J. Goetz, S. Pogorzalek, F. Deppe, K. G. Fedorov, P. Eder, M. Fischer, F. Wulschner, E. Xie, A. Marx, and R. Gross, ArXiv e-prints (2016). [arXiv:1609.07353](https://arxiv.org/abs/1609.07353) [quant-ph].

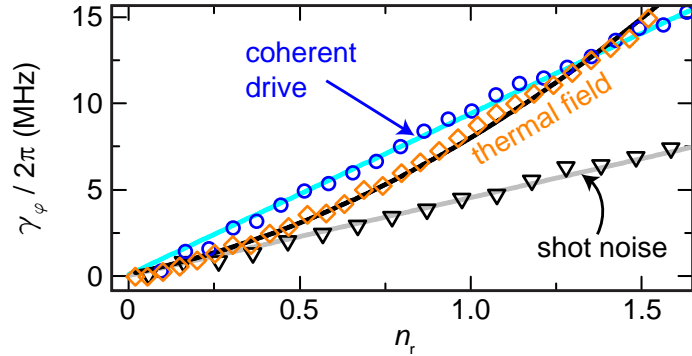


**Figure 2:** Qubit dephasing rates  $\gamma_\varphi$  of prototypical input fields plotted versus the average resonator population  $n_r$ . Solid lines are numerical fits [2].



## Electronic Correlations in the Organic Metal $\kappa$ -(BETS)<sub>2</sub>Mn[N(CN)<sub>2</sub>]<sub>3</sub> Probed by Magnetic Quantum Oscillations

M.V. Kartsovnik, W. Biberacher <sup>1</sup>  
V.N. Zverev <sup>2</sup>

Magnetic quantum oscillations have proven extremely useful in exploring materials of high current interest such as cuprate [1, 2] and iron-based superconductors [3], topological insulators [4], and organic charge-transfer salts [5]. Here, we report on the high-field magnetoresistance of the organic conductor  $\kappa$ -(BETS)<sub>2</sub>Mn[N(CN)<sub>2</sub>]<sub>3</sub>, demonstrating the power of the Shubnikov - de Haas (SdH) oscillations in studying Fermi surface properties of a quasi-two-dimensional (quasi-2D) correlated electronic system close to a metal-insulator transition.

The present compound is a nice example of a natural nanostructure with alternating single-molecular conducting and magnetic layers. The charge transport is provided by delocalized  $\pi$ -electrons in BETS layers, while magnetic properties are dominated by localized  $d$ -electron spins in the insulating anionic layers. In addition to an interesting, still not understood crosstalk between the two subsystems [6, 7], the narrow half-filled conduction band is a likely candidate for a Mott instability [8]. The material undergoes a metal-insulator transition at  $\approx 21$  K. The insulating ground state is suppressed by a quasi-hydrostatic pressure of about 1 kbar, giving way to a metallic and even superconducting state with  $T_c \approx 5$  K [8].

An example of the oscillating low-temperature interlayer resistance of  $\kappa$ -(BETS)<sub>2</sub>Mn[N(CN)<sub>2</sub>]<sub>3</sub> in a magnetic field perpendicular to the layers is shown in Fig. 1. The applied pressure,  $p = 1.4$  kbar, is sufficient to drive the system into the metallic state, though not far away from the insulating domain of the phase diagram. A close-up of the SdH oscillations at fields between 16 and 18 T, shown in the lower inset in Fig. 1, reveals two oscillatory components, confirming the theoretically predicted Fermi surface [8]. The weak, relatively slow oscillations with the frequency  $F_\alpha \approx 1130$  T originate from the rhombus-like  $\alpha$ -orbit on the border of the Brillouin zone, see the upper inset in Fig. 1. The dominant oscillations have a frequency of  $\approx 4220$  T, corresponding to the full first Brillouin zone area. The relevant  $\beta$ -orbit (green arrows in the upper inset in Fig. 1) is caused by magnetic breakdown (MB) between different parts of the Fermi surface.

The field and temperature dependence of the oscillation amplitude  $A_j$  can be analyzed within the 2D Lifshitz-Kosevich-Shoenberg (LKS) formula [9] using the standard damping factors  $R_T$ ,  $R_D$ , and  $R_{MB}$  caused,

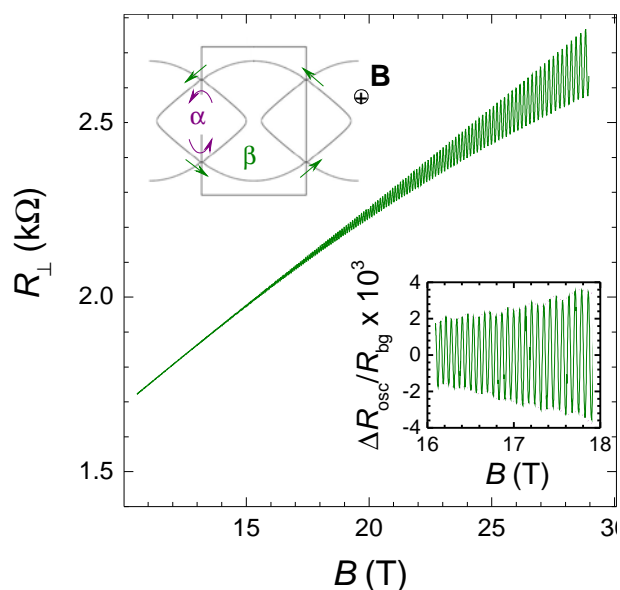


**Figure 1:** Interlayer resistance of  $\kappa$ -(BETS)<sub>2</sub>Mn[N(CN)<sub>2</sub>]<sub>3</sub> versus magnetic field  $B \perp$  layers, at  $T = 0.35$  K,  $p = 1.4$  kbar. Upper inset: 2D rectangular Brillouin zone and the Fermi surface. The purple and green arrows indicate, respectively, the classical,  $\alpha$ , and magnetic-breakdown,  $\beta$ , cyclotron orbits. Lower inset: close-up of the oscillatory part of the magnetoresistance normalized to the monotonic background. The dotted purple lines are envelopes emphasizing the weak  $\alpha$  oscillations superposed on the dominant fast  $\beta$  oscillations.

<sup>1</sup>The work was supported by the German Research Foundation grant No. KA 1652/4-1 and by the LNCMI-CNRS, member of the European Magnetic Field Laboratory (EMFL).

<sup>2</sup>Institute of Solid State Physics, Chernogolovka, Russia

respectively, by finite temperature, scattering, and MB effects. From the experimentally obtained temperature dependence we evaluate the effective cyclotron masses corresponding to the  $\alpha$ - and  $\beta$ -orbits, respectively [10]:  $m_{c,\alpha} = 5.55m_e$  and  $m_{c,\beta} = 6.90m_e$ , where  $m_e$  is the free electron mass. These values, are significantly higher than the calculated band masses, suggesting strong many-body renormalization effects. Particularly interesting is that the mass ratio  $m_{c,\alpha}/m_{c,\beta} \approx 0.8$  is  $\sim 60\%$  higher than usually met in similar metallic  $\kappa$ -type salts of BETS and BEDT-TTF [11].

We also analyze the field dependence of the oscillation amplitudes shown in Fig. 2. Here, it is important to properly consider the different influence of many body interactions on the damping factors in the LKS formula [10]. For the temperature damping factor  $R_T$  this influence consists in a renormalization of the cyclotron mass. By contrast, for  $R_D$ , renormalization effects on the mass and Dingle temperature are predicted to cancel each other [12, 13]. By taking this into account, the data in Fig. 2 can be fitted, yielding a rather low MB field  $B_0 = 70$  mT and almost equal Dingle temperatures  $T_D = 3.1$  and  $3.5$  K for the  $\alpha$  and  $\beta$  orbits, respectively. Remarkably, the fit reveals a considerable difference between the ratios of the renormalized cyclotron masses entering  $R_{T,\alpha}$  and  $R_{T,\beta}$  and of the band masses entering the Dingle factors [10]. This points to a significant enhancement of electron correlations on the  $\alpha$  part of the Fermi surface, most likely due to the nesting instability on its extended flat segments. Thus, in addition to the standard set of the Fermi surface parameters, the SdH oscillations provide important information on electronic correlations in the present compound.

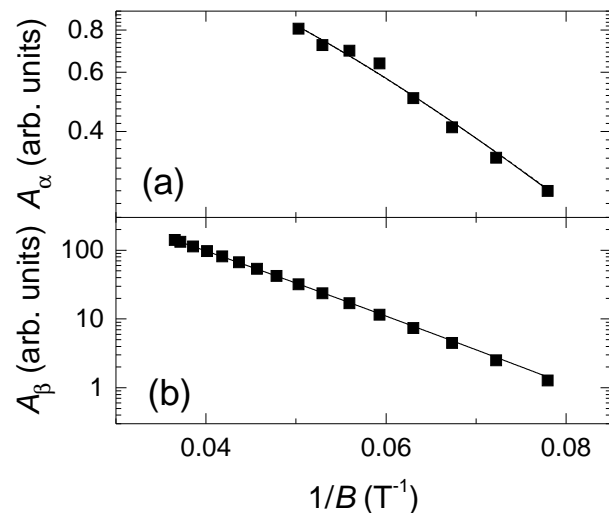


**Figure 2:** Amplitude of the  $\alpha$  oscillations (a) and the  $\beta$  oscillations (b) plotted against inverse magnetic field. Both amplitudes are measured in the same units. The lines are fits according to the LKS theory.

## References

- [1] S. E. Sebastian, and C. Proust, *Annu. Rev. Condens. Matter Phys.* **6**, 411 (2015).
- [2] T. Helm, M. V. Kartsovnik, C. Proust, B. Vignolle, C. Putzke, E. Kampert, I. Sheikin, E.-S. Choi, J. S. Brooks, N. Bittner, W. Biberacher, A. Erb, J. Wosnitzer, and R. Gross, *Phys. Rev. B* **92**, 094501 (2015).
- [3] A. Carrington, *Reports on Progress in Physics* **74**, 124507 (2011).
- [4] Y. Ando, *Journal of the Physical Society of Japan* **82**, 102001 (2013).
- [5] M. V. Kartsovnik, *Chem. Rev.* **104**, 5737 (2004).
- [6] O. Vyaselev, M. Kartsovnik, W. Biberacher, L. Zorina, N. Kushch, and E. Yagubskii, *Phys. Rev. B* **83**, 094425 (2011).
- [7] O. M. Vyaselev, S. V. Simonov, N. D. Kushch, W. Biberacher, and M. V. Kartsovnik. Magnetic torque in  $\kappa$ -(BETS)<sub>2</sub>Mn[N(CN)<sub>2</sub>]<sub>3</sub>. [arXiv:1512.07013](https://arxiv.org/abs/1512.07013) (2015).
- [8] V. N. Zverev, M. V. Kartsovnik, W. Biberacher, S. Khasanov, R. P. Shibaeva, L. Ouahab, L. Toupet, N. D. Kushch, E. B. Yagubskii, and E. Canadell, *Phys. Rev. B* **82**, 155123 (2010).
- [9] D. Shoenberg. *Magnetic Oscillations in Metals* (Cambridge University Press, Cambridge, 1984).
- [10] M. V. Kartsovnik, V. N. Zverev, W. Biberacher, S. V. Simonov, I. Sheikin, N. D. Kushch, and E. B. Yagubskii. Shubnikov-de Haas oscillations and electronic correlations in the layered organic metal  $\kappa$ -(BETS)<sub>2</sub>Mn[N(CN)<sub>2</sub>]<sub>3</sub>. [arXiv:1608.03755](https://arxiv.org/abs/1608.03755) (2016).
- [11] J. Merino, and R. H. McKenzie, *Phys. Rev. B* **62**, 2416 (2000).
- [12] M. Fowler, and R. E. Prange, *Physics* **1**, 315 (1965).
- [13] G. W. Martin, D. L. Maslov, and M. Y. Reizer, *Phys. Rev. B* **68**, 241309 (2003).

## Interlayer Coupling and Magnetoresistance in $\kappa$ -(BETS)<sub>2</sub>FeCl<sub>4</sub>

M. Kunz, W. Biberacher, M.V. Kartsovnik<sup>1</sup>  
N.D. Kushch<sup>2</sup>, A. Miyazaki<sup>3</sup>

Magnetic quantum oscillations and classical angular magnetoresistance oscillations (AMRO) are known as powerful tools for studying the Fermi surface (FS) of low-dimensional metals [1]. By investigating quantum oscillations, the area of closed FS orbits can be directly determined from the oscillation frequency, while their temperature and field dependencies allow one to estimate the cyclotron mass and the scattering time. The AMRO, being a semi-classical geometrical effect, can be used to observe different FS sheets, both open and closed.  $\kappa$ -(BETS)<sub>2</sub>FeCl<sub>4</sub> ( $\kappa$ -FeCl) is a system of high interest because of the interplay between magnetic and conducting systems [2]. The general shape of the FS of this salt was predicted by band structure calculations [3] and experimentally verified by Shubnikov-de Haas (SdH) oscillations [4]. In addition, we studied AMRO in order to get more information about the FS. According to C epas *et al.* [5] it should also be possible to gain information on the interaction between the magnetic and conducting systems from SdH oscillations. To this end we studied the angle dependence of the SdH oscillations in  $\kappa$ -FeCl.

For fields perpendicular to the layers SdH oscillations with two main frequencies  $F_\alpha = 873$  T, originating from the elliptical FS orbit  $\alpha$ , and  $F_\beta = 4280$  T, originating from the magnetic breakdown orbit  $\beta$ , are observed. The cyclotron masses are found to be  $m_\alpha^* = 3.3$  and  $m_\beta^* = 6.0$ , where  $m^* = m_c/m_e$  is the cyclotron mass  $m_c$  in units of the free electron mass  $m_e$ . These values are in good agreement with an earlier report [4].

Figure 1 shows field sweeps at several values of the polar angle  $\theta$  between 20° and 70°. In the inset of Fig. 1 an enlarged part of the  $\theta = 20^\circ$  curve can be seen, where both main frequencies are visible by eye. For higher angles the SdH oscillations become weaker. The  $\beta$  oscillations vanish for  $\theta > 30^\circ$ .

For the  $\alpha$  oscillations a beating behaviour is observed at angles of  $\theta > 48^\circ$ . In Fig. 2, the  $\alpha$  component of the SdH oscillations is shown for several values of  $\theta$ . The arrows indicate the node positions. This beating behaviour can be explained by the presence of an effective exchange field  $B_e$  on the electron spins caused by the exchange interaction with saturated localised  $d$ -electron spins of Fe<sup>2+</sup> in the insulating layers. In such a case the spin damping factor acquires a field dependence modulating the oscillation amplitude:

$$R_s = \cos \left[ 2\pi \frac{gm^*}{4 \cos \theta} \left( \frac{B_e}{B} - 1 \right) \right], \quad (1)$$

where  $g$  is the Land e factor. This equation allows to derive the exchange field from the measured beat frequency. As indicated by the arrows, the node positions monotonically move to lower fields at higher angles, which is in agreement with the assumption of the nodes being

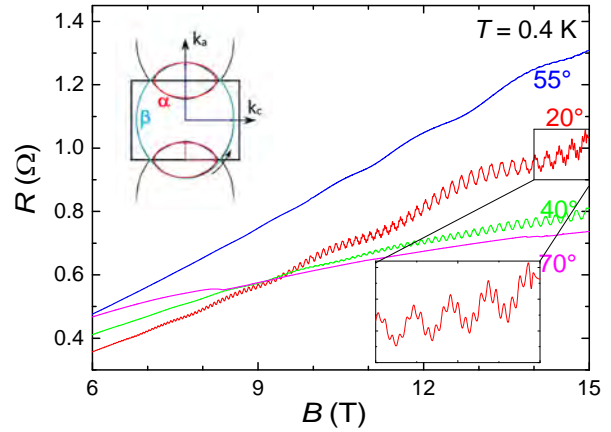


Figure 1: (a) High field magnetoresistance at different polar angles  $\theta$  including the FS with the elliptical orbits  $\alpha$  and  $\beta$ . The inset shows an enlarged excerpt of the  $\theta = 20^\circ$  curve showing  $\alpha$  and  $\beta$ -oscillations.

<sup>1</sup>This work was supported by the German Research Foundation through grant number KA 1652/4-1.

<sup>2</sup>Institute of Problems of Chemical Physics, Chernogolovka, Russia

<sup>3</sup>Faculty of Engineering, University of Toyama, Toyama, Japan

caused by the exchange field with  $B > B_e$  and contradicts, to the best of our knowledge, all other possible explanations for nodes in the SdH oscillations.

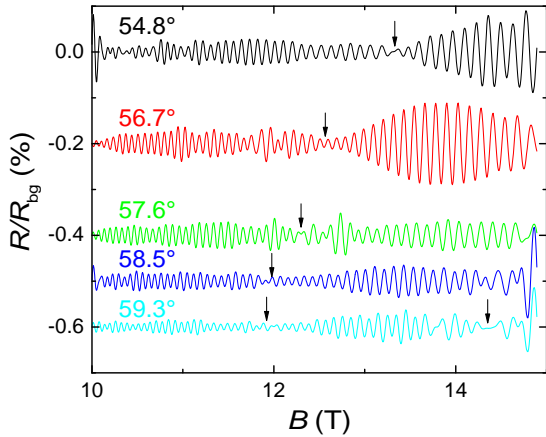


**Figure 2:** The  $\alpha$  component of the SdH oscillations normalised to the background resistance for several values of  $\theta$ . The arrows mark the node positions.

called Lebed magic angle (LMA) resonances, originating from the open FS sheets, which are best seen at intermediate fields (indicated by pink arrows in Fig. 3).

The 2D AMROs allow a construction of the respective FS orbits as shown in the inset of Fig. 3. The resulting orbits can be very well approximated by an elliptical shape and the sizes are in good agreement with the values obtained from the SdH frequencies.

The LMA, however, show a surprising behaviour: While the period behaves exactly as expected, the actual positions of the characteristic resistance dips of the LMA are shifted by half a period with respect to the expected values. We cannot definitely state, what causes the shift. One possible scenario is that there is a relation to the positions of the  $\text{FeCl}_4^-$ -anions, which are shifted by half a period in both  $a$  and  $c$  directions in adjacent layers. A similar anomaly of the LMA was also found in the sister compound  $\kappa$ -(BETS) $_2$ FeBr $_4$  [7].

## References

- [1] M. V. Kartsovnik, *Chem. Rev.* **104**, 5737–5782 (2004).
- [2] M. Kunz, W. Biberacher, N. D. Kushch, A. Miyazaki, and M. V. Kartsovnik, *Phys. Rev. B* **94**, 205104 (2016).
- [3] H. Kobayashi, H. Tomita, T. Naito, A. Kobayashi, F. Sakai, T. Watanabe, and P. Cassoux, *J. Am. Chem. Soc.* **118**, 368–377 (1996).
- [4] N. Harrison, C. H. Mielke, D. G. Rickel, L. K. Montgomery, C. Gerst, and J. D. Thompson, *Phys. Rev. B* **57**, 8751–8754 (1998).
- [5] O. Cépas, R. H. McKenzie, and J. Merino, *Phys. Rev. B* **65**, 100502 (2002).
- [6] T. Mori, and M. Katsuhara, *J. Phys. Soc. Jpn.* **71**, 826–844 (2002).
- [7] L. Schaidhammer. *Magnetotransport studies of the organic superconductor and antiferromagnet  $\kappa$ -(BETS) $_2$ FeBr $_4$* . Masterarbeit, Technische Universität München (2014).

Fitting the node positions with Eq. (1) yields the exchange field  $B_e = (7.4 \pm 0.3) \text{ T}$ , what is in good agreement with the theoretical prediction [6]. One question, however, remains: We have found only the third, fourth and fifth order nodes. The reason for the absence of the lower order nodes, which should be visible at lower angles, is unclear.

In Fig. 3 the angle-dependent magnetoresistance of  $\kappa$ -FeCl at  $T = 1.4 \text{ K}$  is shown for different fields. A Fourier analysis reveals three components of AMRO. The dominant component originates from the closed magnetic-breakdown orbit  $\beta$ . Further, at lower  $B$  we see AMROs associated with the basic elliptic FS orbit  $\alpha$  (indicated by green arrows in Fig. 3) and quasi 1D AMRO,

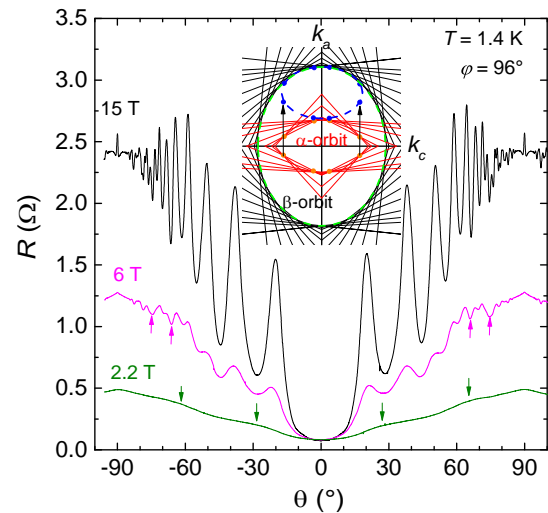


**Figure 3:** Resistance plotted versus  $\theta$  for different fields. Strong AMROs are visible. The inset shows the elliptical FS orbits constructed from the measured AMROs.

# Anisotropic Superconductivity under Hydrostatic Pressure in $\alpha$ -(BEDT-TTF)<sub>2</sub>KHg(SCN)<sub>4</sub>

M. Kunz, W. Biberacher, M.V. Kartsovnik <sup>1</sup>  
H. Müller <sup>2</sup>

The organic charge transfer salt  $\alpha$ -(BEDT-TTF)<sub>2</sub>KHg(SCN)<sub>4</sub> ( $\alpha$ -KHg) is a system of high interest because it shows superconductivity in the vicinity of a charge density wave (CDW) state. At zero pressure, the CDW state sets in below 8 K and coexists with a filamentary superconducting (SC) state at  $T < 0.3$  K [1]. Above a pressure of  $p_c \approx 2.6$  kbar,  $\alpha$ -KHg exhibits a homogeneous SC state with a maximum  $T_c$  of 110 mK [1]. The anisotropy of the SC state in  $\alpha$ -KHg was already extensively studied slightly above the critical pressure [2, 3]. We performed studies of  $\alpha$ -KHg at a pressure of  $p = 4.7$  kbar to see how the SC state behaves far above the critical pressure. We compare the new data with the earlier studies at lower pressures.

For magnetic fields perpendicular to the conducting layers the temperature dependence of the critical field is linear. This was expected, since for this field direction the critical field is limited only by the orbital pair breaking effect. Comparing to the lower pressures, not only the critical temperature but also the slope  $dH_{c2,\perp}/dT$  has decreased, indicating a significant increase of the in-plane coherence length  $\xi_{\parallel,0} = \sqrt{\frac{\Phi_0}{2\pi T_c dB_{c2,\perp}/dT}} = 710$  nm at 4.7 kbar. This is a much higher value than conventionally observed in other organic superconductors.

This value of  $\xi_{\parallel,0}$  is higher than the London penetration depth  $\lambda_L$ , which we estimated as  $\lambda_L = (m_s/\mu_0 n_s q_s^2)^{1/2} \approx 390$  nm, where  $m_s$  is the mass,  $q_s$  the charge and  $n_s$  the density of the SC charge carriers;  $m_s$  and  $n_s$  were estimated from Shubnikov-de Haas oscillations. This raised the question, whether a field-direction-dependent crossover from the type-II to the type-I SC regime occurs in this system for highest pressures. However, no sign of such a crossover could be found. Earlier estimations of the mean free path of this sample [4] yielded a value  $\ell \approx (1.0 \pm 0.5)$   $\mu$ m, which also lies in the same order of magnitude as  $\xi_{\parallel}$  and  $\lambda_L$ , indicating that the system may be not clean enough to observe such a crossover.

In order to trace the in-plane anisotropy of the critical field  $B_{c2,\parallel}(\varphi)$  (angles are defined in Fig. 1(a)), we have done a series of polar angle ( $\theta$ ) sweeps at different  $\varphi$  values, in a magnetic field slightly below  $B_{c2,\parallel}$ . At these conditions the resistance shows a sharp dip around the parallel orientation, as seen in an example sweep in Fig. 1(b). A larger magnitude of the dip  $\Delta R_{\text{dip}}$  can be considered as a signature of a stronger critical field. Using the described method, a significant anisotropy is found. The experiment at  $p = 4.7$  kbar reveals a similar in-plane anisotropy as it was found for the lower overcritical pressures [2, 3]. However, there is a noticeable difference to the behaviour at zero

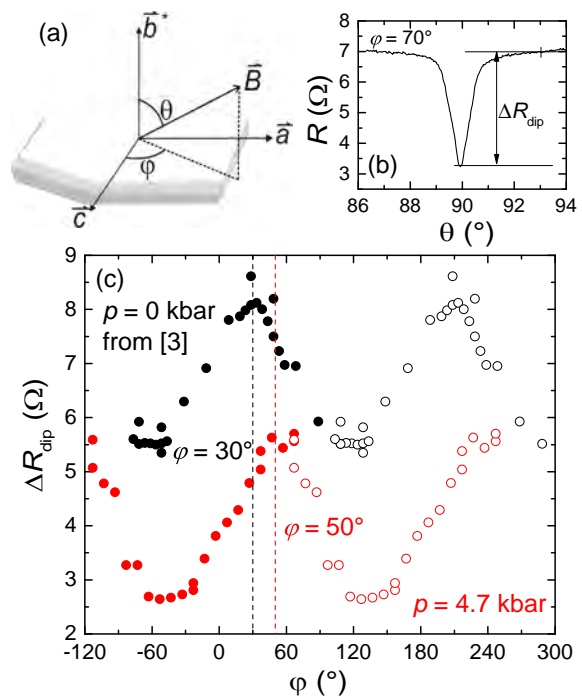


**Figure 1:** (a)  $R(\theta)$  of at  $T = 24$  mK and  $B = 30$  mT. (b) Definition of the angles. (c)  $\varphi$  dependence of the critical field. Explanation of the graph is in the text.

<sup>1</sup>This work was supported by the German Research Foundation through grant number KA 1652/4-1.

<sup>2</sup>European Synchrotron Radiation Facility, 38043 Grenoble, France



pressure, where SC state coexists with the CDW state. This can be seen in Fig. 1(c), where the  $\varphi$ -dependencies for  $p = 0$  kbar and  $p = 4.7$  kbar are shown. The filled points were taken directly from the experiment, while the hollow points are the same data shifted by  $180^\circ$ . As indicated by the vertical dashed lines in Fig. 1(c), the strongest superconductivity (maximum depth of the dip) at  $p = 0$  kbar and  $p = 4.7$  kbar is found at  $30^\circ \pm 5^\circ$  and  $50^\circ \pm 5^\circ$ , respectively. For both pressures this direction of superconductivity seems not to be connected with any special direction of the crystal or the Fermi surface. Together with the twofold symmetry this does not yield us any direct clue, which electron systems or mechanisms might be responsible for the superconductivity in this compound. However, the comparison of the two pressure values shows a  $\sim 20^\circ$  shift of the angle. Having in mind that the Fermi surface reconstruction in the CDW state causes the direction of the 1D Fermi surface sheets to turn by  $\sim 20^\circ$ , this suggests that the SC state is somehow connected with these open sheets.

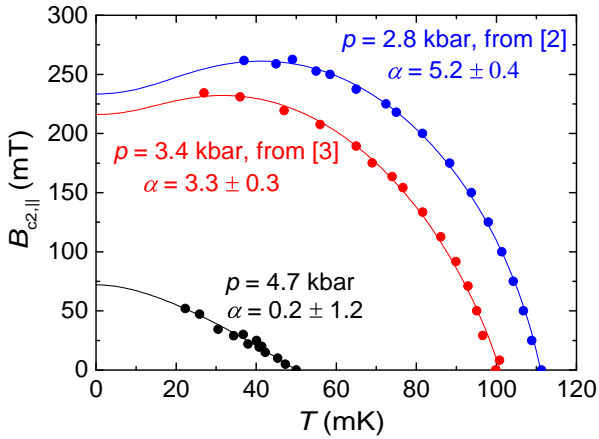


**Figure 2:** SC phase diagram for  $B\parallel ab$ -plane for several pressures at the respective  $\varphi$  with the strongest superconductivity. Solid lines are fits [5] yielding the Maki parameter  $\alpha$ .

tion for the critical field of a type-II superconductor in the dirty limit [5]. Here,  $B_{c2,\parallel}^{\text{orb}}$  and  $B_p$  are the orbital and paramagnetic critical fields, respectively. The resulting fits are shown by the solid lines in Fig. 2 together with the resulting values for  $\alpha$ . The  $\alpha$  values derived for the two lower pressure values should be sufficient for the observation of a Fulde-Ferrell-Larkin-Ovchinnikov (FFLO) phase, which was predicted for very clean superconductors with  $\alpha > 1.8$ . However, our measurements show no evidence of a FFLO state. Possible explanations are that either we did not reach sufficiently low temperatures or our sample is not in the clean limit as already discussed above in the context of a type-I/type-II crossover.

## References

- [1] D. Andres, M. V. Kartsovnik, W. Biberacher, K. Neumaier, E. Schuberth, and H. Müller, *Phys. Rev. B* **72**, 174513 (2005).
- [2] S. Jakob. *Magnetic field effects in the layered organic superconductor  $\alpha$ -(BEDT-TTF) $_2$ KHg(SCN) $_4$* . Diplomarbeit, Technische Universität München (2007).
- [3] M. Kunz. *Magnetoresistance in the normal and superconducting states of the layered organic metal  $\alpha$ -(BEDT-TTF) $_2$ KHg(SCN) $_4$  under pressure*. Diplomarbeit, Technische Universität München (2011).
- [4] M. V. Kartsovnik, D. Andres, S. V. Simonov, W. Biberacher, I. Sheikin, N. D. Kushch, and H. Müller, *Phys. Rev. Lett.* **96**, 166601 (2006).
- [5] D. Saint-James, G. Sarma, and E. J. Thomas. *Type II Superconductivity*, Vol. 17 of *International series of monographs in natural philosophy* (Pergamon Press, Oxford, 1969).



## Absence of Static Magnetic Proximity Effects in the Pt/Y<sub>3</sub>Fe<sub>5</sub>O<sub>12</sub> System

S. Geprägs, S. Meyer, S.T.B. Gönnenwein, M. Opel, R. Gross <sup>1</sup>  
 C. Klewe, T. Kuschel <sup>2</sup>  
 K. Ollefs, F. Wilhelm, A. Rogalev <sup>3</sup>

The thorough understanding of spin transport phenomena across interfaces is of growing importance in the fields of spintronics and spin caloritronics. A common detection scheme for spin currents makes use of the inverse spin Hall effect (SHE) in a non-ferromagnetic metallic electrode [1]. The standard material used in such experiments is Pt due to its large spin Hall angle implying a high detection efficiency. Since Pt is close to the Stoner criterion for ferromagnetism, however, it may show additional Hall or Nernst effects due to proximity magnetism and has therefore generated some controversy regarding the correct interpretation of magnetotransport data [2–4].

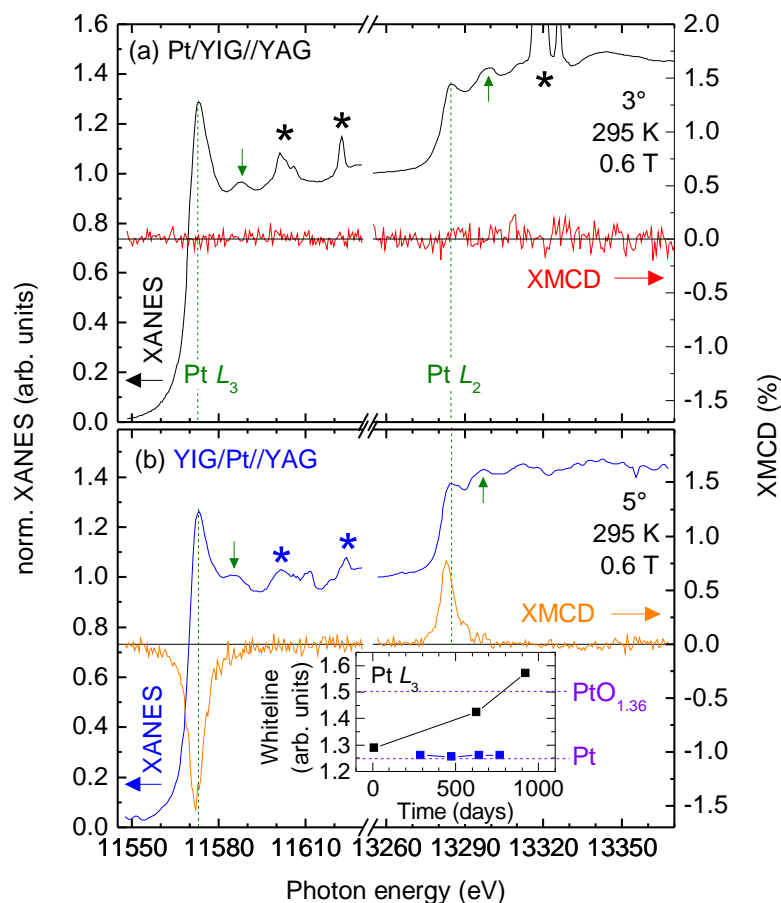


**Figure 1:** Normalized Pt  $L_{2,3}$  edge X-ray absorption near edge spectra (XANES) (black/blue, left axis) and XMCD (red/orange, right axis) spectra measured at 295 K: (a) standard bilayer, (b) inverted bilayer sample. Diffraction peaks are marked by asterisks (\*). Both samples display EXAFS wiggles at 11588 eV and 13300 eV, indicated by olive vertical arrows. The inverted bilayer in (b) shows a pronounced XMCD signal at both absorption edges, compatible with a spin magnetic moment of  $0.037\mu_B/\text{Pt}$  and an orbital magnetic moment of  $0.0065\mu_B/\text{Pt}$ . The inset presents a compilation of the normalized XANES Pt  $L_3$  whiteline intensities from different consecutive measurements as a function of time after thin film deposition for the standard (black) and the inverted bilayer (blue). For comparison, the values for Pt and  $\text{PtO}_{1.36}$  are indicated by dashed horizontal lines.

In a recent Letter [3], Lu *et al.* reported on “ferromagneticlike transport properties” of thin films of Pt, deposited *ex situ* via sputtering on the ferrimagnetic insulator (FMI) Y<sub>3</sub>Fe<sub>5</sub>O<sub>12</sub>. The authors found a magnetoresistance in Pt displaying a hysteresis corresponding to the coercive field of Y<sub>3</sub>Fe<sub>5</sub>O<sub>12</sub>, consistent with our earlier findings [5]. Whereas we interpreted our data in terms of a spin Hall magnetoresistance (SMR) [5], Lu *et al.* attributed their observation to

<sup>1</sup>This work was supported by the European Synchrotron Radiation Facility (ESRF) via HE-3784 and DFG via SPP 1538 (Projects GO 944/4-2, GR 1132/18-2 and KU 3271/1-1).

<sup>2</sup>Center for Spinelectronic Materials and Devices, Department of Physics, Bielefeld University, 33615 Bielefeld, Germany

<sup>3</sup>European Synchrotron Radiation Facility (ESRF), 38043 Grenoble Cedex 9, France

a magnetic proximity magnetoresistance (MPMR) effect [3]. Such static magnetic proximity effects were extensively investigated in the past via X-ray magnetic circular dichroism (XMCD) and have been confirmed for Pt when in contact to ferromagnetic metals (FMM) with a finite spin polarization at the Fermi edge, like Fe, Co, Ni, or  $\text{Ni}_{81}\text{Fe}_{19}$ . The situation is different for Pt on FMIs like  $\text{Y}_3\text{Fe}_5\text{O}_{12}$ , where we could not detect a finite magnetic moment [4]. While XMCD gives only the mean polarization of the Pt film, X-ray resonant magnetic reflectivity (XRMR) is a direct measure of the spin polarization at the interface due to the interference of the reflected light from the Pt surface and the Pt/FMI interface. However, XRMR results did also not indicate proximity magnetism in Pt on FMIs like  $\text{NiFe}_2\text{O}_4$  [6].

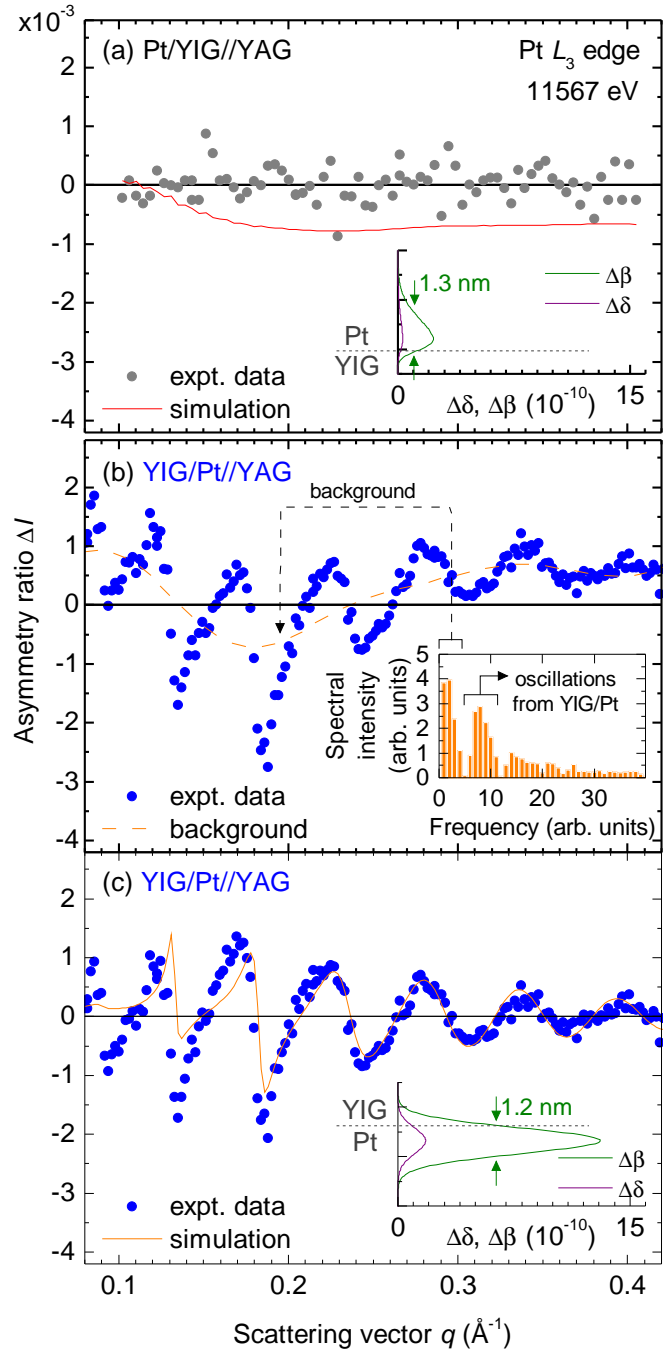


**Figure 2:** XRMR asymmetry ratios  $\Delta I$  at the Pt  $L_3$  edge (black/blue symbols: experimental data, red/orange lines: simulated data). (a) The asymmetry ratio of the standard bilayer does not show any XRMR response. The simulation using the magnetooptic depth profile (inset) gives an upper limit of  $0.002 \mu_B$  per spin-polarized Pt atom. (b) The raw data of the inverted bilayer shows clear oscillations in the asymmetry ratio  $\Delta I$ . A Fourier analysis (inset) identifies two main contributions: oscillations from the YIG/Pt and a background at very low frequencies, which was extracted and back-transformed as the dashed orange line. (c) Asymmetry ratio after subtraction of the background contribution from (b). The simulation using the magnetooptic depth profile (inset) gives a magnetic moment of  $0.008 \mu_B$  per spin-polarized Pt atom at the YIG/Pt interface. For details see [7].

In a joint effort with the Center for Spinelectronic Materials and Devices of the Bielefeld University, we performed a combined XMCD/XRMR investigation in the same samples to unambiguously clarify the controversially discussed issue of proximity magnetism in the Pt/ $\text{Y}_3\text{Fe}_5\text{O}_{12}$  system. We compared bilayer thin film samples with differently arranged layers

and different interface properties, fabricated at WMI. The  $\text{Y}_3\text{Fe}_5\text{O}_{12}$  thin films were deposited by laser-molecular beam epitaxy, the Pt layers were grown via electron-beam evaporation. [4] In contrast to many other reports, we prepared our thin film bilayer samples completely *in situ* without breaking the vacuum and could therefore directly control the interface quality. “Standard” Pt/ $\text{Y}_3\text{Fe}_5\text{O}_{12}$  bilayer samples with sharp and clean interface did not show a magnetic proximity effect of the metallic paramagnetic Pt top electrode, neither in XMCD (Fig. 1(a)) nor in XRMR (Fig. 2(a)). In “inverted”  $\text{Y}_3\text{Fe}_5\text{O}_{12}$ /Pt bilayer samples with a gradual and intermixed interface, however, Pt displayed a magnetic signature comparable to the situation in all-metallic Pt/Fe bilayer thin films. Both XMCD (Fig. 1(b)) and XRMR (Fig. 2(b,c)) provided evidence for a finite spin polarization in Pt [7].

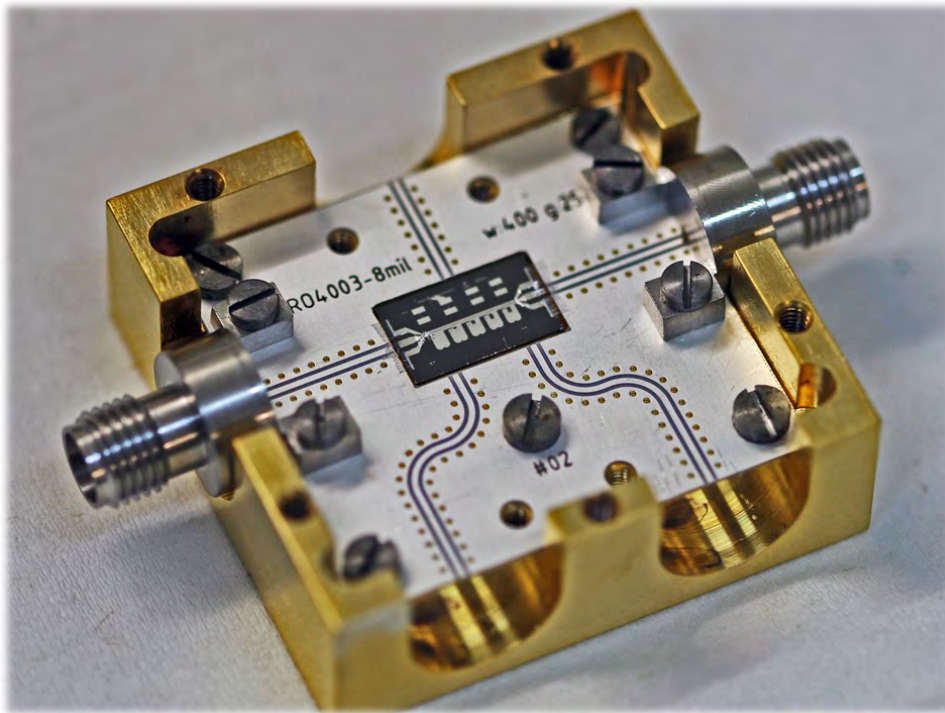
Our data presented here and published earlier [4] unambiguously demonstrate that in bilayer thin film samples the appearance of magnetic proximity effects in paramagnetic metallic Pt on ferrimagnetic insulating  $\text{Y}_3\text{Fe}_5\text{O}_{12}$  crucially depends on the quality of the interface. For rough interfaces with a partial intermixing of the two layers, Pt becomes ferromagnetic. In this case an anisotropic magnetoresistance (AMR) occurs (not shown here) in the angle-resolved magnetotransport, which can be considered a “magnetic proximity magnetoresistance” [3]. In contrast, for sharp and clean interfaces the induced magnetic moment of Pt is negligible [4]. In this case we do not find any indication for proximity magnetism even in ultrathin Pt layers ( $t_{\text{Pt}} < 2$  nm). Simultaneously, the angle-resolved magnetotransport does not show any AMR contribution, but is instead fully consisted with the SMR model [5].

## References

- [1] E. Saitoh, M. Ueda, H. Miyajima, and G. Tatara, *Applied Physics Letters* **88** (2006).
- [2] S. Y. Huang, X. Fan, D. Qu, Y. P. Chen, W. G. Wang, J. Wu, T. Y. Chen, J. Q. Xiao, and C. L. Chien, *Phys. Rev. Lett.* **109**, 107204 (2012).
- [3] Y. M. Lu, Y. Choi, C. M. Ortega, X. M. Cheng, J. W. Cai, S. Y. Huang, L. Sun, and C. L. Chien, *Phys. Rev. Lett.* **110**, 147207 (2013).
- [4] S. Geprägs, S. Meyer, S. Altmannshofer, M. Opel, F. Wilhelm, A. Rogalev, R. Gross, and S. T. B. Goennenwein, *Applied Physics Letters* **101**, 262407 (2012).
- [5] H. Nakayama, M. Althammer, Y.-T. Chen, K. Uchida, Y. Kajiwara, D. Kikuchi, T. Ohtani, S. Geprägs, M. Opel, S. Takahashi, R. Gross, G. E. W. Bauer, S. T. B. Goennenwein, and E. Saitoh, *Phys. Rev. Lett.* **110**, 206601 (2013).
- [6] T. Kuschel, C. Klewe, J.-M. Schmalhorst, F. Bertram, O. Kuschel, T. Schemme, J. Wollschläger, S. Francoual, J. Stempfer, A. Gupta, M. Meinert, G. Götz, D. Meier, and G. Reiss, *Phys. Rev. Lett.* **115**, 097401 (2015).
- [7] C. Klewe. *Static and non-equilibrium magnetic proximity effects in Pt/NiFe<sub>2</sub>O<sub>4</sub> and Pt/Ni<sub>1-x</sub>Fe<sub>x</sub> heterostructures*. Ph.D. thesis (2016).



# Application-Oriented Research



Sample box with printed circuit board and superconducting quantum circuit chip.





## Flux-driven Non-degenerate Josephson Parametric Amplifiers: Hysteretic Flux Response and Gain Measurements

*S. Pogorzalek, K. G. Fedorov, J. Goetz, F. Wulschner, M. Fischer, P. Eder, E. Xie, A. Marx, F. Deppe, R. Gross*<sup>1</sup>

Josephson parametric amplifiers (JPA) have become key devices in quantum science and technology with superconducting circuits. In particular, they can be utilized as quantum-limited amplifiers or as a source of squeezed microwave fields. A particularly prominent application of the latter is the generation of entanglement in the form of two-mode squeezed propagating microwave states [1] as required for many quantum communication and quantum teleportation protocols with continuous variables [2].

We investigate flux-driven JPAs [3] consisting of a quarter-wavelength coplanar waveguide resonator which is short-circuited to ground by a dc-SQUID. The dc-SQUID provides a flux-tunable non-linear inductance which contributes to the quasi-static resonant frequency  $\omega_0$  of the JPA. Thus, an applied magnetic flux can be used to tune the dc-SQUID inductance and, in this way, the resonant frequency of the whole circuit. The dependence of  $\omega_0$  on the external magnetic flux  $\Phi_{\text{ext}}$  is strongly influenced by the dimensionless screening parameter  $\beta_L \equiv 2L_{\text{loop}}I_c/\Phi_0$ , as presented in more detail in Ref. [4]. In general, the dependence on the external magnetic flux is nontrivial and has to be calculated numerically. This is achieved by considering a steady state phase particle in the dc-SQUID potential with either increasing or decreasing  $\Phi_{\text{ext}}$ .

Figure 1(b) shows the flux-dependent JPA resonant frequency of a strongly hysteretic JPA together with numerical fits. The flux dependence is described very well by the model calculations. The hysteresis over a large frequency window is explained by a large screening parameter  $\beta_L = 0.55$ . With increasing  $\beta_L$ , the rigid coupling between the two phase differences across the junctions of the dc-SQUID is lost, allowing for multiple classes of minimal energy states of the dc-SQUID for a given external flux.

Furthermore, an on-chip antenna couples inductively to the dc-SQUID loop with inductance  $L_{\text{loop}}$ , and can be used to apply a strong coherent pump tone with a frequency  $\omega_{\text{pump}} = 2\omega_0$ . This leads to parametric amplification. Here, we report on the non-degenerate gain of two

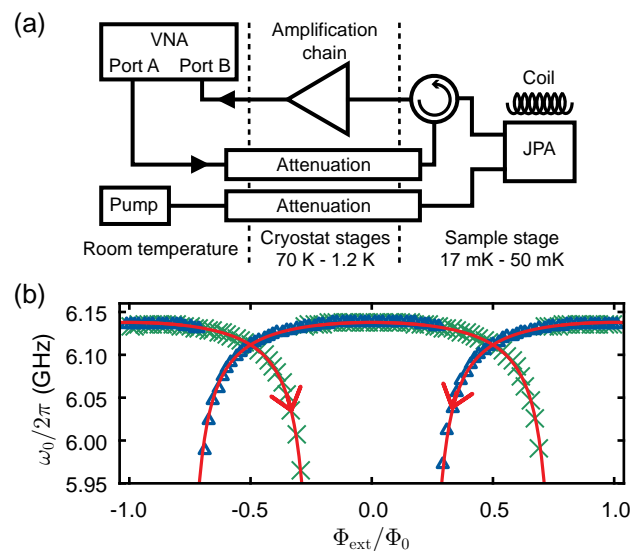


**Figure 1:** (a) Setup for the characterization of JPAs with a VNA. The reflected signal from the JPA is separated from the input signal by a measurement circulator. The current through a superconducting coil determines the dc-flux through the dc-SQUID loop. (b) JPA resonant frequency  $\omega_0$  as a function of the applied flux  $\Phi_{\text{ext}}$  (symbols) as well as numerical fits (red lines). Green crosses and blue triangles mark the data taken for increasing and decreasing  $\Phi_{\text{ext}}$ , respectively, with arrows further indicating the sweep direction. The JPA temperature is stabilized at 30 mK.

<sup>1</sup>We acknowledge support from DFG through project FE 1564/1-1, the doctorate program ExQM of the Elite Network of Bavaria, the IMPRS ‘Quantum Science and Technology’, and the German Excellence Initiative via the ‘Nanosystems Initiative Munich’ (NIM). We also acknowledge the fruitful collaboration with K. Inomata, T. Yamamoto and Y. Nakamura.

JPAs, where one JPA has an overcoupled and the other an undercoupled behavior. To this end, a certain flux value  $\Phi_{\text{ext}}$  corresponding to a certain resonant frequency  $\omega_0$  of the JPA is fixed. Then, a pump tone with frequency  $\omega_{\text{pump}} = 2\omega_0$  is applied to the JPA.

The experimentally obtained spectrum of the signal mode as a function of the pump power for the overcoupled JPA is depicted in Fig. 2(a). Amplification can only be observed within a frequency window defined by the resonator bandwidth and centered at the resonant frequency. However, for the undercoupled JPA [see Fig. 2(d)], the incident signal is deamplified by up to  $-30$  dB. We find very good agreement of our measurements with theoretical fits from explicit expressions for the non-degenerate signal and idler gain of a flux-driven JPA [see Eq. (8) in Ref. [4] for the detailed expressions]. Only the coupling constant between the pump amplitude at the microwave source and the modulation of the JPA resonant frequency  $\epsilon$  is used as a free fitting parameter, while the quality factors and the resonant frequency are fixed to independently determined experimental values.

In summary, we have developed an efficient approach to describe both the hysteretic and non-hysteretic dependence of the resonant frequency  $\omega_0$  of flux-driven JPAs on the applied magnetic flux. Additionally, we have observed that the gain of non-degenerate JPAs with different resonator characteristics shows a distinct behavior which is accurately reproduced by model calculations based on a simple and explicit formalism for the flux-driven JPA. For undercoupled devices, the device is no longer an amplifier but acts as a tunable microwave attenuator.

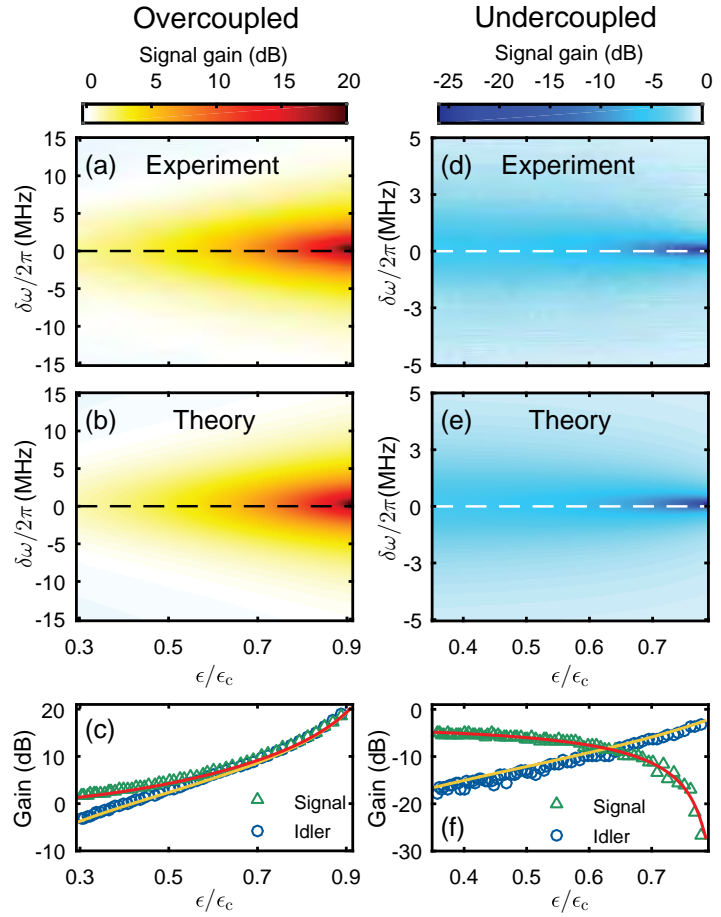


**Figure 2:** (a,d) Experimental spectra of the non-degenerate signal gains as a function of  $\epsilon/\epsilon_c$  and signal detuning  $\delta\omega$  from half the pump frequency.  $\epsilon_c$  is a critical modulation of  $\omega_0$ . (b,e) Theoretical calculations of the signal spectra. (c,f) Signal and idler gains as a function of  $\epsilon/\epsilon_c$  along the black and white dashed lines. The symbols mark the experimental data and solid lines are fits to the data. The JPAs are stabilized to 50 mK and 30 mK, respectively.

## References

- [1] K. G. Fedorov, L. Zhong, S. Pogorzalek, P. Eder, M. Fischer, J. Goetz, E. Xie, F. Wulschner, K. Inomata, T. Yamamoto, Y. Nakamura, R. Di Candia, U. Las Heras, M. Sanz, E. Solano, E. P. Menzel, F. Deppe, A. Marx, and R. Gross, *Phys. Rev. Lett.* **117**, 020502 (2016).
- [2] R. Di Candia, K. G. Fedorov, L. Zhong, S. Felicetti, E. P. Menzel, M. Sanz, F. Deppe, A. Marx, R. Gross, and E. Solano, *EPJ Quan. Tech.* **2**, 25 (2015).
- [3] T. Yamamoto, K. Inomata, M. Watanabe, K. Matsuba, T. Miyazaki, W. D. Oliver, Y. Nakamura, and J. S. Tsai, *Appl. Phys. Lett.* **93**, 042510 (2008).
- [4] S. Pogorzalek, K. G. Fedorov, L. Zhong, J. Goetz, F. Wulschner, M. Fischer, P. Eder, E. Xie, K. Inomata, T. Yamamoto, Y. Nakamura, A. Marx, F. Deppe, and R. Gross (2016). [arXiv:1609.09041](https://arxiv.org/abs/1609.09041).

## Characterization of Tunable Resonators for Quantum Simulation

*M. Fischer, C. Besson, P. Eder, J. Goetz, S. Pogorzalek, F. Wulschner, E. Xie, K. Fedorov, F. Deppe, A. Marx, R. Gross*<sup>1</sup>

Quantum simulation is believed to be an important tool to investigate the quantum mechanical behaviour of systems, which are too complex to be handled analytically [1]. One such system, where quantum simulation is beneficial, consists of interacting bosons in a lattice. The system has already been studied by performing quantum simulations on different platforms, e.g., using cold atoms. However, the implementation of such a simulation in the realm of circuit quantum electrodynamics (QED) promises access to the driven dissipative regime. Here, the loss of particles in the lattice can be compensated by an external microwave drive which creates new particles inside the lattice. In a circuit QED environment, we can create a 1D lattice for photons using series-connected, capacitively coupled coplanar waveguide resonators. The resonators can each be individually driven by an external microwave source through a capacitively coupled transmission line. To achieve interaction between the photons, we introduce a nonlinearity in the form of galvanically coupled SQUIDs, placed in the current maximum of each resonator [Fig. 1(a)] [2]. The nonlinearity can be tuned by external coils and on-chip antennas. This driven system is described by a Bose-Hubbard-like Hamiltonian  $H_{\text{HB}}$

$$H_{\text{HB}} = \Delta \sum_{j=1}^N a_j^\dagger a_j - J \sum_{j=1}^{N-1} (a_j^\dagger a_{j+1} + a_j a_{j+1}^\dagger) + \frac{U}{2} \sum_{j=1}^N a_j^\dagger a_j (a_j^\dagger a_j - 1) + \sum_{j=1}^N \left( \frac{\Omega_j}{2} a_j^\dagger + \frac{\Omega_j^*}{2} a_j \right), \quad (1)$$

where  $a_j$  ( $a_j^\dagger$ ) is the annihilation (creation) operator of a photon at the  $j^{\text{th}}$  resonator,  $J$  is the coupling rate between two neighbouring resonators,  $U$  is the nonlinearity of the resonators,  $\Delta$  is the detuning between the resonant frequency and drive and  $\Omega_j$  the Rabi frequency of the microwave drive.

As a first step towards longer chains or 2D lattices, which are more challenging experimentally, we examine a system consisting of two resonators with a single drive. Here, we are still able to calculate the behaviour analytically in the regime of small excitation numbers. We calculate the second order correlation functions  $g^{(2)}(0)$  of the microwave field inside each resonator and

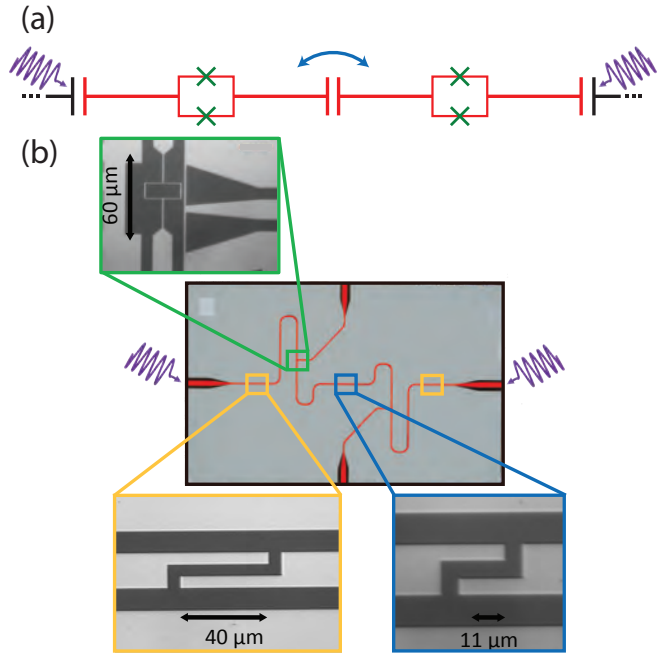


**Figure 1:** (a) Sketch of a series of tunable nonlinear (green) resonators (red) with coupling (blue) and drive (purple). (b) False color micrographs of the sample with blow ups of key areas of the chip.

<sup>1</sup>We acknowledge support from DFG through project FE 1564/1-1, the doctorate program ExQM of the Elite Network of Bavaria, the IMPRS ‘Quantum Science and Technology’, and the German Excellence Initiative via the ‘Nanosystems Initiative Munich’ (NIM).

the cross-correlation  $\text{cross-}g^{(2)}(0)$  between the fields of the two resonators. We find regimes, where the second-order correlation function of the field in one resonator is smaller than one, which means the field is antibunched. At the same time, the cross-correlation between the two resonators shows bunching ( $\text{cross-}g^{(2)}(0) > 1$ ).

By adjusting the nonlinearity and the Rabi frequency of the microwave drive, we can switch this behaviour to the opposite case, where the field inside one resonator is bunched, but there is antibunching between the two resonator fields. Fig. 2 shows a map of the different regimes in the  $U - \Omega$  space calculated for the experimentally accessible parameter range of  $J = 10$  MHz and  $\Delta = -1$  MHz.

In order to experimentally validate the expected behaviour, we fabricate superconducting quantum circuits as shown in Fig. 1(b) by e-beam lithography and aluminium shadow evaporation on a  $500 \mu\text{m}$  thick silicon substrate. The Josephson junctions are Al/AIO<sub>x</sub>/Al contacts. The resonators are capacitively coupled to each other and to outside control lines by finger capacitors.

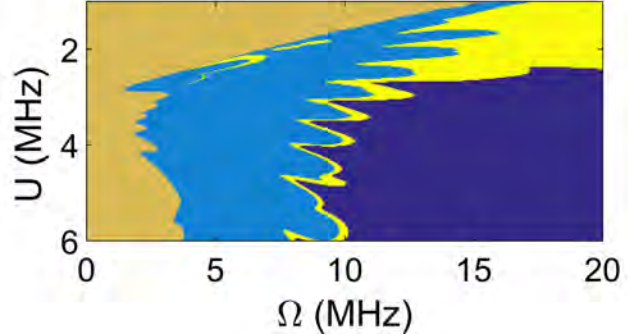


**Figure 2:** Map of different regimes of the second order correlation functions dependent on the nonlinearity  $U$  and the Rabi frequency  $\Omega$  of a drive at one resonator. Light blue:  $g^{(2)}(0) > 1$  (bunched) and  $\text{cross-}g^{(2)}(0) > 1$  (bunched), dark blue:  $g^{(2)}(0) < 1$  (antibunched) and  $\text{cross-}g^{(2)}(0) < 1$  (antibunched), ocher:  $g^{(2)}(0) < 1$  (antibunched) and  $\text{cross-}g^{(2)}(0) > 1$  (bunched), yellow:  $g^{(2)}(0) > 1$  (bunched) and  $\text{cross-}g^{(2)}(0) < 1$  (antibunched).

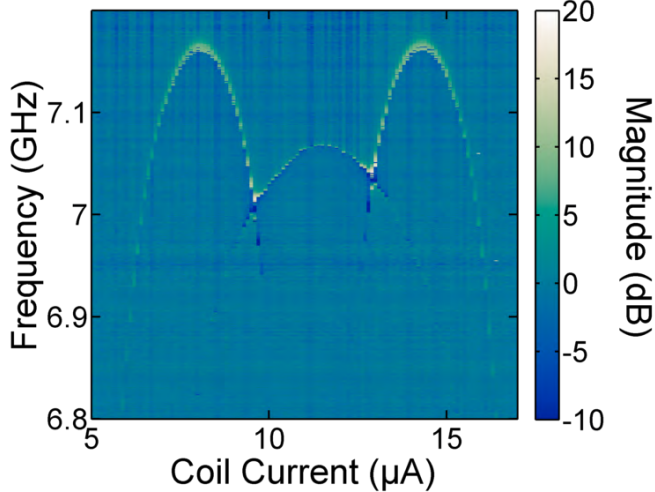


**Figure 3:** Calibrated transmission magnitude through the resonators showing the dependence of their resonance frequency on the current through the coil.

In preliminary experiments we measured the dependence of the resonant frequency of the two resonators on the external flux which is applied with a superconducting coil (Fig. 3). Even though the resonators show different maximal frequencies and different flux periodicity, we can tune the resonators into resonance and observe the expected anti-crossing of the resonator modes. Further experiments will determine the exact parameters of the system, but first estimations show that the coupling strength  $J$ , the tunability of the resonance frequency and, in turn, the nonlinearity  $U$  should be close enough to the design values in order to reach the regimes shown in Fig. 2. The next step

towards the simulation of the Bose-Hubbard Hamiltonian will be to implement an experimental setup for the measurement of the second order correlation functions of the resonator fields.

## References

- [1] A. A. Houck, H. E. Türeci, and J. Koch, *Nat. Phys.* **8**, 292–299 (2012).
- [2] M. Leib, F. Deppe, A. Marx, R. Gross, and M. J. Hartmann, *New J. Phys.* **14**, 75024 (2012).



## On-chip Environments Characterized with a Superconducting Qubit

*P. Eder, F. Deppe, M. Fischer, J. Goetz, S. Pogorzalek, K. F. Wulschner, E. Xie, K. G. Fedorov, A. Marx, R. Gross*<sup>1</sup>

Microwave beam splitters, interferometer and qubits are important components in circuit quantum electrodynamics (QED) [1, 2]. By positioning a transmon qubit in one arm of a Michelson interferometer, we implement a highly sensitive spectroscopic measurement of a transmon qubit placed in a controlled on-chip electromagnetic environment (see Fig 1).

We implement the whole circuit by standard WMI technology [3–6] using optical and e-beam lithography on an SiO<sub>2</sub>-coated silicon chip. The interferometer shown in Fig. 2(a) is made from sputter-deposited Nb and the transmon qubit is realized by aluminum shadow evaporation. Since the beam splitters have a significant bandwidth, they must be interpreted in terms of a continuous bath rather than a single-mode resonant environment. Here, we present first results on the spectroscopic characterization of the system. By comparing the measured microwave transmission with predictions based on a model calculations, we generally find good agreement. The observed small deviations between experiment and model calculations assuming an ideal interferometer environment provide insight into the residual environment formed by the substrate and/or spurious electromagnetic modes. In order to analyze our data, we adapt the spin-boson model [7, 8] to the case of a transmon qubit in an ideal Michelson interferometer. In this way, we obtain a transfer matrix description for the coupled qubit-interferometer system in absence of any residual environment due to spurious electromagnetic modes [9, 10].

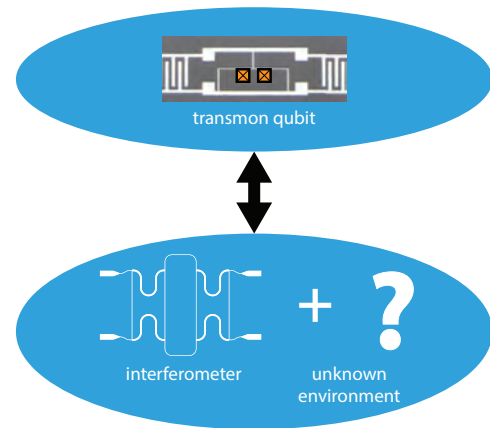


**Figure 1:** Basic idea of the experiment. A transmon qubit is placed in one arm of a Michelson interferometer. The latter can be straightforwardly modelled as a model electromagnetic environment. The transmon qubit sees this ideal model environment together with some unknown residual environment due to spurious electromagnetic modes.

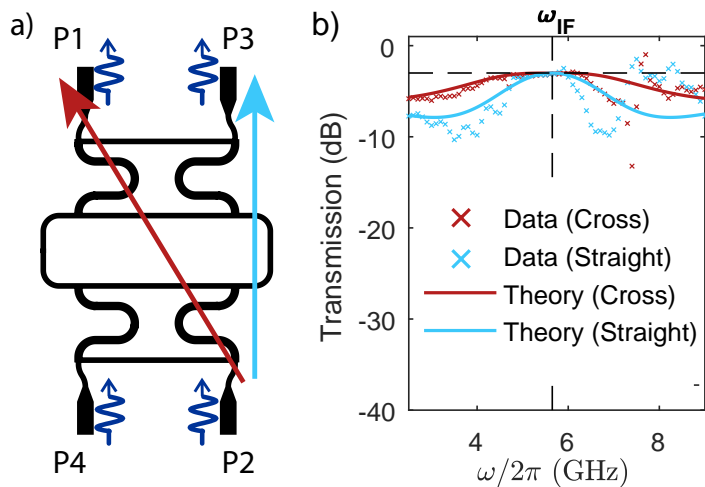


**Figure 2:** a) Chip-layout of the interferometer. P1–P4 denote the interferometer ports. b) Transmission amplitude plotted versus frequency obtained from model calculations and from measurements on an interferometer without transmon qubit. Here,  $\omega_{IF}$  is the center frequency of the interferometer.

<sup>1</sup>We acknowledge support from DFG through project FE 1564/1-1, the doctorate program ExQM of the Elite Network of Bavaria, the IMPRS ‘Quantum Science and Technology’, and the German Excellence Initiative via the ‘Nanosystems Initiative Munich’ (NIM). We also thank Edwin Menzel for his support in sample fabrication and setting up the experiment, and J.J. Garcia-Ripoll and T. Ramos for fruitful discussions.

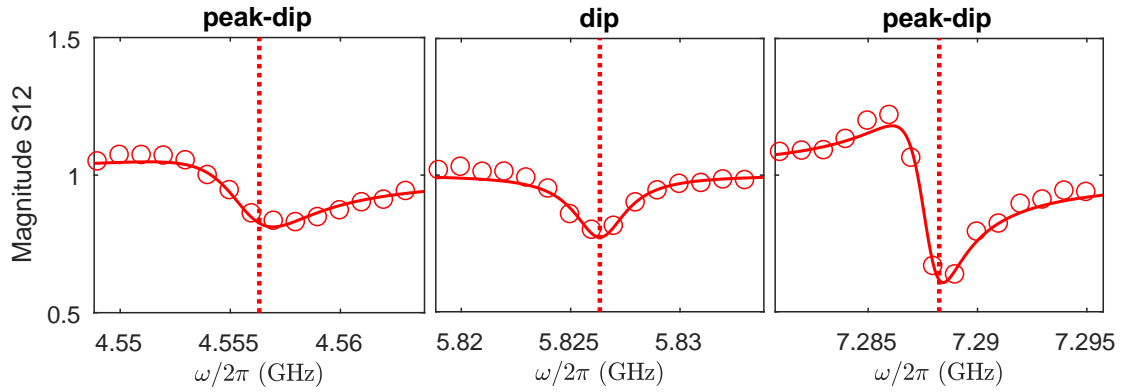


**Figure 3:** Coupled interferometer-transmon qubit system. The transmission magnitude  $S_{12}$  (see Fig. 2 for the port configuration)) is plotted as a function of frequency near the qubit resonance frequency for three different values of  $\omega_{qb}$  marked by the dotted vertical lines. The effect of transmon qubit appears in the transmission as peak-dip or dip feature, depending on the frequency. The symbols show experimental data, the lines are model fits.

In a first step, we analyze the interferometer without the transmon qubit. We find that the model calculations can well describes the measured interferometer transmission (see Fig. 2). Next, we investigate the coupled interferometer-transmon qubit system. Figure 3 shows that the measured transmission magnitude shows Fano-type resonant features [11] of two different types: (i) peak-dip and (ii) dip features. Except for very few points of the accessible frequency range (4 – 9.5 GHz), the experimental data can be well fitted by model calculations based on a transfer matrix element approach. The relevant fitting parameters in the model calculations are the qubit frequency  $\omega_{qb}$ , as well as the relaxation rate  $\Gamma_1$  and the dephasing rate  $\Gamma_\phi$  of the qubit. The derived relaxation and dephasing rates as a function of  $\omega_{qb}$  follow the expected behavior over a wide frequency redime (data not shown). Only for qubit frequencies above 7.2 GHz,  $\Gamma_1$  and  $\Gamma_\phi$  show significant deviations from the model expectation. This suggests that this region is dominated by the unknown residual environment, e.g., due to spurious electromagnetic modes.

The thorough investigation of coupled interferometer-transmon qubit system is the basis for further experiments with similar sample layouts, heading towards controlled phase gates in all microwave quantum computing and two-photon scattering matrix analysis.

## References

- [1] J. Goetz, F. Deppe, P. Eder, M. Fischer, M. Müting, J. P. Martínez, S. Pogorzalek, F. Wulschner, E. Xie, K. G. Fedorov, A. Marx, and R. Gross (2016). [arXiv:1609.07351](#).
- [2] J. Goetz, S. Pogorzalek, F. Deppe, K. G. Fedorov, P. Eder, M. Fischer, F. Wulschner, E. Xie, A. Marx, and R. Gross (2016). [arXiv:1609.07353](#).
- [3] F. Loacker. *Design and characterization of a superconducting beam-splitter for quantum information processing*. Master thesis, Walther-Meißner-Institut (2013).
- [4] M. Fischer. *On-chip Superconducting Microwave Interferometer*. Master thesis, Walther-Meißner-Institut (2014).
- [5] C. Schneider. *On-chip Superconducting Microwave Beam Splitter*. Master thesis, Walther-Meißner-Institut (2014).
- [6] J. P. Martinez. *Circuit quantum electrodynamics with transmon qubits*. Master thesis, Walther-Meißner-Institut (2015).
- [7] A. J. Leggett, S. Chakravarty, A. T. Dorsey, M. P. A. Fisher, A. Garg, and W. Zwerger, *Rev. Mod. Phys.* **59**, 1–85 (1987).
- [8] M. Haeberlein, F. Deppe, A. Kurcz, J. Goetz, A. Baust, P. Eder, K. Fedorov, M. Fischer, E. P. Menzel, M. J. Schwarz, F. Wulschner, E. Xie, L. Zhong, E. Solano, A. Marx, J. J. Garcia-Ripoll, and R. Gross (2015). [arXiv:1506.09114](#).
- [9] D. M. Pozar. *Microwave Engineering* (John Wiley & Sons Inc., New York, 2005).
- [10] O. Astafiev, A. M. Zagoskin, A. A. Abdumalikov, Y. A. Pashkin, T. Yamamoto, K. Inomata, Y. Nakamura, and J. S. Tsai, *Science* **327**, 840–843 (2010).
- [11] U. Fano, *Phys. Rev.* **124**, 1866–1878 (1961).



## A Scalable 3D Quantum Memory

*E. Xie, F. Deppe, D. Repp, P. Eder, M. Fischer, J. Goetz, F. Wulschner, K. G. Fedorov, A. Marx, R. Gross*<sup>1</sup>

Quantum information processing with superconducting qubits is a promising approach to a future quantum computer. Apart from information processing, an important issue is the storage of the processed quantum information. Storing and retrieving information in the quantum regime proves to be difficult due to the fragility of quantum information. Moreover, a quantum memory has to be scalable in order to be implemented in future applications with a large number of qubits and memory cells.

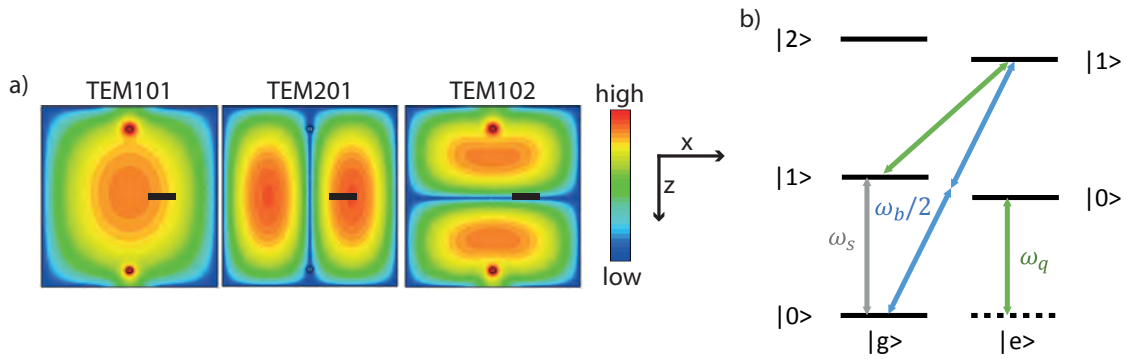


**Figure 1:** (a) Color-coded representation of the electric field intensity of the first three cavity modes. The qubit chip position is schematically marked with a black rectangle. The antenna positions are marked with a small circle. The coupling of the qubit to the TEM<sub>102</sub> mode is small in comparison with its coupling to the readout (TEM<sub>101</sub>) and storage (TEM<sub>201</sub>) modes. (b) Level scheme of the qubit coupled to the storage mode. The qubit transition frequency (green), the storage mode frequency (grey) and the blue sideband transition frequency (blue) are shown.

In this report, we introduce a scalable quantum memory architecture based on a 3D superconducting cavity and a transmon qubit. The cavity and qubit parameters are summarized in Tab. 1. From the multimode structure of the cavity, we use two distinct modes: an undercoupled, highly coherent one as the storage mode and an overcoupled one as the readout mode [cf. Fig. 1a)]. A transmon qubit is placed in the resonator in such a way that it couples to both modes with equal coupling strength. Hence, no additional readout resonator is necessary, which results in a much more compact system compared to conventional 3D circuit QED systems and gives more flexibility in scaling up.

	$\omega_q/2\pi$ (GHz)	$E_C/2\pi$ (MHz)	$E_J/E_C$	$\alpha_{\text{rel}}$
qubit	7.602	186	206	2.5%
	$\omega_{r/s}/2\pi$ (GHz)	$Q_{r/s}$	$g_{r/s}/2\pi$ (MHz)	$\Delta_{r/s}/2\pi$ (GHz)
readout mode	5.604	2000	62.3	1.944
storage mode	8.904	$8.47 \cdot 10^4$	63.8	1.356

**Table 1:** Characteristic parameters of the transmon qubit, the readout and the storage mode.  $E_C$  is the transmon charging energy,  $E_J$  the Josephson energy,  $\alpha_{\text{rel}}$  the relative anharmonicity of the transmon,  $\Delta_{r/s}$  the detuning between the transmon frequency and the corresponding cavity mode, and  $Q_{r/s}$  the quality factor of the respective mode.

The level scheme of the storage mode and the qubit is shown in Fig. 1b). By using a second-order process, we are able to transfer an excitation from the qubit into the storage mode.

<sup>1</sup>We acknowledge support from DFG through project FE 1564/1-1, the doctorate program ExQM of the Elite Network of Bavaria, the IMPRS ‘Quantum Science and Technology’, and the German Excellence Initiative via the ‘Nanosystems Initiative Munich’ (NIM).

We start in the ground state of the qubit and with no photons in the cavity ( $|g0\rangle$ ). For a storage operation, we first drive the blue sideband transition with a  $\pi$ -pulse. Because of selection rules, we use a two-photon drive at half the blue sideband frequency  $(\omega_q + \omega_s)/2$ . Subsequently, we drive the system from  $|e1\rangle$  to  $|g1\rangle$  by a  $\pi$ -pulse on the qubit. State retrieval is done with the reverse process, followed by a measurement of the qubit state. If the qubit then is in  $|g\rangle$ , the excitation has not decayed while being in the storage mode.

The experiment is carried out at mK temperatures in a custom-made wet dilution refrigerator [1]. For the sample characterization in the time domain, we use a setup similar to that of Ref. 2. Moreover, an automatic put in tune procedure has been implemented, which automatically searches for the correct  $\omega_b$  and the  $\pi$ -pulse lengths in order to gain a higher setup stability.

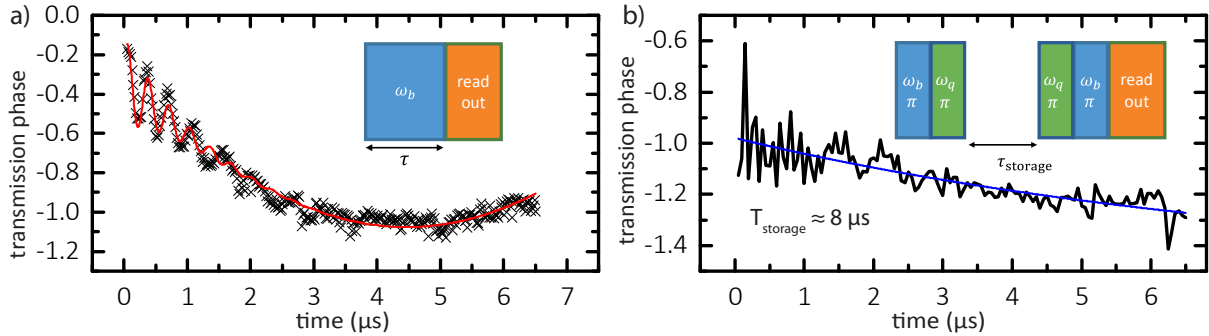


**Figure 2:** a) Rabi oscillations on the blue sideband. The inset shows the pulsing scheme. The red line is a fit to the data (black crosses). (b) Quantum memory storage time. The inset shows the full protocol. The blue line is an exponential function fit to the data (black line).

In Fig. 2(a), Rabi oscillations on the blue sideband are shown. On a timescale of several microseconds, a collapse and revival feature is visible in our data. Most likely, this behavior can be explained by taking the  $|f\rangle$  state of the transmon qubit into account, which is potentially populated during the high-power blue sideband drive pulse due to the qubit's low anharmonicity. Still, further investigation is necessary at this point. For the quantum memory protocol, only the first period of the Rabi oscillations is of interest in order to determine the  $\pi$ -pulse length.

We characterize the memory by the decay time  $T_{\text{storage}}$  of the  $|g1\rangle$  state [cf. Fig.2b)]. Until now, the exponential decay is still superposed by oscillations with frequencies of 1.54 MHz and 7.54 MHz. Again, this is presumably due to the low anharmonicity of the transmon, and a similar explanation as for the blue sideband Rabi oscillation data can be given. Nevertheless, the decay time  $T_{\text{storage}}$  is approximately  $8\ \mu\text{s}$  exceeding the pure qubit lifetime by a factor of three. In our experiment,  $T_{\text{storage}}$  reaches almost the limit of the mode photon lifetime, which is  $10\ \mu\text{s}$  in our case. In order to increase the pure mode photon lifetime, the cavity antennas can be placed more carefully into the node of the mode, leading to a smaller photon loss rate caused by external coupling.

In summary, we have implemented a scalable 3D quantum memory. We find that the memory lifetime is close to the lifetime of the storage mode. In the future, we plan to use optimal control pulses to further optimize the protocol.

## References

- [1] J. Goetz, F. Wulschner, J. Höß, K. Neumaier, C. Probst, F. Deppe, A. Marx, and R. Gross, *WMI Ann. Rep.* **2013**, 75–76 (2013).
- [2] J. Goetz, M. Müting, F. Deppe, A. Marx, and R. Gross, *WMI Ann. Rep.* **2015**, 47–48 (2015).

## Circuit Electromechanics with Aluminium Nanobeams

*M. Pernpeintner, P. Schmidt, D. Schwienbacher, R. Gross, H. Huebl*<sup>1</sup>

Circuit electromechanics explores the photon-phonon interaction of a mechanical resonator and a microwave (MW) circuit. Such hybrid systems are a promising platform for quantum experiments, enabling, e.g., the preparation and transfer of non-classical states [1, 2]. At the WMI, we investigate tensile stressed nanobeam resonators integrated into a superconducting MW circuit. This allowed us to demonstrate optomechanical features in the MW domain [3] and study material parameters of the nanobeam [4]. While in those experiments a silicon nitride nanobeam covered with a niobium thin film was employed, we here pursue an alternative approach based on a pure aluminum nanobeam integrated in an aluminium microwave resonator. This scheme reduces the number of sample fabrication steps and allows for the integration of a standard aluminium transmon qubit serving e.g. as a single photon source or a cavity photon detector. In particular, the direct coupling of a nanobeam to a transmon qubit would open the path to a new class of experiments, as proposed in Ref. [5]. Besides, aluminium-based nano-electromechanical systems are one approach to achieve higher coupling strengths, using for instance focused ion beam milling as a fabrication technique to produce ultra-narrow gaps between the nanobeam and the adjacent ground plane [6].

Figure 1 shows a chip with a superconducting Al microwave resonator into which an Al nanobeam has been integrated. The fabrication process involves two steps of e-beam lithography as well as e-beam evaporation, lift-off and reactive ion etching. After the initial deposition of the Al layer, we use an annealing step to generate a tensile stress in the Al film. Following the final cleaning procedure, the sample is dried in a critical point dryer. This prevents adhesion of the nanobeam to the adjacent Al ground plane caused by strong capillary forces present during the evaporation of the solvent.

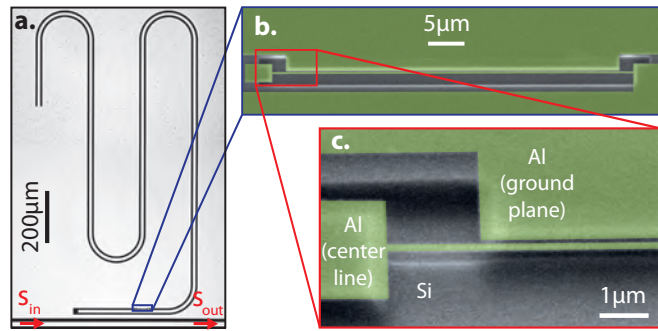


**Figure 1:** **a.** Micrograph of the MW resonator into which a nanomechanical beam has been integrated. **b-c.** False-colored SEM image of the nanobeam, including its clamping pads and the adjacent aluminium ground plane.

The nanobeam is capacitively coupled to the MW resonator, i.e. a displacement of the nanobeam modifies the capacity between the MW resonator's centerline and the ground plane and thus changes its resonance frequency  $\omega_c$ . An oscillation of the nanobeam therefore modulates  $\omega_c$  and leads to the observation of side-bands in a homodyne detection setup (see Fig. 2a).

From the experimental data, we extract the resonance frequency  $\Omega_m/2\pi = 4.872$  MHz and the linewidth  $\Gamma_m/2\pi = 13.2$  Hz of the fundamental in-plane mode of the nanobeam resonator. This corresponds to a quality factor of  $Q_m = 3.69 \times 10^5$  at  $T = 50$  mK. From the measured resonance frequency, we determine the tensile stress in the nanobeam  $\sigma_0 = 641$  MPa. Compared to the prestress at room temperature (RT),  $\sigma_0^{\text{RT}} = 234$  MPa, we observe an increase by 407 MPa, which is consistent with estimations based on the thermal expansion coefficient of aluminium [7]. Thus, a pre-characterization of the eigenfrequency at RT, e.g., by optical means, allows the prediction of the nanobeam's eigenfrequency at mK-temperature.

In Fig. 2b, the linewidth is plotted as a function of temperature between 50 and 400 mK. We observe a nearly linear temperature dependence,  $\Gamma_m(T) = \Gamma_{m,0} + \gamma T$ , with  $\gamma/2\pi \approx 66$  Hz/K

<sup>1</sup>The authors acknowledge support from the German Excellence Initiative via the 'Nanosystems Initiative Munich' (NIM).

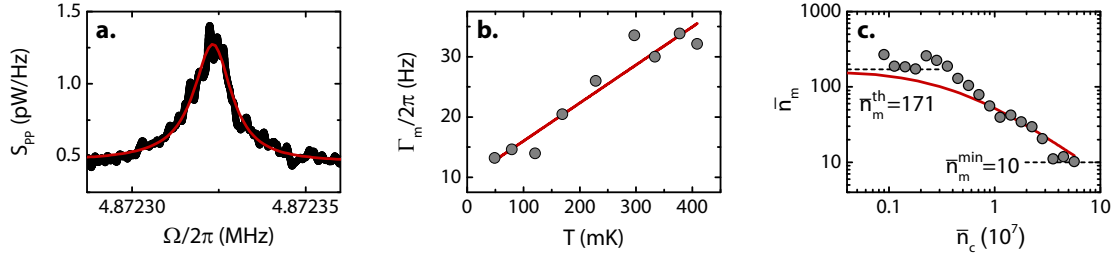


**Figure 2:** **a.** Thermal motion spectrum of the fundamental in-plane mode of the nanobeam with Lorentzian fit ( $T = 50$  mK). **b.** Linewidth as a function of temperature (with linear fit). **c.** Phonon number versus cavity photon number for an ideally red-detuned drive (black circles: experimental data, red line: theoretical prediction).

and  $\Gamma_{m,0}/2\pi \approx 10$  Hz. This behavior is consistent with observations reported in literature for pure aluminium nanobeams [6, 8] and  $\text{Si}_3\text{N}_4/\text{Nb}$  nanobeams [9]. The linear  $T$ -dependence of  $\Gamma_m(T)$  suggests that coupling of phonons to two-level states (TLS) is the dominating loss mechanism in this type of nanobeam resonator at low temperatures. These TLS can be modeled as a double-well potential whose major damping mechanism is given by tunneling between the potential minima. In a nanobeam resonator, the potential is modulated periodically by the oscillating strain, which couples the TLS to the nanobeam motion. The relaxation rate of the TLS depends on the phonon density and thus on the environment temperature  $T$ .

Using an ideally red-detuned MW drive, the electromechanical coupling can be used to cool the motion of the mechanical resonator via the MW circuit. Starting at a thermal phonon number of  $\bar{n}_m^{\text{th}} \approx 171$ , we are able to cool down the fundamental in-plane mode of the nanobeam to  $\bar{n}_m^{\text{min}} \approx 10$ , corresponding to an effective mode temperature of  $T_m^{\text{min}} \approx 2.3$  mK (see Fig. 2c) [7]. Thanks to the relatively high mechanical resonance frequency, the mode cooling process is not dominated by side-band noise from the MW source (cf. [9]). Instead, the minimum attainable phonon number is limited by the available MW power, as the electromechanical coupling of our sample is slightly smaller than for the sample discussed in Ref. [9].

In future samples, a reduction of the gap size between nanobeam and adjacent ground plane will allow us to increase the electromechanical coupling, which is the basis for ground-state cooling with a coherent side-band drive. Besides, first experiments have demonstrated the feasibility of a three-body hybrid system, consisting of a MW resonator, a nanobeam resonator and a transmon qubit on a single chip. This paves the way towards novel protocols for the preparation of non-classical states and the realization of three-partite entanglement in a circuit electromechanical system [5].

## References

- [1] E. E. Wollman, C. U. Lei, A. J. Weinstein, J. Suh, A. Kronwald, F. Marquardt, A. A. Clerk, and K. C. Schwab, *Science* **349**, 952 (2015).
- [2] J.-M. Pirkkalainen, E. Damskäg, M. Brandt, F. Massel, and M. A. Sillanpää, *Phys. Rev. Lett.* **115**, 243601 (2015).
- [3] X. Zhou, F. Hocke, A. Schliesser, A. Marx, H. Huebl, R. Gross, and T. J. Kippenberg, *Nat. Phys.* **9**, 179 (2013).
- [4] F. Hocke, M. Pernpeintner, X. Zhou, A. Schliesser, T. J. Kippenberg, H. Huebl, and R. Gross, *Appl. Phys. Lett.* **105**, 133102 (2014).
- [5] M. Abdi, M. Pernpeintner, R. Gross, H. Huebl, and M. J. Hartmann, *Phys. Rev. Lett.* **114**, 173602 (2015).
- [6] J. Sulkko, M. A. Sillanpää, P. Häkkinen, L. Lechner, M. Helle, A. Fefferman, J. Parpia, and P. J. Hakonen, *Nano Lett.* **10**, 4884 (2010).
- [7] M. Pernpeintner. *Nanomechanical hybrid systems*. Ph.D. thesis, Walther-Meißner-Institut and Technische Universität München (2016).
- [8] F. Hoehne, Y. A. Pashkin, O. Astafiev, L. Faoro, L. B. Ioffe, Y. Nakamura, and J. S. Tsai, *Phys. Rev. B* **81**, 184112 (2010).
- [9] F. Hocke. *Microwave circuit-electromechanics in a nanomechanical hybrid system*. Ph.D. thesis, Walther-Meißner-Institut and Technische Universität München (2013).

## A Combined Circuit Qed Circuit Nanomechanical System

*P. Schmidt, D. Schwienbacher, M. Pernpeintner, F. Wulschner, F. Deppe, A. Marx, R. Gross, H. Huebl*<sup>1</sup>

Opto- and electromechanical systems investigate ultra-sensitive force detection and test quantum mechanics in the literal sense [1]. Typically, the effective coupling between the mechanical and the optical or electrical subsystem is rather weak and of linear type in most cases. The generation of non-classical and, in particular, mechanical Fock states therefore requires a non-linear circuit element. Thus circuit elements such as SQUIDs and superconducting qubits are natural candidates to reach this goal [2].

As a first experimental step in this direction, we integrated a transmon qubit and a nano-string in a single superconducting microwave (mw) resonator. Figure 1 shows the schematic of the device in panel (a) as well as scanning electron microscopy images of the nano-string and the transmon in panel (b) and (c), respectively. The realization of such a hybrid system, however, remains challenging, although fabrication of the individual parts is well established at the WMI (see Refs. [3–6] for qubits and Refs. [7–10] for cavity electromechanics). Starting with a 6 mm × 10 mm single-crystalline silicon chip we use e-beam lithography to pattern an aluminum coplanar waveguide resonator as well as the nano-string on the bare substrate. After the Al thin film deposition, the sample is annealed to generate high tensile stress in the aluminum film. Next, the qubit is fabricated using e-beam lithography and shadow evaporation. Finally, the nano-string is released via isotropic reactive ion etching (RIE) and a critical point drying process (CPD). Note, that releasing the string is the most critical step, since a RIE process can destroy Josephson junctions via an electrostatic discharge. Furthermore, as capillary forces can destroy the nano-string during the drying process, we employ CPD increasing the fabrication yield for our Al nano-strings from 50% to ≥ 80%.

The transmon qubit has been characterized in a spectroscopy experiment. We measure the dispersive shift [11], i.e. a qubit state-dependent frequency shift of the microwave resonator eigenfrequency. In this way, we can map the dispersion of the qubit using a two-tone microwave spectroscopy scheme as shown in Fig. 2(a). The maximum qubit frequency  $\omega_{\text{qb}}$  located at the so-called sweet spot (here  $I_{\text{coil}} = 220 \mu\text{A}$ ), allows to determine the Josephson energy via  $E_J = \omega_{\text{qb}}^2 / (8E_C)$  [12]. Using  $E_C/h = 200 \text{ MHz}$  obtained from spectroscopy of two-photon absorption processes, we find a characteristic energy ratio  $E_J/E_C = 195$  for our transmon qubit.

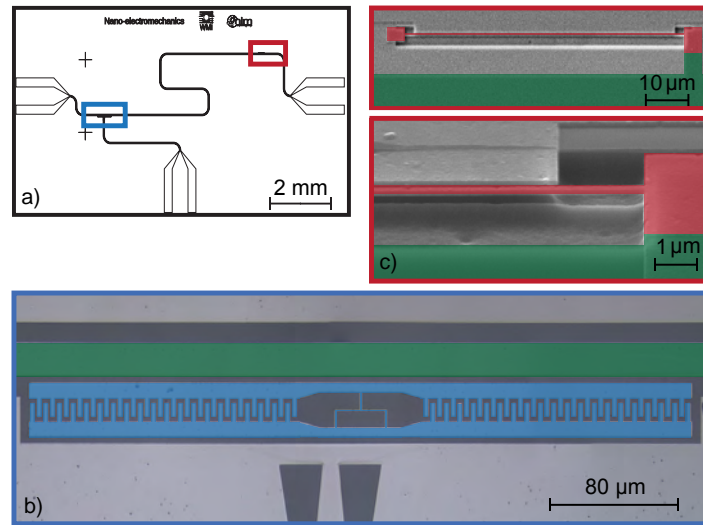


**Figure 1:** (a) Layout of the hybrid device. A mw-resonator is coupled to a transmon qubit (blue box) and a nano-string (red box). (b) displays two false-colored SEM images of the nano-string resonator (red) and the mw resonator (green). (c) shows a false-colored microscope image of the qubit (blue).

<sup>1</sup>We acknowledge support from the doctorate program ExQM of the Elite Network of Bavaria, the IMPRS ‘Quantum Science and Technology’, and the German Excellence Initiative via the ‘Nanosystems Initiative Munich’ (NIM).



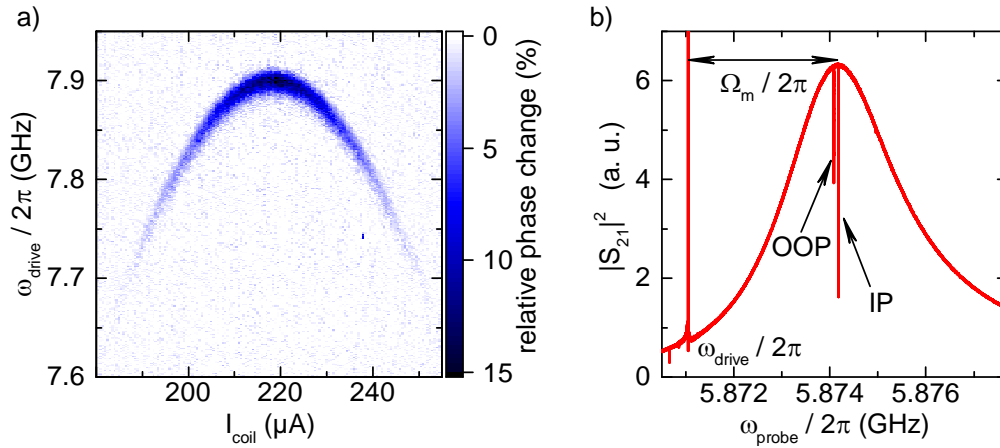


**Figure 2:** (a) Dispersion of the transmon qubit as function of the applied magnetic flux measured via the dispersive shift of the microwave resonator. (b) Transmission of the microwave resonator using an additional strong red-detuned drive tone resulting in EMIA signatures caused by the in- and out-of-plane mode of the nano-string.

For a characterization of the nano-string we employ a two-tone microwave spectroscopy scheme to investigate electromechanically induced absorption (EMIA). We probe the transmission through the microwave resonator while driving the nano-string on the red-detuned side-band. Via an anti-Stokes process, which upconverts a drive photon using a phonon from the nanobeam, we populate the mw resonator at the frequency  $\approx \omega_c$ . When the probe-tone is resonant with the anti-Stokes field, they interfere causing a narrow absorption feature in the transmission data, as shown in Fig. 2(b). From this data, we can identify the in-plane (IP) and out-of-plane (OOP) mode of the nano-string, with eigenfrequencies of about 3.15 MHz.

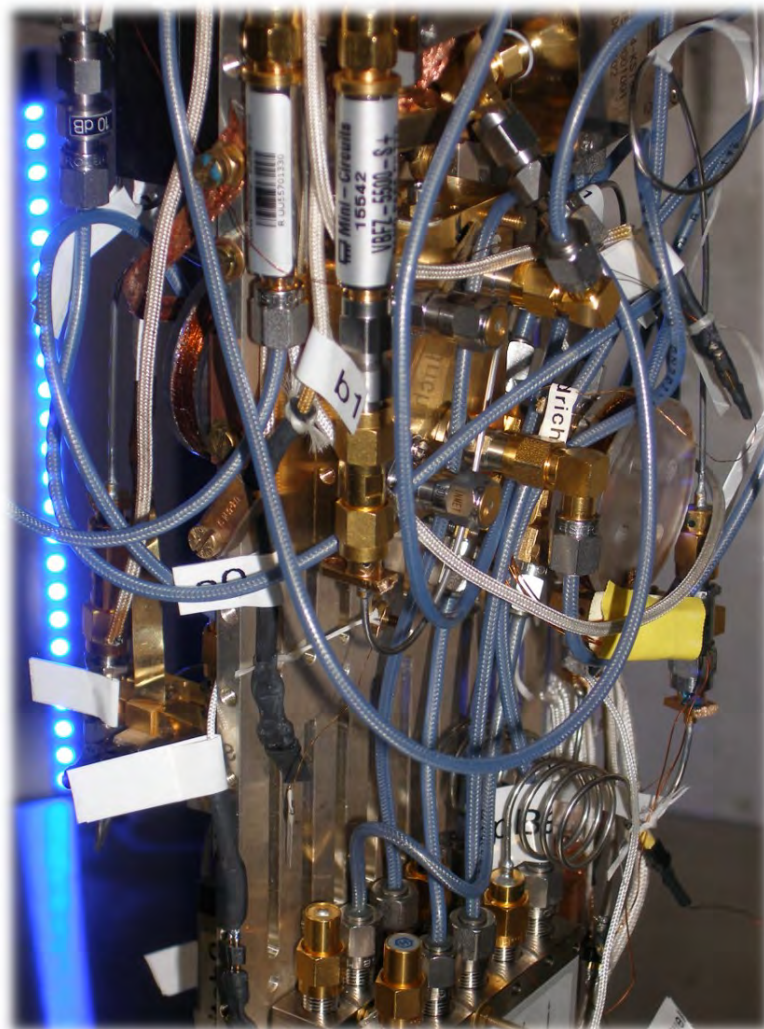
This work experimentally demonstrates the successful fabrication and operation of a nano-string resonator and a transmon qubit coupled to a single superconducting microwave resonator forming a nano-electromechanical circuit QED device. Thus this work is a step in the direction of non-linear nano-electromechanics as envisaged in Ref. [2].

## References

- [1] M. Aspelmeyer, T. Kippenberg, and F. Marquardt, *Rev. Mod. Phys.* **86**, 1391 (2014).
- [2] M. Abdi, M. Pernpeintner, R. Gross, H. Huebl, and M. Hartmann, *Phys. Rev. Lett.* **114**, 17360 (2015).
- [3] T. Niemczyk, F. Deppe, H. Huebl, E. Menzel, F. Hocke, M. Schwarz, J. Garcia-Ripoll, D. Zueco, T. Hümmer, E. Solano, A. Marx, and R. Gross, *Nat. Phys.* **6**, 772 (2010).
- [4] M. J. Schwarz, J. Goetz, Z. Jiang, T. Niemczyk, F. Deppe, A. Marx, and R. Gross, *New J. Phys.* **15**, 045001 (2013).
- [5] A. Baust, E. Hoffmann, M. Haerberlein, P. Eder, J. Goetz, F. Wulschner, E. Xie, L. Zhong, F. Quijuandia, D. Zueco, J. Garcia-Ripoll, L. Garcia-Alvares, G. Romero, E. Solano, K. Federov, E. Menzel, F. Deppe, A. Marx, and R. Gross, *Phys. Rev. B* **93**, 214501 (2016).
- [6] J. Goetz, S. Pogorzalek, F. Deppe, K. Federov, P. Eder, M. Fischer, F. Wulschner, E. Xie, A. Marx, and R. Gross. [arXiv:1611.03842](https://arxiv.org/abs/1611.03842) (2016).
- [7] F. Hocke, X. Zhou, A. Schliesser, T. Kippenberger, H. Huebl, and R. Gross, *New J. Phys.* **14**, 123037 (2013).
- [8] X. Zhou, F. Hocke, A. Marx, H. Huebl, R. Gross, and T. Kippenberg, *Nat. Phys.* **9**, 179 (2013).
- [9] M. Pernpeintner, T. Faust, F. Hocke, J. Kotthaus, E. Weig, H. Huebl, and R. Gross, *Appl. Phys. Lett.* **105**, 123106 (2014).
- [10] F. Hocke, M. Pernpeintner, X. Zhou, A. Schliesser, T. Kippenberger, H. Huebl, and R. Gross, *Appl. Phys. Lett.* **105**, 133102 (2014).
- [11] D. Schuster, A. Wallraff, A. Blais, L. Frunzio, R.-S. Huang, J. Majer, S. Girvin, and R. Schoelkopf, *Phys. Rev. Lett.* **94**, 123602 (2005).
- [12] K. Jens, T. Yu, J. Gambetta, A. Houck, D. Schuster, J. Majer, A. Blais, M. Devoret, S. Girvin, and R. Schoelkopf, *Phys. Rev. A* **76**, 042319 (2007).



# Materials, Thin Film and Nanotechnology, Experimental Techniques



Installation of microwave cables and components on the mK part of a dilution refrigerator system used for experiments on solid state quantum systems.



## Magnetoresistance of the Electron Underdoped Cuprate Superconductor $\text{Nd}_{2-x}\text{Ce}_x\text{CuO}_4$

A. Dorantes, A. Alshemi, H. Zengle<sup>1</sup>, A. Erb, M. Kartsovnik

The parent compound of the electron-doped superconductor  $\text{Nd}_{2-x}\text{Ce}_x\text{CuO}_4$  (NCCO) is an antiferromagnetic (AF) Mott insulator. According to literature, superconductivity is observed from  $x = 0.13$  to  $x = 0.18$  but there is no definite separation between the AF and superconducting (SC) regions of the phase diagram and it is not clear if these two states coexist [1]. To understand the presence and range of the AF order, the magnetic properties of underdoped NCCO crystals should be studied. The magnetic structure of NCCO is determined by the  $\text{Cu}^{2+}$  spins. The spins in two adjacent planes can be oriented in two different ways. In the collinear structure the spins point either parallel or antiparallel to a single direction, and in the noncollinear structure the spins in adjacent layers are orthogonal to each other [2]. It is possible to trigger a spin flop transition that switches the spins from a noncollinear to a collinear orientation by the application of a magnetic field parallel to the  $\text{CuO}_2$  layers. Previous studies on the angle dependent magnetoresistance (AMR) of very low doped NCCO have linked a jump-like feature to the spin flop, which occurs when the field is increased or rotated with respect to the crystal axes [3].

In order to look for a manifestation of long range AF order, we have measured the field and angular dependence of the out-of-plane magnetoresistance (MR) of NCCO single crystals with  $x = 0.10, 0.12$  and  $0.125$ . We performed field sweeps with the field oriented in either [100] or [110] directions. The AMR was measured upon rotating the field in the conducting layers. The crystals were grown using the Traveling Solvent Floating Zone method. The samples were annealed according to the dopant concentration,  $900^\circ\text{C}$  for the NCCO10 sample and  $910^\circ\text{C}$  for the NCCO12 and NCCO12.5 for 40 hours, respectively [4], and then contacted with the 4-probe method.

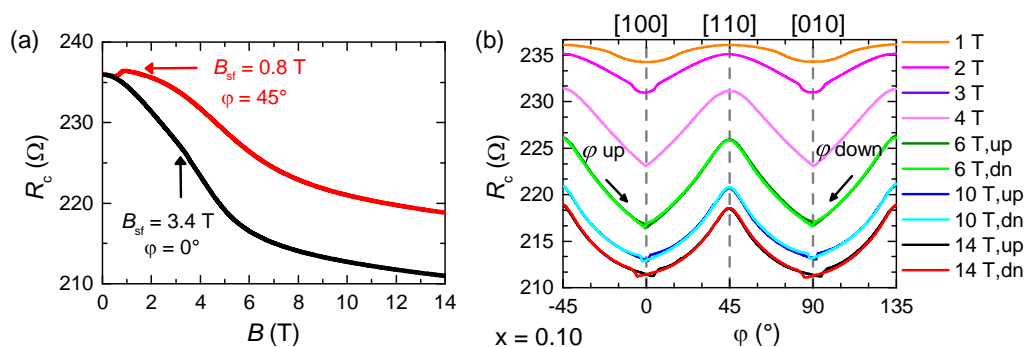
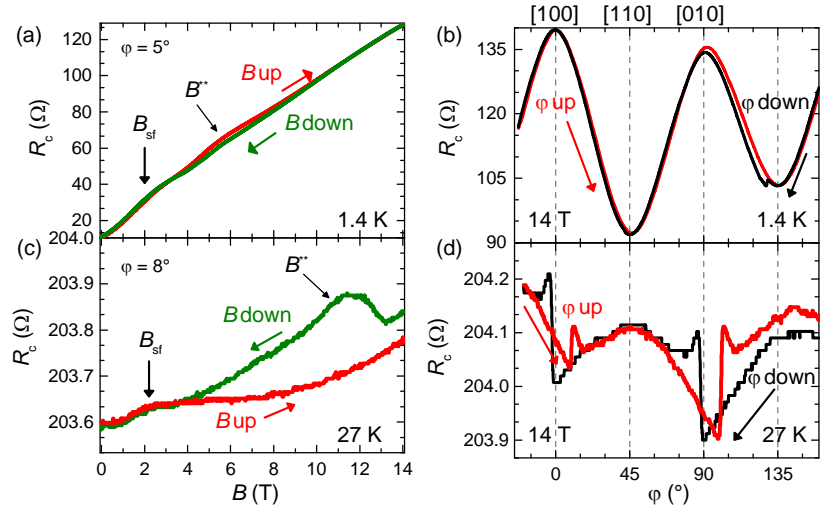


**Figure 1:** Out-of-plane MR for a NCCO10 crystal at  $T = 1.4$  K. (a) Field sweeps for  $B \parallel [100]$  and  $B \parallel [110]$ . (b) Angle dependent MR for different fields. Rotations were done parallel to the  $\text{CuO}_2$  layers. This is described by the angle  $\phi$ , where  $\phi = 0^\circ$  and  $\phi = 45^\circ$  correspond to  $B \parallel [100]$  and  $B \parallel [110]$ , respectively.

The NCCO10 sample did not show a SC transition. Figure 1(a) and (b) show the MR as a function of a magnetic field and the AMR, respectively, for  $T = 1.4$  K. During the field sweep, at  $B \approx 0.8$  T and  $3.4$  T for  $B \parallel [110]$  and  $B \parallel [100]$ , respectively, there is a step-like feature. This behavior matches other reports [3] and indicates the transition from non-collinear to collinear structure. Although the feature at  $3.4$  T is very weak, the derivative  $dR_c/dB$  indicates the presence of the spin flop. In Fig. 1(b), the AMR at different fields shows fourfold symmetry and the presence of step-like features when the field passes through the [100] direction. As the field increases, this feature starts to develop a hysteresis between field rotation from low to high angle and vice versa.

<sup>1</sup>Lee's Pharmaceutical-Kanya Lee Scholarship

**Figure 2:** Out-of-plane MR of NCCO12.5, top  $T = 1.4$  K, bottom  $T = 27$  K. (a) Field sweeps at  $T = 1.4$  K. The field was applied at  $\varphi = 5^\circ$  and increased to 14 T. (b) Angle dependent MR with  $B = 14$  T. When both angular sweeps were finished the field was rotated back to  $\varphi = 5^\circ$  and then the field was swept down. (c) and (d) Similar data at  $T = 27$  K.



Samples NCCO12 and 12.5 showed a very similar behavior. We show only the results for NCCO12.5. This sample was superconducting with  $T_c = 12$  K. In Fig. 2(a-d) we show the field and angular sweeps at  $T = 1.4$  K and  $T = 27$  K. At  $T = 1.4$  K, the spin flop feature at  $\varphi = 0^\circ$  became difficult to see, so the field was set slightly off to make the feature clearer. At  $B \approx 2.5$  T, there is a bending in the resistance for  $\varphi = 5^\circ$ . In the field sweep at  $T = 27$  K, the MR shows a feature at  $B \approx 2.3$  T for  $\varphi = 8^\circ$ . Additionally, we observed other features at 5.6 T and 11.5 T for 1.4 and 27 K, respectively. This is labelled as  $B^{**}$  and it can only be seen when the field is firstly applied at [100] and then moved to an angle where the spin flop occurs, followed by a removal of the field. At 1.4 K, the AMR shows only one small jump around  $\varphi = 135^\circ$  but no other signal of reorientation of the spins. The presence of one weak feature might be due to the SC state in the sample and its high sensitivity to misalignments. However, at 27 K the step-like feature is undoubtedly present as the field rotates away from the [100] direction. This jump also shows a similar hysteretic behavior as NCCO10.

The similarities in the behavior of the MR for different dopant concentrations is a safe indication that the AF order continues to exist up to  $x = 0.125$ . Other features like  $B^{**}$  in the field sweeps and the hysteretic jump in the AMR around  $\varphi = 0^\circ$  and  $90^\circ$ , should be further studied, but we believe they both originate from a reorientation of the spins from the metastable [100] or [010] direction to an intermediate equilibrium state, which is dependent on the field direction [5]. By the observation of the spin flop transition in the field sweeps and in the AMR, we clearly demonstrate the presence of long range AF order in our samples. For NCCO12 and 12.5 we have observed these features below and above the SC transition of the sample, which hints into the possible coexistence of both AF and SC states. But the origin of the coexistence remains to be resolved.

## References

- [1] N. P. Armitage, P. Fournier, and R. L. Greene, *Rev. Mod. Phys.* **82**, 2421–2487 (2010).
- [2] T. Wu, C. H. Wang, G. Wu, D. F. Fang, J. L. Luo, G. T. Liu, and X. H. Chen, *Journal of Physics: Condensed Matter* **20**, 275226 (2008).
- [3] M. Matsuda, K. Yamada, K. Kakurai, H. Kadowaki, T. R. Thurston, Y. Endoh, Y. Hidaka, R. J. Birgeneau, M. A. Kastner, P. M. Gehring, A. H. Moudden, and G. Shirane, *Phys. Rev. B* **42**, 10098–10107 (1990).
- [4] M. Lambacher, T. Helm, M. Kartsovnik, and A. Erb, *Eur. Phys. J. Special Topics* **18**, 61–72 (2010).
- [5] V. P. Plakhty, S. V. Maleyev, S. V. Gavrilov, F. Bourdarot, S. Pouget, and S. N. Barilo, *EPL (Europhysics Letters)* **61**, 534 (2003).

## Pure Spin Current Transport in Gallium-Doped Zinc Oxide

M. Althammer, S. Geprägs, S.T.B. Gönnenwein, M. Opel, R. Gross <sup>1</sup>  
J. Mukherjee, M.S. Ramachandra Rao <sup>2,3</sup>

The generation and detection of pure spin currents, i.e. the charge-less flow of angular (spin) momentum, has been extensively studied in various experiments. One prominent example is the spin Hall magnetoresistance (SMR) which manifests itself in ferromagnetic insulator (FMI) | normal metal (NM) bilayer samples as a dependence of the longitudinal electrical resistance of the NM on the orientation of the magnetization in the FMI. Since its discovery during a close collaboration between WMI, the TU Delft (The Netherlands) and the Tohoku University at Sendai (Japan) three years ago, the SMR has received significant attention, and our original publication [1] was cited more than 190 times in the Web of Science.

Most SMR studies are based on FMI | NM bilayer structures where the magnitude of the SMR depends on the size of the spin Hall angle in the NM. Only in a few experiments, an additional conductive interlayer was inserted at the FMI | NM interface to rule out the contribution of a proximity-polarized NM layer [2]. However, trilayer structures also allow to study the transport of pure spin currents in an interlayer material with a negligible spin Hall angle. In particular, the role of interlayer resistivity and spin diffusion length on the SMR together with a quantitative comparison between a spin diffusive theory model and experiment was still missing for such trilayer systems. In close collaboration with the Indian Institute of Technology (IIT) Madras at Chennai (India), we addressed this problem in detail and investigated trilayer thin film samples consisting of bismuth-substituted yttrium iron garnet ( $\text{Bi}_{0.3}\text{Y}_{2.7}\text{Fe}_5\text{O}_{12}$ , Bi:YIG) | gallium-doped zinc oxide ( $\text{Ga}_{0.01}\text{Zn}_{0.99}\text{O}$ , Ga:ZnO) | Pt [3].

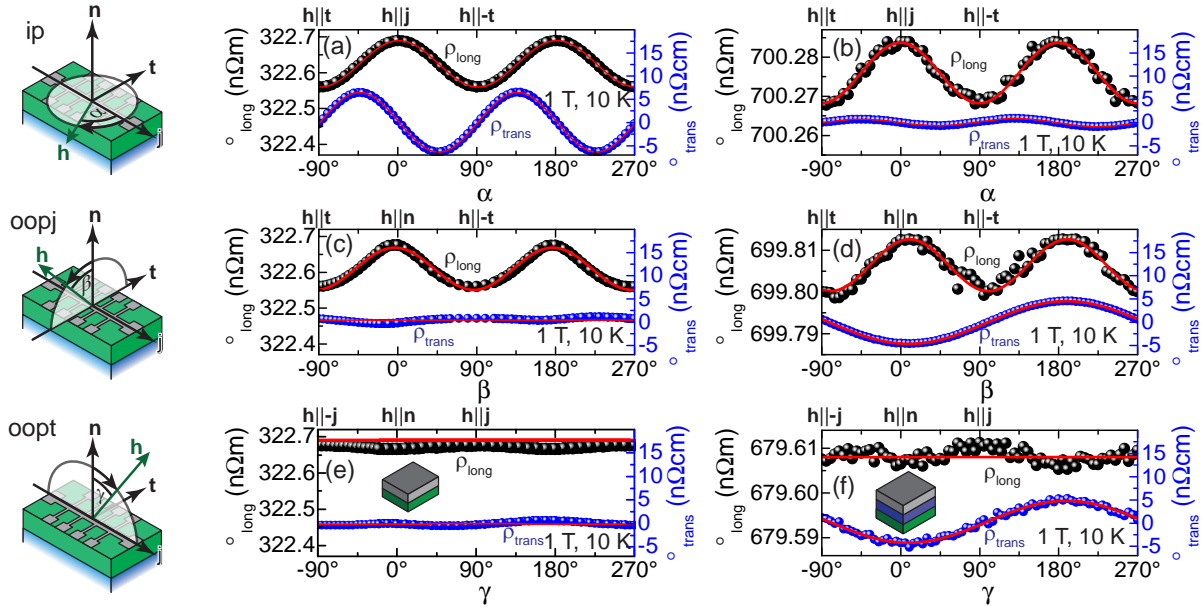


**Figure 1:** ADMR data of (a,c,e) a Bi:YIG | Pt bilayer and (b,d,f) a Bi:YIG | Ga:ZnO | Pt trilayer sample at 10 K. The three orthogonal rotation planes for the magnetic field are sketched in the left column. In the plot, black and blue symbols represent the experimental data of the longitudinal  $\rho_{\text{long}}$  and transverse resistivity  $\rho_{\text{trans}}$ , respectively. The red lines are simulations.

<sup>1</sup>We acknowledge financial support by DAAD via project no. 57085749.

<sup>2</sup>Department of Physics, Nano Functional Materials Technology Centre and Materials Science Research Centre, Indian Institute of Technology Madras, Chennai, Tamil Nadu 600036, India

<sup>3</sup>M.S.R. and J.M. would like to thank for funding from Department of Science and Technology, New Delhi, that facilitated the establishment of Nano Functional Materials Technology Centre (Grant: SR NM/NAT/o2-2005).



The samples were fabricated at WMI *in-situ*, i.e. without breaking the vacuum, on (111)-oriented yttrium aluminium garnet (YAG) substrates in an ultra high vacuum deposition system. Bi:YIG and Ga:ZnO layers were deposited via laser-molecular beam epitaxy and Pt via electron-beam evaporation [3]. The samples were then patterned into Hall bar structures by photolithography and Ar-ion milling, and then mounted in a superconducting magnet cryostat. We performed angle-dependent magnetoresistance (ADMR) measurements, where the magnetic field is rotated in three orthogonal planes: in the film plane (ip), in the plane perpendicular to the  $\mathbf{j}$ -direction (oopj), and in the plane perpendicular to the  $\mathbf{t}$ -direction (oopt) (cf. Fig. 1).

For the bilayer, we measured the typical fingerprint expected for SMR [2]. In ip geometry, we observed a  $\sin^2(\alpha)$ -dependence of  $\rho_{\text{long}}$  and a  $\sin(\alpha)\cos(\alpha)$ -dependence of  $\rho_{\text{trans}}$  (Fig. 1(a)), in oopj we observed a  $\sin^2(\beta)$ -dependence of  $\rho_{\text{long}}$  (Fig. 1(c)), while we did not see any sizeable angular-dependence of  $\rho_{\text{long}}$  in the oopt rotation plane (Fig. 1(e)). Furthermore,  $\rho_{\text{trans}}$  showed only a very small cosine dependence in the oopj and oopt rotation planes, due to the nearly vanishing ordinary Hall coefficient (OHC) of Pt thin films at low temperatures. For the trilayer sample, the angular dependence looked qualitatively the same (Fig. 1(b,d,f)). Since the observed ADMR data reflected the symmetry expected for SMR, we can safely assume the SMR to be the only cause of the magnetoresistance in the bilayer sample as well as in the trilayer sample.

We then studied the dependence of the SMR magnitude on the value of the magnetic field, the temperature, and the thickness of the Ga:ZnO interlayer and compared them to the Bi:YIG|Pt bilayer (Fig. 2). We found that the SMR amplitude is reduced by almost one order of magnitude upon inserting a Ga:ZnO interlayer, and continuously decreases with increasing interlayer thickness. Nevertheless, the SMR stayed finite even for a 12 nm thick Ga:ZnO interlayer. These results show the possibility to transfer a pure spin current through a degenerate ZnO interlayer. Our results also highlight the importance of interface quality for the SMR effect. Finally, our results demonstrate how SMR experiments in trilayers can be utilized to investigate pure spin currents in materials with vanishing spin Hall angle  $\theta_{\text{SH,NM}}$ .

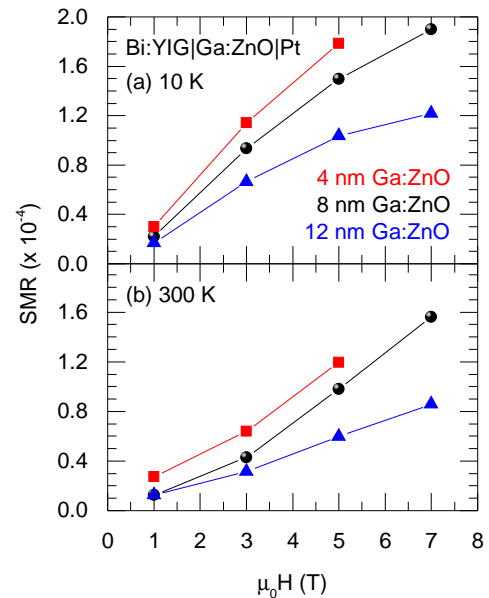


**Figure 2:** SMR amplitude as a function of the magnetic field  $\mu_0 H$  at (a) 10 K and (b) 300 K for different thicknesses of the Ga:ZnO interlayer of 4 nm (red), 8 nm (black), and 12 nm (blue).

## References

- [1] H. Nakayama, M. Althammer, Y.-T. Chen, K. Uchida, Y. Kajiwara, D. Kikuchi, T. Ohtani, S. Geprags, M. Opel, S. Takahashi, R. Gross, G. E. W. Bauer, S. T. B. Goennenwein, and E. Saitoh, *Phys. Rev. Lett.* **110**, 206601 (2013).
- [2] M. Althammer, S. Meyer, H. Nakayama, M. Schreier, S. Altmannshofer, M. Weiler, H. Huebl, S. Geprags, M. Opel, R. Gross, D. Meier, C. Klewe, T. Kuschel, J.-M. Schmalhorst, G. Reiss, L. Shen, A. Gupta, Y.-T. Chen, G. E. W. Bauer, E. Saitoh, and S. T. B. Goennenwein, *Phys. Rev. B* **87**, 224401 (2013).
- [3] M. Althammer, J. Mukherjee, S. Geprags, S. T. B. Goennenwein, M. Opel, M. R. Rao, and R. Gross. Pure spin current transport in gallium doped zinc oxide. Submitted for publication in *J. Appl. Phys.*, [arXiv:1612.07239](https://arxiv.org/abs/1612.07239) (2016).



## Combined Brillouin Light Scattering and Microwave Absorption Study of Magnon-Photon Coupling in a Split-Ring Resonator/Yig Film System

*S. Klingler, H. Maier-Flaig, H. Huebl, S. T.B. Goennenwein, R. Gross, and M. Weiler*<sup>1</sup>

*C.-M. Hu*<sup>2</sup>

In recent years, hybrid quantum systems have been discussed as potential candidates for the up- and down-conversion of quantum signals from the optical to the microwave domain and vice versa. One possible hybrid quantum system consists of spin ensembles coupled to microwave resonators [1]. Here, we report on the optical observation of strong coupling of microwave photons in a micropatterned split-ring resonator [2] (SRR) and magnons in an yttrium iron garnet (YIG) film. We simultaneously use Brillouin light scattering (BLS) spectroscopy and microwave absorption (MA) measurements to probe both magnonic and photonic excitations in the SRR/YIG film system. We find a clear mode anti-crossing indicating a hybridization of the magnon and microwave photon modes in the strong coupling regime. Our findings represent an up-conversion of the hybridized mode frequencies to optical frequencies by inelastic optical photon-magnon scattering.

A sketch of the experimental setup is shown in Fig. 1(a). The setup consists of three parts: (i) A YIG film on a GGG (gadolinium gallium garnet) substrate with lateral dimensions of  $5 \times 5 \text{ mm}^2$  and a YIG layer thickness of  $1 \mu\text{m}$  placed on a SRR of comparable dimensions. An external magnetic field  $H$  is applied in the film plane as indicated, (ii) the microwave circuit to excite and detect GHz-frequency photons, and (iii) the BLS setup to analyze the magnonic excitations up-converted to the optical frequency range. In Fig. 1(b) the microwave absorption is plotted versus the applied magnetic field  $H$  and microwave frequency  $f$ . At  $\mu_0 H \leq 103 \text{ mT}$  and  $\mu_0 H \geq 112 \text{ mT}$ , a single strong resonance at  $f_{\text{SRR}}$  occurs corresponding predominately to the pure microwave eigenmode of the loaded SRR. For  $\mu_0 H \approx 108 \text{ mT}$ , the detuning between the unperturbed photon and magnon modes is zero, and the mode coupling results in two hybridized modes with frequencies  $f_+$  and  $f_-$ . Since the effective coupling strength  $g_{\text{eff}}$  is larger than both the loss rates of the SRR and the magnon resonance, the mode coupling is observed as a pronounced anti-crossing. It is evident from Fig. 1(b), that the  $f_+$  and  $f_-$  modes approach the purely photon and magnon modes for large detuning. Fig. 1(c) shows the simultaneously recorded BLS signal. Here, three different modes are visible: (i) The most prominent mode appears at a frequency which depends almost linearly on the applied magnetic field. This mode is attributed to the detection of the YIG ferromagnetic resonance at frequency  $f_{\text{FMR}}$  excited directly by the feedline. (ii) The two faint modes at  $f_+$  and  $f_-$  resemble the hybridized modes of the magnon-photon system. Their field and frequency dependence is identical to that of the hybridized modes detected in the microwave absorption experiments. The low intensity of these modes in the BLS measurement indicates a small BLS scattering cross-section. Note that the pure photon modes of the SRR are not detected by BLS.

For a quantitative analysis of the hybridized mode frequencies  $f_+$  and  $f_-$  a model of two coupled harmonic oscillators is used [1]:  $f_{\pm} = f_{\text{SRR}} + \Delta/2 \pm \sqrt{\Delta^2 + (g_{\text{eff}}/2\pi)^2}/2$  with  $\Delta = f_{\text{FMR}} - f_{\text{SRR}}$ . The resonance frequency  $f_{\text{SRR}}$  is assumed to be independent of the applied magnetic field, and  $f_{\text{FMR}}$  is modeled by the Kittel equation which describes the precession frequency of a macrospin in an in-plane magnetized ferromagnetic film [3]:  $f_{\text{FMR}} = \frac{\gamma}{2\pi} \mu_0 \sqrt{H(H + M_{\text{eff}})}$ . Here,  $\gamma = g_J \mu_B / \hbar$  is the gyromagnetic ratio,  $g_J$  the Landé factor,  $\mu_B$  the

<sup>1</sup>Financial support from the German Research Foundation via SPP 1538 "Spin Caloric Transport" (projects GO 944/4-2 and GR 1132/18-2) is gratefully acknowledged.

<sup>2</sup>Department of Physics and Astronomy, University of Manitoba, Winnipeg, Manitoba R3T2N2, Canada

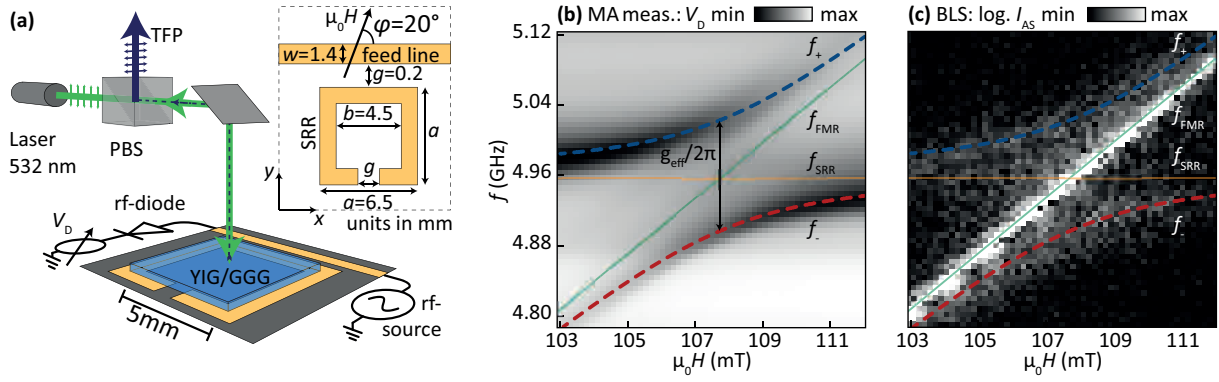


**Figure 1:** (a) Experimental setup: A microwave signal is applied to the feed line which is inductively coupled to the SRR. The YIG film is placed onto the SRR. The microwave transmission through the feedline is detected with a microwave diode and a voltmeter as  $V_D$ . A linearly-polarized laser beam passes a polarizing beam splitter (PBS) and is focussed on the surface of the YIG film by a microscope objective lens (not shown). The cross-polarized backscattered light is directed to the Tandem-Fabry-Pérot interferometer (TFP). Inset: Sketch of the SRR system. (b) Diode voltage versus applied magnetic field and microwave frequency. (c) BLS anti-Stokes intensity as a function of field and microwave frequency. The dashed lines in (b) and (c) were obtained by simultaneously fitting the anti-crossing from (b) and the FMR mode from (c) to  $f_{\pm}$  (see text). The solid lines show the uncoupled modes.

Bohr magneton,  $\hbar$  the reduced Planck constant and  $M_{\text{eff}}$  the effective magnetization of the YIG film. Simultaneously fitting of  $f_{\pm}$  to the  $f_+$  and  $f_-$  modes in the MA and the  $f_{\text{FMR}}$  mode in the BLS data yields the dashed fit curves in Figs. 1(b) and (c). Excellent agreement of model and data is observed and  $g_{\text{eff}}/2\pi = 63 \pm 1$  MHz,  $\mu_0 M_{\text{eff}} = 182 \pm 5$  mT and  $g_J = 2.003 \pm 0.004$  are extracted from the fit. The loss rate of the loaded resonator  $\kappa/2\pi = 25$  MHz is determined from the half width at half maximum (HWHM) of the resonance at  $\mu_0 H = 40$  mT, where the magnon and photon systems are well decoupled. The loss rate of the spin system  $\eta_{\text{FMR}}/2\pi = 4.1$  MHz is obtained from the BLS measurement. Taken together, both  $g_{\text{eff}}/\kappa > 1$  and  $g_{\text{eff}}/\eta_{\text{FMR}} > 1$ , and thus the microwave photon and magnon modes are strongly coupled.

In conclusion, the presented microwave absorption and BLS measurements reveal strong magnon-photon coupling and its up-conversion to optical frequencies in a system consisting of a micropatterned split-ring resonator and a YIG film. A coupling constant of  $g_{\text{eff}}/2\pi = 63$  MHz is found, which exceeds the loss rates of both the pure spin system and the split-ring resonator. The experiments presented here provide a powerful platform for the study of time-dependent oscillations of the coupled system in between the purely magnonic and photonic states during coherent magnon-photon exchange, as well as limiting decoherence processes. More details can be found in Ref. 4.

## References

- [1] H. Huebl, C. W. Zollitsch, J. Lotze, F. Hocke, M. Greifenstein, A. Marx, R. Gross, and S. T. B. Goennenwein, *Physical Review Letters* **111**, 127003 (2013).
- [2] B. Bhoi, T. Cliff, I. S. Maksymov, M. Kostylev, R. Aiyar, N. Venkataramani, S. Prasad, and R. L. Stamps, *Journal of Applied Physics* **116**, 243906 (2014).
- [3] C. Kittel, *Physical Review* **73**, 155–161 (1948).
- [4] S. Klingler, H. Maier-Flaig, R. Gross, C.-M. Hu, H. Huebl, S. T. B. Goennenwein, and M. Weiler, *Applied Physics Letters* **109**, 072402 (2016).

## Pulsed Electron Spin Resonance of Phosphorus Donors at Millikelvin Temperatures

*S. Weichselbaumer, C. W. Zollitsch, K. Müller, P. Natzkin, S. T. B. Goennenwein, R. Gross, H. Huebl<sup>1</sup>*

*M. S. Brandt<sup>2</sup>*

Besides fast processing elements, quantum computers also require long-term storage solutions for quantum information. Possible candidates for such a quantum memory are solid-state spins, as they show remarkably long coherence times [1, 2]. To coherently exchange quantum information between the spin ensemble and, for example, a superconducting microwave resonator effectively, they need to be strongly coupled. In this coupling limit, they form a so-called hybrid quantum system [3]. Previously, high cooperativity coupling was demonstrated for a hybrid system consisting of an ensemble of phosphorus donors in isotopically pure  $^{28}\text{Si}$  and a superconducting microwave resonator [4].

However, for the application of storing quantum states in a spin system, the measurements have to be conducted at temperatures compatible to the operation of other quantum information processing elements. For the case of superconducting quantum circuits, this is in the range of  $T \approx 50$  mK. Here, the spin splitting exceeds thermal energy, and thus automatically prepares the spin ensemble in its ground state. This is in contrast to the temperature regime of conventional paramagnetic resonance (EPR) experiments and thus poses additional challenges to the experimental setup.

For the implementation of a pulsed EPR excitation scheme at millikelvin temperatures we extended the existing microwave circuitry by a pulsed excitation and a phase-sensitive time-domain detection scheme. This setup is schematically shown in Fig. 1. A fast arbitrary waveform generator (AWG) generates arbitrarily shaped pulses at an intermediate frequency (IF). Using an IQ-microwave mixer, the pulses are up-converted to the resonator frequency by a vector-modulated frequency source. Inside the cryostat, attenuators suppress thermal microwave photons and thus allow one to prepare the spin ensemble in its ground state. In the detection line, circulators shield the sample from thermal noise from the input of the low-noise amplifier. This low-noise amplifier pre-amplifies the signal. The room temperature detection circuitry further amplifies the signal, down-converts it to the intermediate frequency and finally records the signal with a fast digitizer. To prevent overloading the detection circuitry during an microwave excitation pulse, we implement a fast high-frequency switch prior the room-temperature amplifier.

To put the new millikelvin pulsed EPR setup to the test, we measure a standard Hahn echo sequence, which consists of gaussian shaped  $\pi/2$ - and  $\pi$ -pulses, separated by an evolution

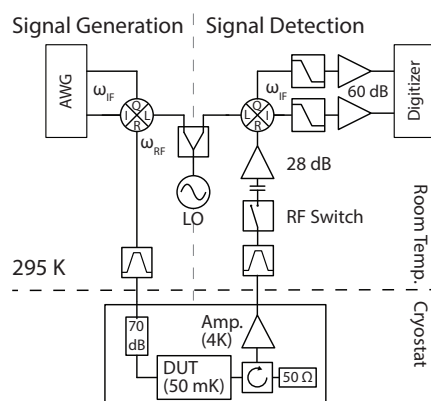


**Figure 1:** Schematic of the microwave circuitry of the pulsed millikelvin EPR setup. Arbitrarily shaped pulses are generated using a fast arbitrary waveform generator in combination with a microwave vector source. The resulting pulse or pulse sequence coherently controls the spin ensemble. For the analysis of its dynamic response, the microwave signal is preamplified in the detector channel, down-converted to the IF frequency, and phase-sensitively digitized.

<sup>1</sup>The authors acknowledge financial support from the German Research Foundation (DFG) via the focus program SPP 1601 (project HU 1861/2-1), the collaborative research center SFB 631 and the Nanosystems Initiative Munich (NIM).

<sup>2</sup>Walter-Schottky-Institut, Technical University of Munich

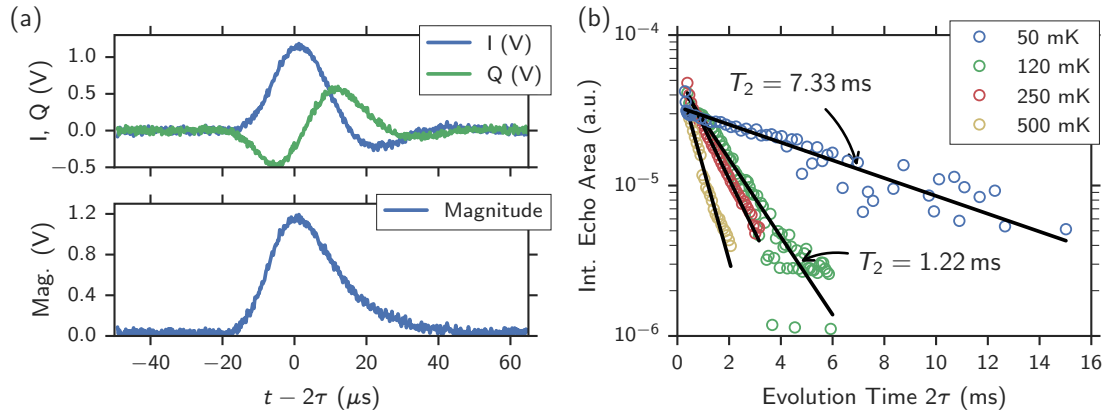


**Figure 2:** (a) Quadrature components I and Q (upper panel) and magnitude (lower panel) of a single-shot Hahn echo with Gaussian pulses ( $5\ \mu\text{s}$ – $250\ \mu\text{s}$ – $10\ \mu\text{s}$ ). (b) Integrated echo area (symbols) of the signal magnitude as a function of the evolution time  $2\tau$  for several temperatures. Black lines are fits of a mono-exponential decay to extract the coherence time  $T_2$ .

time  $\tau$ . We plot both quadratures as well as the magnitude of the detected single-shot echo signal in Fig. 2(a). We observe a clear echo signal after twice the evolution time with an exceptional signal-to-noise ratio  $\text{SNR} \approx 45$  for approximately  $10^8$  spins. This large SNR for a single-shot experiment is attributed to the fact that the thermal spin polarization of the phosphorus donors is close to unity at  $T = 50$  mK.

The Hahn-echo sequence is the standard method to measure the coherence time  $T_2$  of a quantum system. We plot the integrated echo area as a function of the free evolution time  $2\tau$  in Fig. 2(b) for various temperatures and find a mono-exponential decay yielding the characteristic, here temperature dependent, decay time or coherence time  $T_2$ . We find an unexpectedly long coherence time of  $T_2 = 7.33$  ms for this phosphorus doping concentration of  $[P] = 10 \times 10^{17} \text{ cm}^{-3}$  at the lowest temperature of  $T = 50$  mK. Possibly, this long coherence time is due to the strong coupling between the microwave resonator and the spin ensemble.

These measurements also demonstrate the capability to utilize arbitrarily shaped pulses for EPR experiments. For future studies we plan to employ adiabatic or optimal control pulses, as they allow us to compensate microwave magnetic field inhomogeneities [5] and to shorten the required pulse length [6].

In summary, we present our pulsed EPR setup for measurements in the millikelvin regime and show first measurements of the spin coherence time of a hybrid system consisting of a spin ensemble and a superconducting microwave resonator. We observe a  $T_2$  time of 7.33 ms for phosphorus donors at 50 mK and successfully demonstrate the generation of arbitrary pulse shapes, paving the way towards future experiments enabling optimal control techniques.

## References

- [1] K. Saeedi, S. Simmons, J. Z. Salvail, P. Dluhy, H. Riemann, N. V. Abrosimov, P. Becker, H.-J. Pohl, J. J. Morton, and M. L. Thewalt, *Science* **342**, 830–833 (2013).
- [2] A. M. Tyryshkin, S. Tojo, J. J. L. Morton, H. Riemann, N. V. Abrosimov, P. Becker, H.-J. Pohl, T. Schenkel, M. L. W. Thewalt, K. M. Itoh, and S. A. Lyon, *Nat. Mat.* **11**, 143–147 (2011).
- [3] Z.-L. Xiang, S. Ashhab, J. Q. You, and F. Nori, *Rev. Mod. Phys.* **85**, 623–653 (2013).
- [4] C. W. Zollitsch, K. Mueller, D. P. Franke, S. T. B. Goennenwein, M. S. Brandt, R. Gross, and H. Huebl, *Appl. Phys. Lett.* **107**, 142105 (2015).
- [5] A. J. Sigillito, H. Malissa, A. M. Tyryshkin, H. Riemann, N. V. Abrosimov, P. Becker, H.-J. Pohl, M. L. W. Thewalt, K. M. Itoh, J. J. L. Morton, A. A. Houck, D. I. Schuster, and S. A. Lyon, *Appl. Phys. Lett.* **104**, 222407 (2014).
- [6] T. E. Skinner, T. O. Reiss, B. Luy, N. Khaneja, and S. J. Glaser, *J. Magn. Res.* **167**, 68–74 (2004).

# Experimental Facilities







## Overview of Key Experimental Facilities and Infrastructure

In the following basic information on the key experimental facilities and components of the technical infrastructure installed at the Walther-Meißner-Institute (WMI) is given.

### UHV Laser-MBE

The WMI operates an UHV Laser-Molecular Beam Epitaxy (L-MBE) system for the growth of complex oxide heterostructures. The system has been designed to meet the special requirements of oxide epitaxy. The UHV cluster tool consists of the following main components:

- central transfer chamber;
- load-lock chamber with a heater system for substrate annealing;
- laser deposition chamber with a KrF excimer laser, *in-situ* reflection high energy electron diffraction (RHEED) system, laser substrate heating system, and atomic oxygen/nitrogen source; the RHEED system has been modified to allow for the operation at high oxygen partial pressure up to 0.5 mbar;
- surface characterization chamber with UHV scanning atomic force microscope (Omicron);
- metallization chamber with a four heart electron gun system and a liquid nitrogen cooled sample stage. The sample holder can be tilted for shadow evaporation.

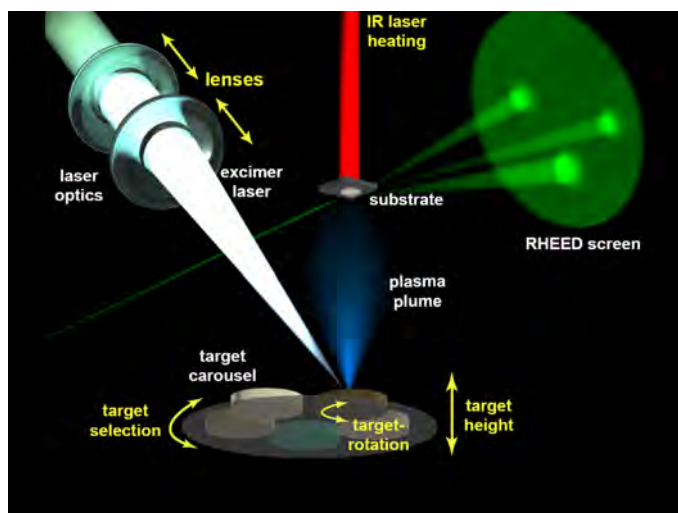
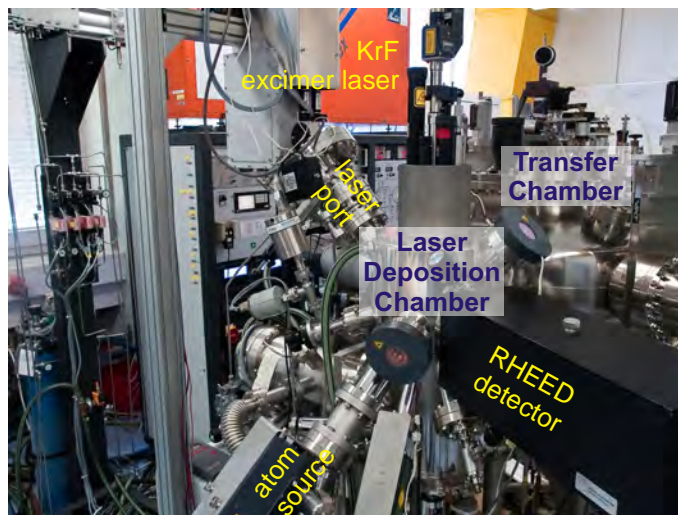


**Figure 1:** Top: UHV laser-molecular beam epitaxy system. Bottom: principle of the deposition process.

The system is used for the growth of complex oxide heterostructures consisting of superconducting, ferromagnetic, ferroelectric, and semiconducting materials such as high-temperature superconductors, doped manganites, (double) perovskites, magnetite, zinc oxide, rare earth iron garnets, pyrochlore iridates, etc.

The original laser molecular beam epitaxy system (laser-MBE) designed already in 1995/96 has been continuously upgraded and modified until now. In particular, the substrate heating system and the temperature control unit were changed from a resistive radiation heater to an infrared laser heating system (see Fig. 3, left) including a pyrometer for determining the sample temperature. In addition, a source for atomic oxygen and nitrogen has been installed. The main advantage of the new heating system is that only the substrate is heated while the surrounding parts are hardly affected (Fig. 3, right). In this way one can achieve a substantially better vacuum at temperatures well above 1000 °C. The achievable substrate temperature is limited by the melting point and the size of the substrate material (approx. 1410 °C for a 5 mm × 5 mm silicon substrate). The laser heating system has already been successfully used for removing the amorphous silicon oxide layer from the surface of silicon substrates at 1150 °C.



**Figure 2:** Pulsed Laser Deposition (PLD): When the pulse of the UV laser (KrF excimer laser, 248 nm) hits the target, the target material is ablated and the so-called laser “plume” containing highly excited atoms and molecules is formed.

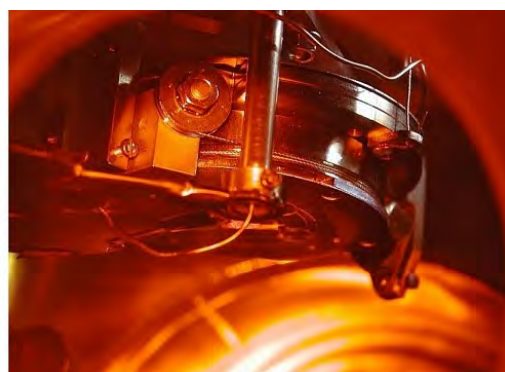
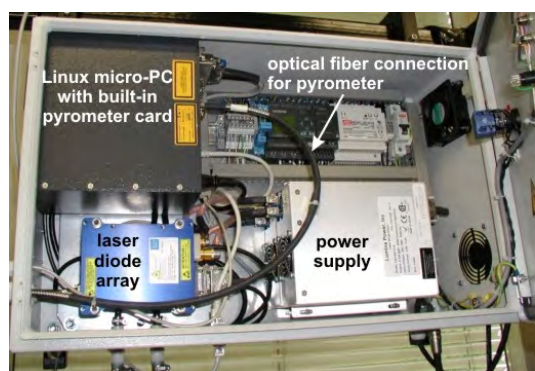


**Figure 3:** Components of the laser heating system: The substrate is heated using an IR diode laser head that is located in a separate box far away from the deposition chamber (left). The laser light is brought to the substrate (right) via an optical fiber.

We have further developed and installed a home-made telescope zoom optics for the pulsed UV laser light, consisting of in total five lenses on sliding lens holders allowing for a movement over a total distance of 1200 mm. The lens holders are attached to independent stepper motors, each connected to a controller providing an accurate positioning precision. The controllers are driven via a PC, thus allowing for a full automation of the lens system itself. With this telescope zoom optics we are able to change the area of the UV laser spot on the target, resulting in an accessible range of laser fluences from  $\rho_L = 0.5 \text{ J/cm}^2$  to  $5 \text{ J/cm}^2$ . To maintain a stable laser fluence at the target, we have installed a so-called *intelligent* window (PVD Products) at the laser entrance port combining two unique features. First, it keeps the inner side of the entrance window free of coatings by blocking the ablated plasma plume via a rotatable disc consisting of UV grade fused silica. Second, an insertable mirror positioned in the light path after the disc allows to guide the incoming UV laser pulse through a side window, where its energy is determined by a pyroelectric detector. These measures help to improve the deposition processes by accurately monitoring  $\rho_L$  as one of the most critical process parameters.

## UHV Electron Beam Evaporation System

The UHV metal MBE system allows for the growth of high quality metallic thin films by electron beam evaporation and molecular beam epitaxy. The system is optimized for the fabrication of superconducting persistent current qubits by aluminum shadow evaporation. It is equipped with an improved substrate holder allowing for multi-angle shadow evaporation. The main components of the system are:

- UHV system with a process chamber with a base pressure of  $\sim 1 \times 10^{-8}$  mbar pumped by a 10001/s turbo molecular pump with magnetic suspension of the rotor adequate for corrosive gases.
- Load-lock chamber equipped with a magnetic transfer system (push-pull positioner) for sample transfer without breaking the vacuum in the process chamber.
- Downstream pressure control by an adaptive pressure controlled gate valve.
- Electron beam evaporator with six  $8 \text{ cm}^3$  crucibles embedded in a linearly movable water cooled rail providing six different materials.
- Film thickness measurement and closed loop evaporation rate control by a quartz crystal microbalance in combination with the evaporation controller.
- Effusion cell for molecular beam epitaxy processes.
- Ion sputtering gun for in-situ sample cleaning
- Manipulator with UHV stepping motors for automated and precise sample tilt and options for rotating and cooling the sample.

A precise and reproducible tilt of the sample is realized by a sample manipulator with process specific degrees of freedom. The downstream pressure control allows for a fast adjustment and precise control of the oxygen partial pressure. This is crucial for a well-defined oxidation process of the Josephson junctions barriers. The entire process can be performed fully automated via a touch screen and is controlled by a LabView program. Up to six effusion cells can be optionally added to the system allowing for further materials. The manipulator allows for further degrees of freedom that can be used to align the sample to the effusion cells, the ion sputtering gun and to measuring equipment such as ellipsometry or RHEED.

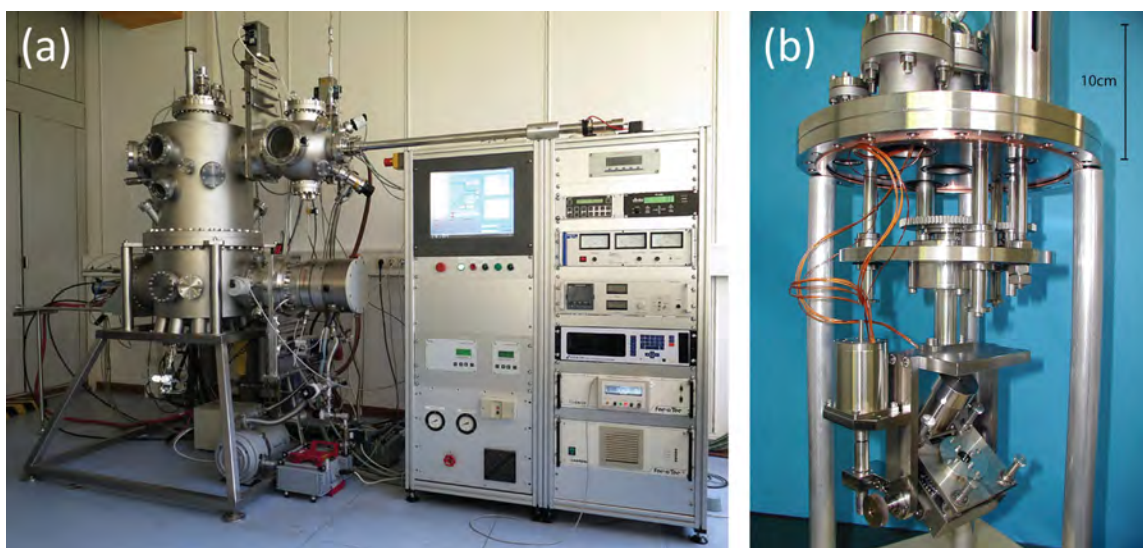


**Figure 4:** (a) Photograph of the UHV electron beam evaporation system. (b) Manipulator with UHV stepping motors for automated and precise sample tilt and options for rotation.



## Single Crystal Growth and Synthesis of Bulk Materials

Transition metal oxides are of great interest due to their various interesting physical properties (e.g. high temperature superconductivity, colossal magnetoresistance, ferroelectricity, nonlinear optical properties etc.) and their high potential for applications. Therefore, the WMI operates a laboratory for the synthesis of bulk materials and single crystals of transition metal oxides. Besides various chamber- and tube furnaces a four-mirror image furnace is used for the crystal growth of various oxide systems. With this furnace crystals of many different compounds of the high temperature superconductors and various other transition metal oxides have been grown as single crystals using the traveling solvent floating zone technique. The furnace consists basically of 4 elliptical mirrors with a common focus on the sample rod and with halogen lamps in their other focus. By irradiation of the focused light the sample rod is locally heated and eventually molten. The molten zone can be moved up and down along the entire sample rod under simultaneous rotation. Due to the anisotropic growth velocity a preferential growth of those grains with the fastest growth velocity along the pulling direction is obtained and the formerly polycrystalline rod is transformed into a single crystal. Single crystal growth can be performed with this furnace at maximum temperatures up to 2200 °C in the pressure range from  $10^{-5}$  mbar up to 10 bar and in oxidizing, reducing as well as inert atmosphere.



**Figure 5:** The four-mirror image furnace installed at the crystal laboratory of the WMI. Crystals can be grown by the floating zone and traveling solvent floating zone techniques at temperatures up to 2200 °C and pressures up to 10 bar.

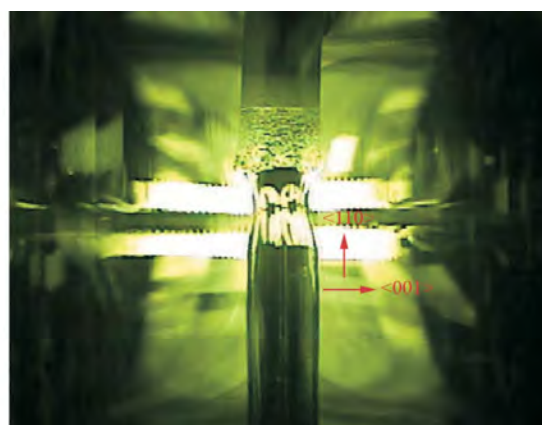
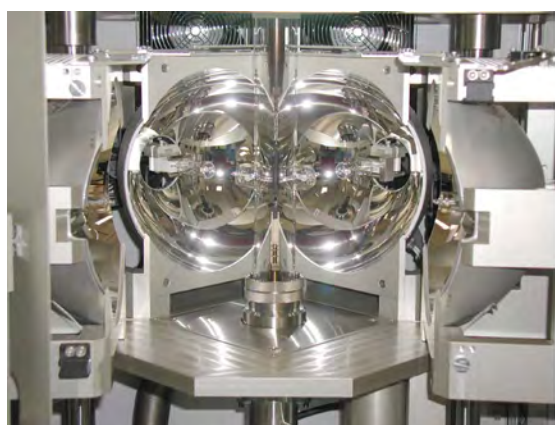


**Figure 6:** Left: Central part of the image furnace with four elliptical mirrors. In the center one can see the quartz tube with a polycrystalline rod. Right: View on the molten zone of  $\text{Pr}_{2-x}\text{Ce}_x\text{CuO}_4$  (melting point: 1280 °C) obtained by a CCD camera.

### The X-ray diffraction systems

For X-ray analysis the WMI operates two X-ray diffractometers (Bruker D8 Advance and D8 Discover). The two-circle system is used for powder diffraction. In this system the samples can be heated in oxygen atmosphere up to 1600 °C. It is equipped with a Göbel mirror and an area detector to save measuring time. The second system is a high resolution four-circle diffractometer that can be used for reciprocal space mappings. It is equipped with a Göbel mirror and an asymmetric two-fold Ge monochromator and allows for the texture analysis of thin film heterostructures, superlattices and single crystalline materials. In both systems measurements can be carried out fully computer controlled.

Beside these two Bruker X-ray systems a Laue camera for single crystal analysis and a Debye-Scherrer camera are available.

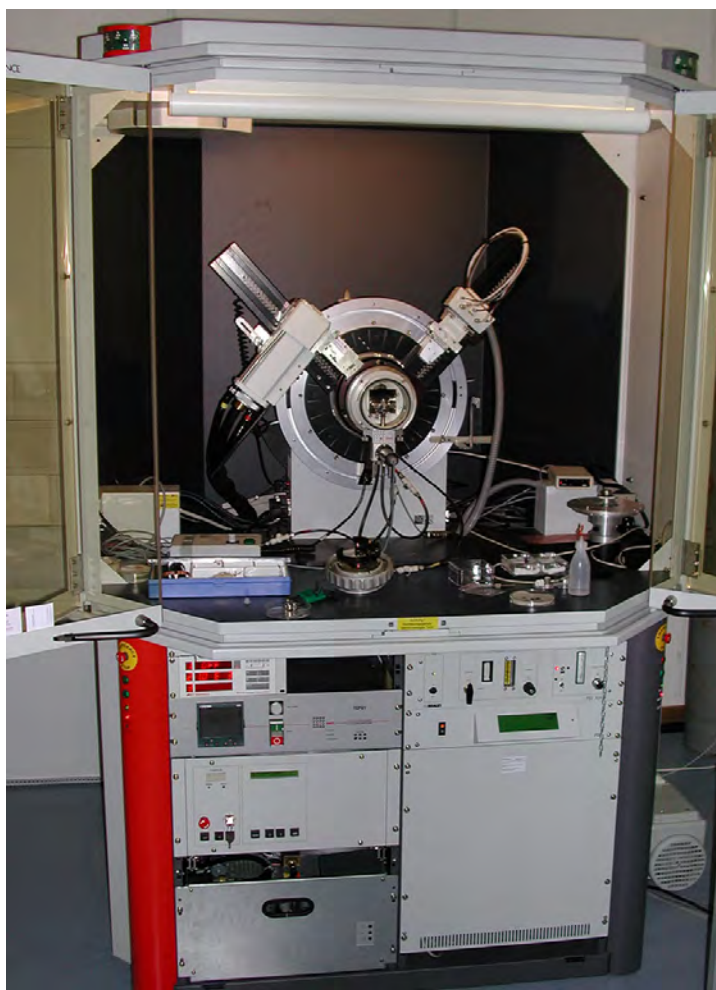


Figure 7: The two-circle X-ray diffractometer Bruker D8 Advance.

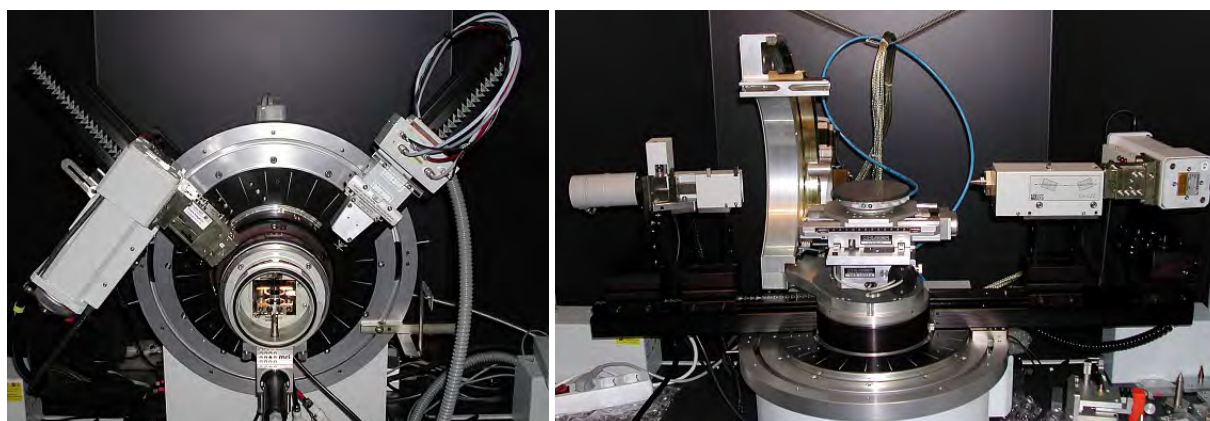


Figure 8: Left: High temperature sample holder of the D8 Advance system. Right: Four-circle high resolution X-ray diffractometer Bruker D8 Discover.





Figure 9: Quantum Design SQUID magnetometer.

### The SQUID magnetometer

For the analysis of the magnetic properties of materials, a Quantum Design SQUID magnetometer system (Fig. 9) is operated at the WMI. The SQUID magnetometer allows for measurements in the temperature regime from 1.8 to 400 K and provides excellent sensitivity particularly in the low field regime. Due to the excellent sensitivity of the system, thin film samples with a very small sample volume can be analyzed. The SQUID magnetometer is equipped with a superconducting solenoid allowing for a

maximum field of 7 T. At present, the magnetometer is used for the characterization of magnetic and superconducting materials (both in bulk and thin film form). Examples are the cuprate high temperature superconductors, the doped manganites, magnetite, the double perovskites, magnetic semiconductors, or multiferroics.

### The High Field Laboratory

Transport and thermodynamic properties of samples are often studied as a function of the applied magnetic field. For such measurements several superconducting magnets are available at the WMI. Two of them (8/10 and 15/17 Tesla magnet system) are located in the high magnetic field laboratory in the basement of the WMI. The magnet systems are installed below the floor level to facilitate the access to the top flange and the change of the sample sticks. The magnet systems

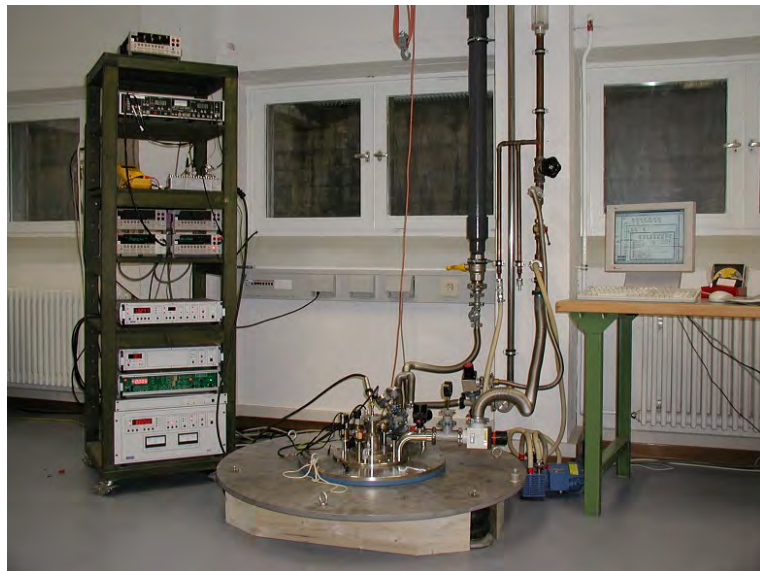


Figure 10: High field laboratory with Oxford 17 T magnet system.

are decoupled from the building to avoid noise due to mechanical vibrations. A variety of sample holders can be mounted allowing for e.g. sample rotation during the measurement. For standard sample holders the accessible temperature regime is  $1.5 \text{ K} < T < 300 \text{ K}$ . However, also  $^3\text{He}/^4\text{He}$  dilution refrigerator inserts ( $T > 20 \text{ mK}$ ) or high temperature units ( $T < 700 \text{ K}$ ) can be mounted. All measurements are fully computer controlled (by the use of the LabView software tool) allowing for remote control and almost continuous measurements.

Since 2012, a 3D vector magnet with variable temperature insert, allowing for 2 T in-plane and 6 T out-of-plane magnetic fields is available for thermal and electrical transport experiments. This system has been named “Chaos” cryostat (acronym for “Cold, Hot And Other Secret experiments”). It consists of a  $^4\text{He}$  flow cryostat with a liquid nitrogen shield and includes a vertically oriented 6 T solenoid combined with two horizontally oriented split coil pairs. The magnet system can be operated in two ways:



- in a single axis mode: up to 6(2) T are provided in the vertical (horizontal) direction.
- in a arbitrary axis mode: the flux density vector can be oriented in arbitrary directions and the magnitude of the flux density is limited to 2 T.

The magnetic field is controlled by a Mercury IPS superconducting magnet power supply master/slave system. It provides output currents of up to 120 A in bipolar operation for each magnet axis. The control of the system is feasible either directly via touch-screen or remote using a LabView based software.

The Chaos cryostat has a IN100 variable temperature insert (VTI), enabling an operation for temperature setpoints between 1.5 K and 300 K. The temperature control of the sample space inside the VTI can be achieved via an automatic needle valve drive for helium flow control and/or an automatic heater system. The temperature of the VTI is read via a Cernox sensor fitted to the heat exchanger. A remote control of the system is realized by a LabView based software. It provides control of the VTI (heater, needle valve, temperature setpoint) and the IPS (control of the magnetic field setpoints and energizing rates for the three vector components of the field) as well as the display of the actual He and liquid nitrogen levels.



**Figure 11:** The 3D vector magnet with control electronics in the “CHAOS” Laboratory.

A further 3D vector magnet allowing for 1 T in-plane and 6 T out-of-plane magnetic fields is installed in the WMI Quantum Laboratories as part of a cryogen-free dilution system.

## The Clean Room Facility

For the fabrication of solid state nanostructures and quantum circuits including superconducting, spintronic and nanomechanical devices the WMI operates a class 1000 clean room facility with an area of about 50 m<sup>2</sup>. This clean room facility has been put into operation at the WMI within the year 2001. The clean room is subdivided into two parts for optical lithography and electron beam lithography, respectively. The clean room facility is equipped with the standard tools for optical lithography such as resist coaters, hot plates, wet benches, a Karl Süss MJB3 mask aligner and an optical projection lithography system. The technical infrastructure for the clean room is located in the basement of the WMI directly below the clean room area.



**Figure 12:** Top: Part of the clean room facility with optical lithography equipment and clean room benches. Bottom: Resist coater and hot plates.

The clean room also is equipped with a reactive ion etching system, Plasmalab 80 Plus with ICP plasma source (Oxford Instruments Plasma Technology).

## Electron Beam Lithography

A 100 kV Electron Beam Lithography System nB5 fabricated by NanoBeam Ltd., UK, is installed in the second part of the clean room facility. The nB5 is a round-beam step-and-repeat system oriented towards high-end R&D applications at universities and research institutes. It is designed for nanopatterning and mix-and-match lithography. The innovative design of the electron optics and automation system enhances its throughput and reliability. It is an ideal tool for nano-device research and production. The electron beam lithography is used for the fabrication of nanostructures in metallic and oxide systems required for the study of quantum effects in mesoscopic samples.



**Figure 13:** 100 kV Electron Beam Lithography System nB5 of NanoBeam Ltd., UK, inside the WMI cleanroom facility.

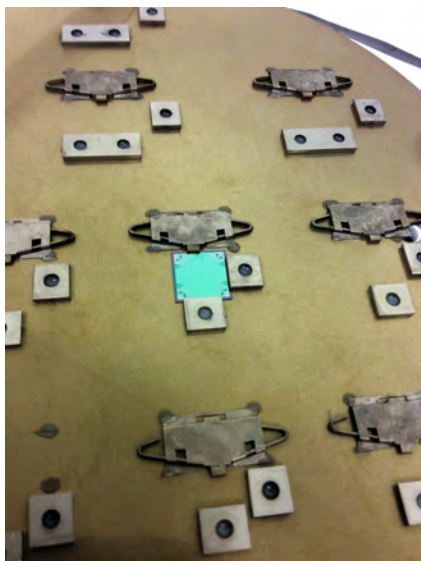


**Figure 14:** Chuck of the nB5 e-beam lithography system with a mounted  $12 \times 12 \text{ mm}^2$  silicon wafer.

The nB5 Electron Beam Lithography System employs low Coulomb-effect electron optics and sophisticated column designs to reduce beam size. The shorter optical column eliminates column bending and reduces system vibration. The modern electronics has low noise and low thermal effects. The perfectly integrated machine structure greatly improves system settling time and total stage move time. The advanced vibration tracking design enables the nB5 system to write on the fly. All these features combined with the fast deflection speed and high data processing rate make the nB5 the highest throughput system available today. Moreover, the nB5 requires undemanding cleanroom conditions, in particular regarding temperature stability, stray field magnitude, and floor vibration level.

The nB5 system is equipped with a thermal field emitter (TFE), an electrostatic lens and magnetic condenser lens, a conjugate beam blanking at  $< 5 \text{ ns}$  slew rate and a dual beam deflection. The latter is used to achieve ultra-high deflection speed for beam writing (clock rate:  $55 \text{ MHz}$ ). The total deflection coverage is combined with the mainfield and the subfield and controlled by two independent deflection sub-systems (field size:  $1000 \mu\text{m}$ , address resolution:  $1 \text{ nm}$ ). The characteristic performance parameters of the electron optics of the nB5 system are: (i) beam voltage range:  $20 \text{ kV}$  to  $100 \text{ kV}$ , (ii) minimum beam current:  $0.1 \text{ nA}$ , (iii) maximum beam current:  $100 \text{ nA}$ , (iv) theoretical beam size:  $2.3 \text{ nm}$  at  $100 \text{ kV}$ , (v) guaranteed writing beam size:  $< 5 \text{ nm}$  at  $2 \text{ nA}$ , (vi) beam current drift:  $< 0.5\%/hour$  at  $5 \text{ nA}$ , (vii) beam position drift:  $< 50 \text{ nm}/hour$  for  $3 \text{ nA}$  beam current, including blanking, deflection and stage move.

The XY-stage allows for a traversal distance of  $200 \text{ mm}$  with a total stage move time of only  $150 \text{ ms}$  for  $1 \text{ mm}$  stage movement and a position measurement resolution of  $0.3 \text{ nm}$  using laser interferometry. The maximum substrate sizes are  $2 - 8 \text{ in}$  for round substrates,  $2 - 5$  for square glass masks up to  $3 \text{ mm}$  thickness. Finally, the nB5 system has airlock operation with automatic loading robotics with a loading cassette for 6 chucks with a maximum diameter of  $8 \text{ inch}$ .

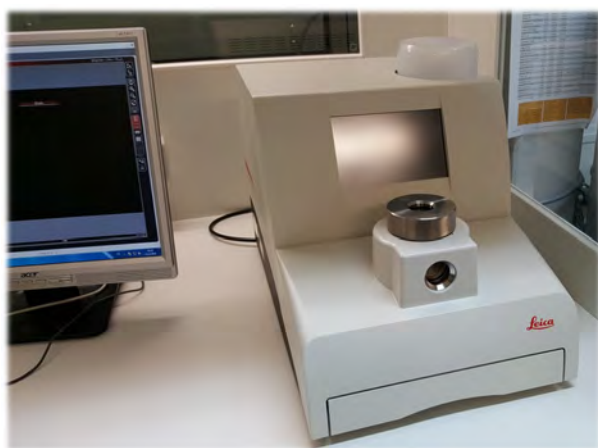


**Figure 15:** The fully automated Critical Point Dryer Leica EM CPD 300.

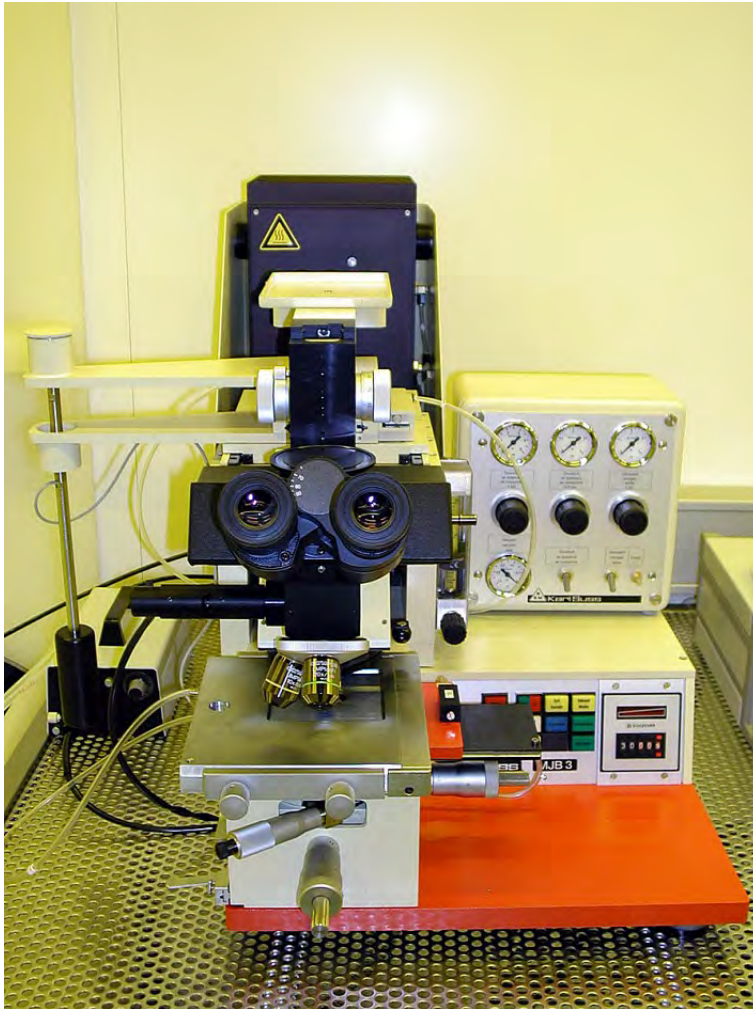
#### Automated Critical Point Dryer Leica EM CPD 300

The fabrication of nanomechanical systems requires the removal of solvent used for wet chemical processing by a critical point dryer. At WMI, we use the Critical Point Dryer Leica EM CPD 300, which allows the fully automated drying of biological specimens such as pollen, tissue, plants, insects etc., as well as NEMS (Nano Electro Mechanical Systems).

To ensure a low  $\text{CO}_2$  consumption and a very short process time a new filler concept is used in the Leica EM CPD 300. Special attention has been put on safety issues by implementing software controlled

cut-off functions and integrating a waste separator.





### Optical Lithography

For optical lithography, a Karl Süss MJB 3 maskaligner or an optical microscope based projection system are used. The maskaligner operates in the 1 : 1 soft or hard contact mode and uses chromium metal masks. In the projection system the mask pattern is demagnified by a factor of 5 to 100. Therefore, cheap foil masks can be used. With both systems microstructures with a lateral dimension down to 1  $\mu\text{m}$  can be fabricated.



**Figure 16:** Top: Süss MJB 3 maskaligner for optical lithography. Bottom: Optical projection lithography based on an optical microscope.

## Low and Ultra-Low Temperature Facilities

At the WMI, we have constructed the first dilution refrigerator with pulse tube pre-cooling for ultra-low temperature experiments. This type of refrigerator works without cryo-liquids, and thus is a lot more practical, more economical and more reliable than cryostats with liquid helium pre-cooling. These days, all major cryo-engineering companies are offering commercial versions of this Millikelvin cooler, and these so-called "dry" refrigerators outsell conventional refrigerators by a wide margin. The general construction concept of most manufacturers is unchanged from our



**Figure 17:** The "dry" dilution refrigerator of the WMI.



**Figure 18:** Low-temperature unit of a WMI dilution refrigerator ready to go into a cryostat.

original prototype, where the refrigerator consists of three basic components. The first cooling stage is a commercial pulse tube cryocooler which reaches a base temperature of 2.5 K. The second stage is a Joule-Thomson stage, and the last stage is a dilution refrigeration stage, where the lowest temperature of the cryostat is about 0.01 K (Fig. 17).



**Figure 19:** Two mixing chamber mounting plates with silver sponges. Those are needed to overcome the thermal resistance (Kapitza resistance) between the liquid  $^3\text{He}$  and the mounting plate of the mixing chamber. To fabricate the mounting of the sponge (square pins embedded in the sponge) a spark erosion technique has been employed.

In many low temperature applications high refrigeration capacities are required. Our design allows for a high circulation rate of  $^3\text{He}$  which in the end determines the cooling power of a dilution refrigerator. Presently our "dry" fridge reaches a refrigeration capacity of  $700\ \mu\text{W}$  at a temperature of the mixing chamber of 0.1 K, seven times the cooling power of the WMI nuclear demagnetization cryostat. Goals of our present work are a further increase of cooling power and a lower base temperature

of the dry dilution refrigerator.

A smaller version of our cryogen-free fridge has become commercially available by *Oxford Instruments* (formerly *VeriCold Technologies, Ismaning*). It has a refrigeration capacity of  $250\ \mu\text{W}$  at a mixing chamber temperature of 0.1 K (Fig. 18).

The WMI also develops and fabricates dilution refrigerator inserts for temperatures down to



about 20 mK. The inserts fit into all cryogenic systems (e.g. superconducting magnets) having a two inch bore. They allow fast sample change and rapid cool down cycles of less than five hours. The dilution refrigerator inserts are engineered and fabricated in-house and are also provided to other low temperature laboratories for ultra-low temperature experiments.

### Millikelvin Temperatures in Combination with 3D Vector Magnetic-Fields



**Figure 20:** The dilution refrigerator with the 3D vector magnet located in the Quantum Laboratories.

In one room of the WMI Quantum Laboratories a cryogen-free dilution refrigerator is installed. This system is equipped with a 3D vector magnet allowing for 1 T in-plane and 6 T out-of-plane magnetic fields. Additional microwave coaxial lines allow for the microwave spectroscopy up to 18 GHz under these experimental conditions.

Scientifically, several directions in the field of fundamental light-matter interaction are envisaged:

(i) Circuit quantum electrodynamics (circuit QED), where superconducting qubits form hybrids with microwave resonators. These experiments are time consuming, because quantum effects arise in the limit of low excitation numbers.

Hereby, challenging requirements are imposed on the detection systems allowing to detect microwave signals in the attowatt regime.

(ii) Storage of quantum states. One possibility is the transfer of the quantum information contained in photons to long-lived spin states. Additionally, exchange coupled systems or ferromagnetic systems come into focus, because the effective coupling strength scales with the square-root of the number of spins contributing. In general, we study the light-matter interaction with long-lived spin systems and integrate them into superconducting quantum circuits.

(iii) Spin systems. Here, our studies are not limited to paramagnetic spin systems, but also involve exchange coupled (ferro- or ferri-) magnetic systems. Hereby, magnetization damping can be investigated as a function of temperature, frequency and magnetic field direction.

(iv) Circuit electro-mechanical hybrid systems consisting of a nano-mechanical element coupled to a superconducting microwave resonator. In this context, sideband cooling of the mechanical system into its ground state and pulsed spectroscopy of hybrid system are performed and will be extended.

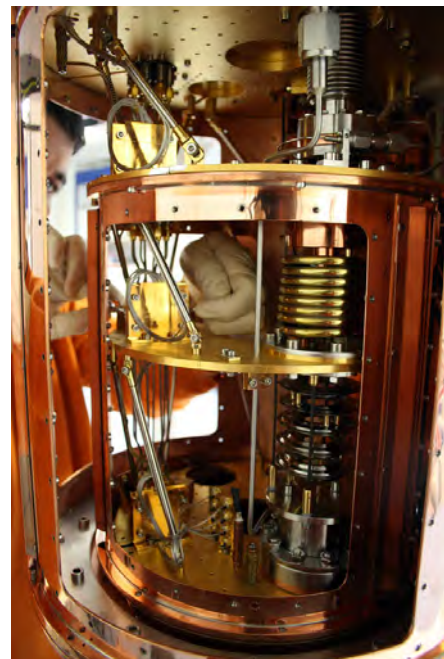


**Figure 21:** Inside of the dilution system. The windows of the 4 K and the still shield are removed providing access to the low temperature stages.



### WMI Millikelvin Facilities for Experiments with Superconducting Quantum Circuits

The research on superconducting quantum circuits at WMI focuses mainly on systems sensitive to externally applied flux (flux qubits), circuit QED systems where flux qubits are coupled to transmission line resonators, squeezing physics in flux driven Josephson parametric amplifiers, and propagating quantum microwaves (e.g., quantum state reconstruction methods). In order to further develop our activities on quantum effects in the microwave regime, additional cryogenic capacities at millikelvin temperatures have been established. In addition to sufficient cooling power, the specifications for these cryostats are mainly dictated by the dimensions (typically a few centimeters in each direction) of bulky microwave components such as circulators or microwave switches.

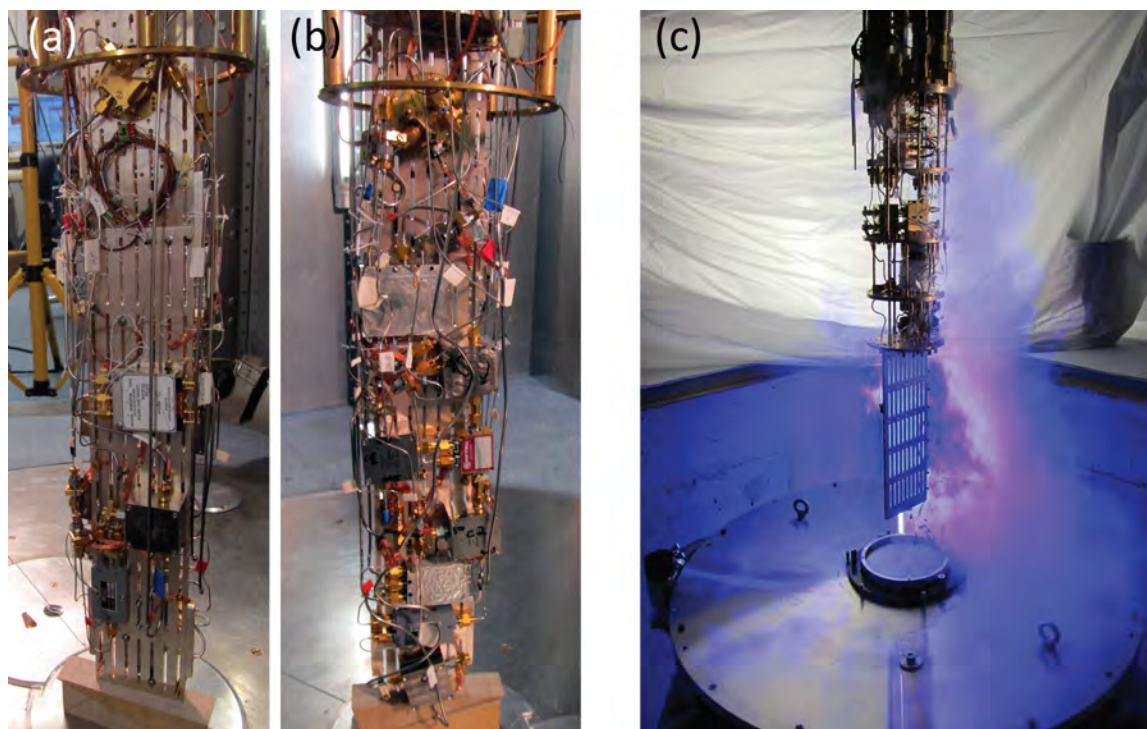


**Figure 22:** Liquid-helium precooled dilution refrigerators for experiments with superconducting quantum circuits. (a), (b) Back and front sides of the sample stage of the K12-refrigerator equipped with four circuit QED experiments. The height of the silver rod is 50 cm. (c) Sample stage and dewar of the dilution refrigerator in the quantum laboratory Ko4.

Two liquid-helium precooled dilution refrigerators are available for experiments with superconducting quantum circuits. The dilution refrigerator in laboratory K12 provides a sample space with a cylindrical volume with 11 cm diameter 55 cm height. The refrigerator is equipped with four microwave amplifiers at the 4 K-stage, seven broadband input lines and 80 twisted pair DC lines. This allows for mounting four experiments simultaneously to avoid idle times by interleaved measurements (see Fig. 22(a) and (b)). The base temperature of this refrigerator is 20 mK.

A new liquid-helium precooled dilution refrigerator for experiments with superconducting quantum circuits has been set up in the quantum laboratory Ko4. To provide enough space at the sample stage we have installed a Cryogenic Ltd. stainless steel dewar with a  $^4\text{He}$  volume of 89 l. The time between two refills exceeds nine days. The cryostat is equipped with 16 coaxial measurement lines suitable for microwave frequencies down to the mixing chamber stage and low-noise cryogenic high electron mobility transistor (HEMT) amplifiers. Presently up to four samples can be mounted simultaneously to the sample stage. By expanding the number of input lines in the near future a more complex experiment can be set up. The cooling power of the mixing chamber at 100 mK was determined to about 140  $\mu\text{W}$ .

A new cryogen-free dilution refrigerator with a pulse tube refrigerator (PTR) for precooling and with a large sample stage has been set up in room K21 of the WMI Quantum Laboratories using the longstanding experience in dry dilution refrigerators at WMI. This refrigerator features large diameters (tens of centimeters) of all temperature stages providing sufficient space for advanced quantum experiments. The main components of the refrigerator are the PTR, a 1K-stage and a dilution unit. The two stages of the PTR cool the incoming  $^4\text{He}$  and the  $^3\text{He}/^4\text{He}$  mixture as well as one radiation shield at each stage. To provide sufficiently high cooling power near 1K to cool microwave components and cables, this refrigerator has been equipped with a 1K-stage operating in a closed cycle. A refrigeration capacity of the 1K-stage of up to 100 mW could be reached. The dilution refrigerator is precooled by a dedicated  $^4\text{He}$  circuit. The minimum base temperature of the refrigerator is below 11 mK. The cooling power at 100 mK was determined to about  $300\ \mu\text{W}$  at the maximum  $^3\text{He}$  flow rate.

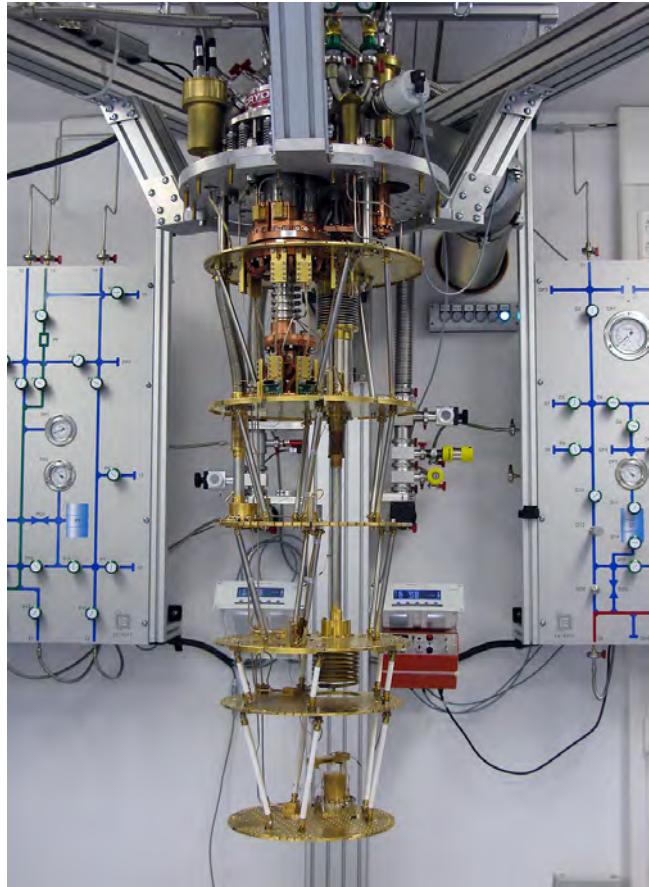


Figure 23: Dry dilution refrigerator with a large sample space.

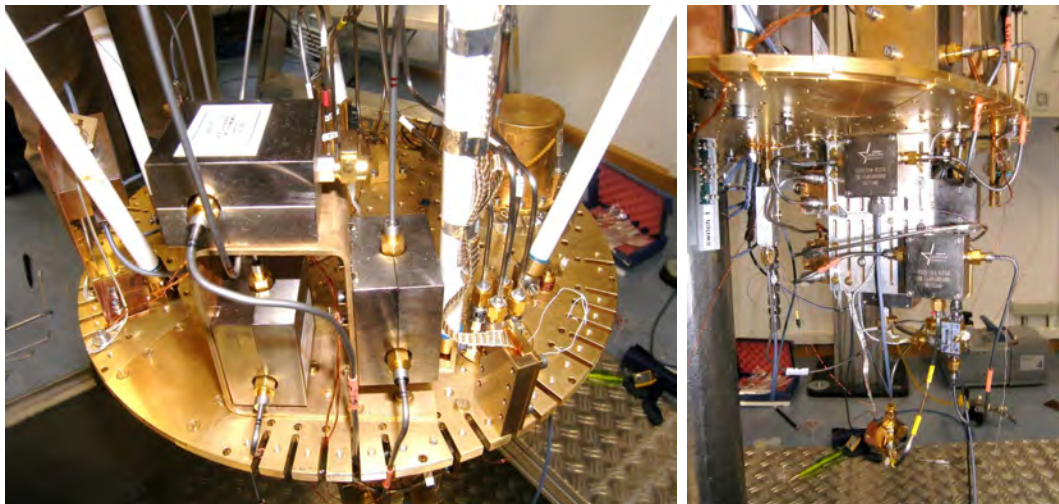


Figure 24: Low temperature platform of K21 dilution refrigerator with experimental setup for circuit QED experiments.



# Statistics





## Publications

1. **Origin of the spin Seebeck effect probed by temperature dependent measurements in  $\text{Gd}_3\text{Fe}_5\text{O}_{12}$**   
Stephan Geprags, Andreas Kehlberger, Tomek Schulz, Christian Mix, Francesco Della Coletta, Sibylle Meyer, Akashdeep Kamra, Matthias Althammer, Gerhard Jakob, Hans Huebl, Rudolf Gross, Sebastian T.B. Goennenwein, Mathias Klauui  
[Nature Communications 7, 10452 \(2016\).](#)
2. **Probing the pairing interaction and multiple Bardasis-Schrieffer modes using Raman spectroscopy**  
S. Maiti, T. A. Maier, T. Boehm, R. Hackl, P. J. Hirschfeld  
[Phys. Rev. Lett. 117, 257001 \(2016\).](#)
3. **Loss mechanisms in superconducting thin film microwave resonators**  
Jan Goetz, Frank Deppe, Max Haeberlein, Friedrich Wulschner, Christoph W. Zollitsch, Sebastian Meier, Michael Fischer, Peter Eder, Edwar Xie, Kirill G. Fedorov, Edwin P. Menzel, Achim Marx, Rudolf Gross  
[J. Appl. Phys. 119, 015304 \(2016\).](#)
4. **A versatile platform for magnetostriction measurements in thin films**  
Matthias Pernpeintner, Rasmus B. Hollander, Maximilian J. Seitner, Eva M. Weig, Rudolf Gross, Sebastian T. B. Goennenwein, Hans Huebl  
[Appl. Phys. Lett. 119, 093901 \(2016\).](#)
5. **Untangling the contributions of cerium and iron to the magnetism of Ce-doped yttrium iron garnet**  
Blai Casals, Marina Espnola, Rafael Cichelero, Stephan Geprags, Matthias Opel, Rudolf Gross, Gervasi Herranz, Josep Fontcuberta  
[Appl. Phys. Lett. 108, 102407 \(2016\).](#)
6. **Emergence of superconductivity in the canonical heavy-electron metal  $\text{YbRh}_2\text{Si}_2$**   
Erwin Schuberth, Marc Tippmann, Lucia Steinke, Stefan Lausberg, Alexander Steppke, Manuel Brando, Cornelius Krellner, Christoph Geibel, Rong Yu, Qimiao Si, Frank Steglich  
[Science 351, 485-488 \(2016\).](#)
7. **New experimental perspectives for soft x-ray absorption spectroscopies at ultra-low temperatures below 50 mK and in high magnetic fields up to 7 T**  
T. Beeck, I. Baev, S. Gieschen, H. Meyer, S. Meyer, S. Palutke, P. Feulner, K. Uhlig, M. Martins and W. Wurth  
[Rev. Sci. Instrum. 87, 045116 \(2016\).](#)
8. **Lamellar Diblock Copolymer Films with Embedded Maghemite Nanoparticles**  
Yuan Yao, Ezzeldin Metwalli, Matthias Opel, Martin Haese, Jean-Franois Moulin, Katia Rodewald, Bernhard Rieger, Peter Muller-Buschbaum  
[Adv. Mater. Interfaces 3, 201500712 \(2016\).](#)
9. **Integrated superconducting detectors on semiconductors for quantum optics applications**  
Michael Kaniber, Fabian Flassig, Gunther Reithmaier, Rudolf Gross, Jonathan J. Finley  
[Appl. Phys. B 122, 115 \(2016\).](#)
10. **Ultrastrong coupling in two-resonator circuit QED**  
A. Baust, E. Hoffmann, M. Haeberlein, M. J. Schwarz, P. Eder, J. Goetz, F. Wulschner, E. Xie, L. Zhong, F. Quijandria, D. Zueco, J.-J. Garcia Ripoll, L. Garcia-Alvarez, G. Romero, E. Solano, K. G. Fedorov, E. P. Menzel, F. Deppe, A. Marx, R. Gross  
[Phys. Rev. B 93, 214501 \(2016\).](#)
11. **Critical spin fluctuations and the origin of nematic order in  $\text{Ba}(\text{Fe}_{1-x}\text{Co}_x)_2\text{As}_2$**   
F. Kretschmar, T. Bohm, U. Karahasanovic, B. Muschler, A. Baum, D. Jost, J. Schmalian, S. Caprara, M. Grilli, C. Di Castro, J. G. Analytis, J.-H. Chu, I. R. Fisher, R. Hackl  
[Nature Physics 12, 560-563 \(2016\).](#)
12. **Revisiting the vortex-core tunnelling spectroscopy in  $\text{YBa}_2\text{Cu}_3\text{O}_{7-\delta}$**

- Jens Bruér, Ivan Maggio-Aprile, Nathan Jenkins, Andreas Erb, Christophe Berthod, Øystein Fischer, Christoph Renner  
[Nature Communications 7, 11139 \(2016\).](#)
13. **Spin Seebeck effect at microwave frequencies**  
 Michael Schreier, Franz Kramer, Hans Huebl, Stephan Geprägs, Rudolf Gross, Sebastian T. B. Goennenwein, Timo Noack, Thomas Langner, Alexander A. Serga, Burkard Hillebrands, Vitaliy I. Vasyuchka  
[Phys. Rev. B 93, 224430 \(2016\).](#)
  14. **Displacement of propagating squeezed microwave states**  
 Kirill G. Fedorov, L. Zhong, S. Pogorzalek, P. Eder, M. Fischer, J. Goetz, E. Xie, F. Wulschner, K. Inomata, T. Yamamoto, Y. Nakamura, R. Di Candia, U. Las Heras, M. Sanz, E. Solano, E. P. Menzel, F. Deppe, A. Marx, R. Gross  
[Phys. Rev. Lett. 117, 020502 \(2016\).](#)
  15. **Magnon based logic in a multi-terminal YIG/Pt nanostructure**  
 Kathrin Ganzhorn, Stefan Klingler, Tobias Wimmer, Stephan Geprägs, Rudolf Gross, Hans Huebl, Sebastian T. B. Goennenwein  
[Appl. Phys. Lett. 109, 022405 \(2016\).](#)
  16. **In-situ study of light production and transport in phonon/light detector modules for dark matter search**  
 The CRESST Collaboration: M. Kiefer, G. Angloher, A. Bento, C. Bucci, L. Canonica, A. Erb, F. v. Feilitzsch, N. Ferreiro Iachellini, P. Gorla, A. Gütlein, D. Hauff, J. Jochum, H. Kluck, H. Kraus, J.-C. Lanfranchi, J. Loebell, A. Münster, F. Petricca, W. Potzel, F. Pröbst, F. Reindl, S. Roth, K. Rottler, C. Sailer, K. Schäffner, J. Schieck, S. Schönert, W. Seidel, M. v. Sivers, L. Stodolsky, C. Strandhagen, R. Strauss, A. Tanzke, M. Uffinger, A. Ulrich, I. Usherov, S. Wawoczny, M. Willers, M. Wüstrich, A. Zöller  
[Nucl. Instr. Meth. Phys. Res. Sect. A 821, 116 - 121 \(2016\).](#)
  17. **New Limits on Double Electron Capture of  $^{40}\text{Ca}$  and  $^{180}\text{W}$**   
 G. Angloher, M. Bauer, P. Bauer, I. Bavykina, A. Bento, C. Bucci, L. Canonica, C. Ciemniak, X. Defay, G. Deuter, A. Erb, F. v. Feilitzsch, N. Ferreiro Iachellini, P. Gorla, A. Gütlein, D. Hauff, P. Huff, C. Isaila, J. Jochum, M. Kiefer, M. Kimmerle, H. Kluck, H. Kraus, J.-C. Lanfranchi, J. Loebell, A. Münster, C. Pagliarone, F. Petricca, S. Pfister, W. Potzel, F. Pröbst, F. Reindl, S. Roth, K. Rottler, C. Sailer, K. Schäffner, J. Schieck, J. Schmalzer, S. Scholl, S. Schönert, W. Seidel, M. v. Sivers, L. Stodolsky, C. Strandhagen, R. Strauss, A. Tanzke, V. Tretyak, H. H. Trinh Thi, C. Türkoglu, M. Uffinger, A. Ulrich, I. Usherov, S. Wawoczny, M. Willers, M. Wüstrich, A. Zöller  
[Journal of Physics G: Nuclear and Particle Physics 43\(9\), 095202 \(2016\).](#)
  18. **Limits on momentum-dependent asymmetric dark matter with CRESST-II**  
 G. Angloher, A. Bento, C. Bucci, L. Canonica, X. Defay, A. Erb, F. v. Feilitzsch, N. Ferreiro Iachellini, P. Gorla, A. Gütlein, D. Hauff, J. Jochum, M. Kiefer, H. Kluck, H. Kraus, J.-C. Lanfranchi, J. Loebell, A. Münster, C. Pagliarone, F. Petricca, W. Potzel, F. Pröbst, F. Reindl, K. Schäffner, J. Schieck, S. Schönert, W. Seidel, L. Stodolsky, C. Strandhagen, R. Strauss, A. Tanzke, H.H. Trinh Thi, C. Türkoglu, M. Uffinger, A. Ulrich, I. Usherov, S. Wawoczny, M. Willers, M. Wüstrich, A. Zöller  
[Phys. Rev. Lett. 117, 021303 \(2016\).](#)
  19. **Charge Variations in Cuprate Superconductors from Nuclear Magnetic Resonance**  
 Steven Reichardt, Michael Jurkatat, Andreas Erb, Jürgen Haase  
[J. Supercond. Nov. Magn. 29, 3017 - 3022 \(2016\).](#)
  20. **Magnetostriction and Magnetostructural Domains in Antiferromagnetic  $\text{YBa}_2\text{Cu}_3\text{O}_6$**   
 B. Náfrádi, T. Keller, F. Hardy, C. Meingast, A. Erb, and B. Keimer  
[Phys. Rev. Lett. 116, 047001 \(2016\).](#)
  21. **Superconductivity and fluctuations in  $\text{Ba}_{1-p}\text{KpFe}_2\text{As}_2$  and  $\text{Ba}(\text{Fe}_{1-n}\text{Co}_n)_2\text{As}_2$**   
 T. Böhm, R. Hosseinian Ahangharnejhad, D. Jost, A. Baum, B. Muechler, F. Kretzschmar, P. Adelman, T. Wolf, H.-H. Wen, J.-H. Chu, I. R. Fisher, R. Hackl  
[physica status solidi \(b\), \(2016\).](#)

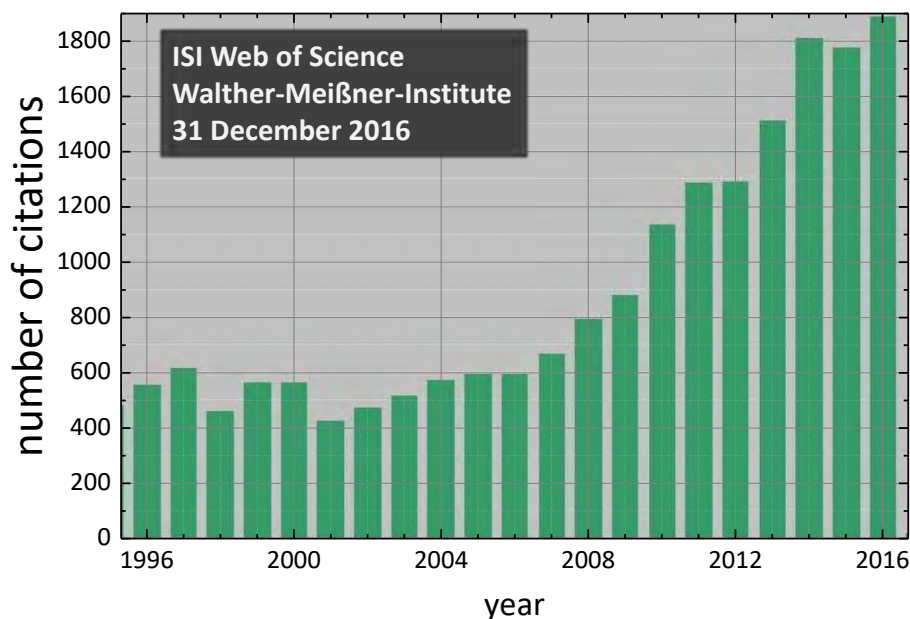


22. **Charge density wave modulation and gap measurements in CeTe<sub>3</sub>**  
U. Ralevic, N. Lazarevic, A. Baum, H.-M. Eiter, R. Hackl, P. Giraldo-Gallo, I. R. Fisher, C. Petrovic, R. Gajic, and Z. V. Popovic  
[Phys. Rev. B \*\*94\*\*, 165132 \(2016\).](#)
23. **Theory of spin Hall magnetoresistance (SMR) and related phenomena**  
Y. T. Chen, S. Takahashi, H. Nakayama, M. Althammer, S. T. B. Goennenwein, E. Saitoh, and G. E. W. Bauer  
[Journal of Physics: Condensed Matter, Volume \*\*28\*\*, Number \*\*10\*\*, 103004 \(2016\).](#)
24. **Results on Light Dark Matter Particles with a Low-Threshold Cresst-II Detector**  
The CRESST Collaboration: G. Angloher, A. Bento, C. Bucci, L. Canonica, X. Defay, A. Erb, F. v. Feilitzsch, N. Ferreiro Iachellini, P. Gorla, A. Gütlein, D. Hauff, J. Jochum, M. Kiefer, H. Kluck, H. Kraus, J. C. Lanfranchi, J. Loebell, A. Münster, C. Pagliarone, F. Petricca, W. Potzel, F. Pröbst, F. Reindl, K. Schäffner, J. Schieck, S. Schönert, W. Seidel, L. Stodolsky, C. Strandhagen, R. Strauss, A. Tanzke, H.H. Trinh Thi, C. Türkoglu, M. Uffinger, A. Ulrich, I. Usherov, S. Wawoczny, M. Willers, M. Wüstrich, A. Zöller  
[Phys. J. C \*\*76\*\*, 25 \(2016\).](#)
25. **Tunable coupling of transmission-line microwave resonators mediated by an rf SQUID**  
F. Wulschner, J. Goetz, F. R. Koessel, E. Hoffmann, A. Baust, P. Eder, M. Fischer, M. Haeberlein, M. J. Schwarz, M. Pernpeintner, E. Xie, L. Zhong, C. W. Zollitsch, B. Peropadre, J.-J. Garcia Ripoll, E. Solano, K. Fedorov, E. P. Menzel, F. Deppe, A. Marx, R. Gross  
[EPJ Quantum Technology \*\*3\*\*, 10 \(2016\).](#)
26. **Alumina shunt for precooling a cryogen-free <sup>4</sup>He or <sup>3</sup>He refrigerator**  
K. Uhlig  
[Cryogenics \*\*79\*\*, 35-37 \(2016\).](#)
27. **Combined Brillouin light scattering and microwave absorption study of magnon-photon coupling in a split-ring resonator/YIG film system**  
Stefan Klingler, Hannes Maier-Flaig, Rudolf Gross, Can-Ming Hu, Hans Huebl, Sebastian T.B. Goennenwein, Mathias Weiler  
[Appl. Phys. Lett. \*\*109\*\*, 072402 \(2016\).](#)
28. **Efficient spin transport through native oxides of nickel and permalloy with platinum and gold overlayers**  
B. L. Zink, M. Manno, L. O'Brien, J. Lotze, M. Weiler, D. Bassett, S. J. Mason, S. T. B. Goennenwein, M. Johnson, and C. Leighton  
[Phys. Rev. B \*\*93\*\*, 184401 \(2016\).](#)
29. **Spin pumping in strongly coupled magnon-photon systems**  
Hannes Maier-Flaig, Michael Harder, Rudolf Gross, Hans Huebl, Sebastian T. B. Goennenwein  
[Phys. Rev. B \*\*94\*\*, 054433 \(2016\).](#)
30. **Spin Hall Magnetoresistance in a Canted Ferrimagnet**  
Kathrin Ganzhorn, Joseph Barker, Richard Schlitz, Matthias Althammer, Stephan Geprägs, Hans Huebl, Benjamin A. Piot, Rudolf Gross, Gerrit E. W. Bauer, Sebastian T. B. Goennenwein  
[Phys. Rev. B \*\*94\*\*, 094401 \(2016\).](#)
31. **Interplay between conducting and magnetic systems in the antiferromagnetic organic superconductor  $\kappa$ -(BETS)<sub>2</sub>FeBr<sub>4</sub>**  
Mark. V. Kartsovnik, Michael Kunz, Ludwig Schaidhammer, Florian Kollmannsberger, Werner Biberacher, Natalia D. Kushch, Akira Miyazaki, Hideki Fujiwara  
[J. Supercond. Nov. Magn. \*\*29\*\*, 3075–3080 \(2016\).](#)
32. **Resistive properties and phase diagram of the organic antiferromagnetic metal  $\kappa$ -(BETS)<sub>2</sub>FeCl<sub>4</sub>**  
Michael Kunz, Werner Biberacher, Natalia D. Kushch, Akira Miyazaki, Mark V. Kartsovnik  
[Phys. Rev. B \*\*94\*\*, 205104 \(2016\).](#)
33. **Electrical Detection of Magnetization Canting in a Magnetic Insulator**  
Kathrin Ganzhorn, Sebastian T. B. Gönnerwein, Benjamin Piot  
[EMFL News \*\*3\*\*, 3 \(2016\).](#)

34. **Impact of the interface quality of Pt/YIG(111) hybrids on their spin Hall magnetoresistance**  
Sabine Pütter, Stephan Geprägs, Richard Schlitz, Matthias Althammer, Andreas Erb, Rudolf Gross, and Sebastian T.B. Goennenwein  
[Appl. Phys. Lett. 110, to appear \(2017\)](#).
35. **Probing Low WIMP Masses with the Next Generation of CRESST Detector**  
The CRESST Collaboration: G. Angloher, A. Bento, C. Bucci, L. Canonica, A. Erb, F. v. Feilitzsch, N. Ferreiro Iachellini, P. Gorla, A. Gütlein, D. Hauff, J. Jochum, M. Kiefer, H. Kluck, H. Kraus, J.-C. Lanfranchi, J. Loebell, A. Münster, F. Petricca, W. Potzel, F. Pröbst, F. Reindl, K. Schäffner, J. Schieck, S. Scholl, S. Schönert, W. Seidel, L. Stodolsky, C. Strandhagen, R. Strauss, A. Tanzke, M. Uffinger, A. Ulrich, I. Usherov, S. Wawoczny, M. Willers, M. Wüstrich, A. Zöller  
[arXiv:1503.08065, submitted for publication \(2015\)](#).
36. **Spin-boson model with an engineered reservoir in circuit quantum electrodynamics**  
Max Haeberlein, Frank Deppe, Andreas Kurcz, Jan Goetz, Alexander Baust, Peter Eder, Kirill Fedorov, Michael Fischer, Edwin P. Menzel, Manuel J. Schwarz, Friedrich Wulschner, Edwar Xie, Ling Zhong, Enrique Solano, Achim Marx, Juan-José García-Ripoll, Rudolf Gross  
[arXiv:1506.09114, submitted for publication \(2015\)](#).
37. **Quantum Memristors with Superconducting Circuits**  
J. Salmilehto, F. Deppe, M. Di Ventra, M. Sanz, E. Solano  
[arXiv:1603.04487, submitted for publication \(2016\)](#).
38. **Observation of the spin Nernst effect**  
Sibylle Meyer, Yan-Ting Chen, Sebastian Wimmer, Matthias Althammer, Stephan Geprägs, Hans Huebl, D. Ködderitzsch, Hubert Ebert, Gerrit E.W. Bauer, Rudolf Gross, Sebastian T.B. Goennenwein  
[arXiv:1607.02277, submitted for publication \(2016\)](#).
39. **Shubnikov-de Haas oscillations and electronic correlations in the layered organic metal  $\kappa$ -(BETS)<sub>2</sub>Mn[N(CN)<sub>2</sub>]<sub>3</sub>**  
M. V. Kartsovnik, V. N. Zverev, W. Biberacher, S. V. Simonov, I. Sheikin, N. D. Kushch, E. B. Yagubskii  
[arXiv:1608.03755, submitted for publication \(2016\)](#).
40. **Investigation of the tunnel magnetoresistance in junctions with a strontium stannate barrier**  
M. Althammer, A.V. Singh, S. Keshavarz, M. K. Yurtisigi, R. Mishra, A. Borisevich, P. LeClair, A. Gupta  
[arXiv:1607.08393, submitted for publication \(2016\)](#).
41. **Second-order decoherence mechanisms of a transmon qubit probed with thermal microwave states**  
J. Goetz, F. Deppe, P. Eder, M. Fischer, M. Müting, J. P. Martínez, S. Pogorzalek, F. Wulschner, E. Xie, K. G. Fedorov, A. Marx, R. Gross  
[arXiv:1609.07351, submitted for publication \(2016\)](#).
42. **Photon Statistics of Propagating Thermal Microwaves**  
J. Goetz, S. Pogorzalek, F. Deppe, K. G. Fedorov, P. Eder, M. Fischer, F. Wulschner, E. Xie, A. Marx, R. Gross  
[arXiv:1609.07353, submitted for publication \(2016\)](#).
43. **Flux-driven Josephson parametric amplifiers: Hysteretic flux response and nondegenerate gain measurements**  
Stefan Pogorzalek, Kirill G. Fedorov, Ling Zhong, Jan Goetz, Friedrich Wulschner, Michael Fischer, Peter Eder, Edwar Xie, Kunihiro Inomata, Tsuyoshi Yamamoto, Yasunobu Nakamura, Achim Marx, Frank Deppe, Rudolf Gross  
[arXiv:1609.09041, submitted for publication \(2016\)](#).
44. **Quantum Illumination Unveils Cloaking**  
U. Las Heras, R. Di Candia, K. G. Fedorov, F. Deppe, M. Sanz, E. Solano  
[arXiv:1611.10280, submitted for publication \(2016\)](#).
45. **Gilbert damping of magnetostatic modes in a yttrium iron garnet sphere**  
Stefan Klingler, Hannes Maier-Flaig, Carsten Dubs, Oleskii Surzhenko, Rudolf Gross, Hans

Huebl, Sebastian T.B. Goennenwein, Mathias Weiler  
[arXiv:1612.02360](#), submitted for publication (2016).

46. **Pure spin current transport in gallium doped zinc oxide**  
 Matthias Althammer, Joynarayan Mukherjee, Stephan Geprägs, Sebastian T. B. Goennenwein, Matthias Opel, M.S. Ramachandra Rao, and Rudolf Gross  
[arXiv:1612.07239](#), submitted for publication (2016).
47. **Frequency control and coherent excitation transfer in a nanostring resonator network**  
 Matthias Pernpeintner, Philip Schmidt, Daniel Schwienbacher, Rudolf Gross, Hans Huebl  
[arXiv:1612.07511](#), submitted for publication (2016).
48. **Dark-Photon Search using Data from CRESST-II Phase 2**  
 G. Angloher, P. Bauer, A. Bento, C. Bucci, L. Canonica, X. Defay, A. Erb, F. v. Feilitzsch, N. Ferreiro Iachellini, P. Gorla, A. Gütlein, D. Hauff, J. Jochum, M. Kiefer, H. Kluck, H. Kraus, J.C. Lanfranchi, J. Loebell, M. Mancuso, A. Münster, C. Pagliarone, F. Petricca, W. Potzel, F. Pröbst, R. Puig, F. Reindl, K. Schäffner, J. Schieck, S. Schönert, W. Seidel, L. Stodolsky, C. Strandhagen, R. Strauss, A. Tanzke, H.H. Trinh Thi, C. Türkoçğlu, M. Uffinger, A. Ulrich, I. Usherov, S. Wawoczny, M. Willers, M. Wüstrich, A. Zöllner  
[arXiv:1612.07662](#), submitted for publication (2016).
49. **Magnon mode selective spin transport in compensated ferrimagnets**  
 Joel Cramer, Er-Jia Guo, Stephan Geprägs, Andreas Kehlberger, Yurii P. Ivanov, Kathrin Ganzhorn, Francesco Della Coletta, Matthias Althammer, Hans Huebl, Rudolf Gross, Jürgen Kosel, Mathias Kläui, and Sebastian T. B. Goennenwein  
 Nano Letter, submitted for publication (2016).



The total number of citations per year of papers published by members of WMI since 1996. This number has about tripled within the last fifteen years and is exceeding 1900 in 2016.



## Bachelor, Master, Doctoral, and Habilitation Theses

### A. Completed and Ongoing Habilitation Theses

The promotion of highly qualified young scholars is a key concern of WMI. The fostering of young scholars goes hand in hand with equipping them to stand on their own in fields that are very competitive on both the national and international scales.

#### 1. Dr. Frank Deppe

Frank Deppe was accepted as a “*Habilitand*” by the Faculty of Physics of TU Munich in October 2010. He then started the habilitation process under the scholarly guidance of a *Fachmentorat* committee consisting of Rudolf Gross (TU Munich, chairman), Jonathan Finley (TU Munich) and Enrique Solano (Universidad del País Vasco and Ikerbasque Foundation, Bilbao, Spain). The *Fachmentorat* is appointed by the Departmental Council for the assessment of the written habilitation thesis and the continuous evaluation of the habilitation project. Meanwhile Frank Deppe submitted his habilitation thesis entitled *Microwave Quantum Science with Superconducting Circuits* to the Faculty of Physics of TU Munich.



It was evaluated positively by the *Fachmentorat* committee and several international experts. It was finally accepted by the Faculty of Physics of TU Munich in October 2016. WMI congratulates Frank Deppe on the successful completion of the habilitation process, which is documented by a certificate signed by the President and the Dean of the Technical University of Munich.

In the past few years, Frank Deppe developed into an internationally renowned junior scientist. He was project leader within the Cooperative Research Center 631 on “Solid State Quantum Information Processing” and presently is Associate Member within the Excellence Cluster “Nanosystems Initiative Munich”. He also was principal investigator in several European Projects such as the EU Collaborative Project (call identifier FP7-ICT-2011-C) on *Quantum Propagating Microwaves in Strongly Coupled Environments – PROMISCE* and the Marie Curie Network for Initial Training (call identifier FP7-PEOPLE-2010-ITN) on *Circuit and Cavity Quantum Electrodynamics (CCQED)*.

#### 2. Dr. Mathias Weiler

Mathias Weiler joined WMI in December 2014 after a two-year postdoctoral stay at the National Institute of Standards and Technology, Boulder, Colorado, USA, where he was working on AC spin currents and spin current transport. His stay abroad was supported by a DAAD fellowship. He started the habilitation process at TU Munich in June 2015 with Rudolf Gross (TU Munich), Christian Pfleiderer (TU Munich) and Christian Back (University of Regensburg) acting as the *Fachmentorat* committee. The research topic of his habilitation project is *Spin-Orbit Interactions in Magnetic Thin Film Systems*.



Mathias Weiler already was taking over the lectures on *Magnetism* and *Spin Electronics* within the winter semester 2015/2016 and the summer semester 2016, respectively, and was contributing to several WMI seminars.

### 3. Dr. Matthias Althammer

Matthias Althammer joined WMI in December 2013 after a postdoctoral stay (10/2012 – 11/2013) at the Center for Materials for Information Technology, University of Alabama, Tuscaloosa, USA, where he worked on oxide based spintronics. From 05/2014 to 02/2015 he was on leave from WMI to acquire experience in industry as an Engineering Consultant at Esprit Engineering GmbH, Munich.

Matthias Althammer was accepted as a “*Habilitand*” by the Faculty of Physics of TU Munich in January 2016. In his case, Rudolf Gross (TU Munich), Martin Brandt (TU Munich) and Arunava Gupta (MINT Center, University of Alabama) form the *Fachmentorat* committee. The research topic of his habilitation project is *Experimental Study of Spin-dependent Transport Phenomena*.





## B. Completed and Ongoing Ph.D. Theses

### Completed Ph.D. Theses:

1. **Nanomechanical Hybrid Systems**  
Matthias Pernpeintner, Technical University of Munich, August 2016.
2. **Controlled Interactions in Superconducting Quantum Circuits**  
Karl Friedrich Wulschner, Technical University of Munich, September 2016.
3. **Superconductivity and Competing Ordered States in Layered Organic Metals**  
Michael Kunz, Technical University of Munich, October 2016.
4. **Single Excitation Transfer in the Quantum Regime: A Spin-Based Solid State Approach**  
Christoph Wilhelm Zollitsch, Technical University of Munich, December 2016.



The four Ph.D. students of the Walther-Meißner-Institute finishing their Ph.D. theses in 2016.

**Ongoing Ph.D. Theses:**

5. **Vibrational Investigations of Luminescence of Molecules**  
Nitin Chelwani, Technical University of Munich, since September 2010.
6. **All Optical Quantum Computing**  
Max Häberlein, Technical University of Munich, since Dezember 2010.
7. **Circuit Quantum Electrodynamics Experiments with Tunable Flux Qubits**  
Jan Goetz, Technical University of Munich, since January 2012.
8. **Spin Transfer Torque Mediated Magnetization Dynamics**  
Michael Sebastian Schreier, Technical University of Munich, since Dezember 2012.
9. **Untersuchung der verschiedenen Phasen eisenbasierter Supraleiter mittels Raman-Streuung**  
Andreas Baum, Technical University of Munich, since April 2012.
10. **Quantum Information Processing with Propagating Quantum Microwaves**  
Peter Eder, Technical University of Munich, since November 2012.
11. **Spin dynamics and spin transport in solid state systems**  
Hannes Maier-Flaig, Technical University of Munich, since November 2013.
12. **A Comparative Study of the Phase Diagrams of CuO<sub>2</sub> and Fe-based Compounds**  
Thomas Böhm, Technical University of Munich, since December 2013.
13. **Circuit Quantum Electrodynamics with Three-dimensional Cavities**  
Edwar Xie, Technical University of Munich, since December 2013.
14. **Spin Currents in Ferrimagnetic Materials**  
Kathrin Ganzhorn, Technical University of Munich, since December 2014.
15. **Chains of Nonlinear and Tunable Superconducting Resonators**  
Michael Fischer, Technical University of Munich, since January 2015.
16. **Magnetization Dynamics in Coupled Photon/Phonon-Magnon Systems**  
Stefan Klingler, Technical University of Munich, since February 2015.
17. **Nanomechanical Quantum Systems**  
Philip Schmidt, Technical University of Munich, since October 2015.
18. **Magnetic Resonance at Millikelvin Temperatures**  
Stefan Weichselbaumer, Technical University of Munich, since December 2015.
19. **Untersuchung des Wärmetransports in porösen Pulvermedien zur Entwicklung einer ökonomischen Hochtemperatur-Vakuumsuperisolation auf Perlitbasis für Anwendungen in Wärmespeichern bis zu 700°C**  
Matthias Johannes Demharter, Technical University of Munich, since February 2016.
20. **Quantum gates with continuous variable microwaves**  
Stefan Pogorzalek, Technical University of Munich, since March 2016.
21. **Momentum and Spatially Resolved Raman Experiments in Correlated Systems**  
Daniel Jost, Technical University of Munich, since October 2016.

## C. Completed and Ongoing Bachelor and Master Theses

### Completed Master Theses:

1. **Magnetoresistance of the Electron-underdoped Cuprate Superconductor  $\text{Nd}_{2-x}\text{Ce}_x\text{CuO}_4$**   
Ahmed Alshemi, Masterarbeit, LMU Munich, January 2016.
2. **Spin Fluctuations and Superconductivity in Doped  $\text{BaFe}_2\text{As}_2$**   
Daniel Jost, Masterarbeit, Technical University of Munich, Januar 2016.
3. **Entwicklung eines Aerosolelektrometers zur ladungsbasierten Messung von ultrafeinen Partikeln und Nanopartikeln sowie Kalibrierung von Partikelanzahlmesssystemen für Verbrennungsmotorabgase**  
Philipp Link, Masterarbeit, Technical University of Munich, Februar 2016.
4. **Magnetic Field and Pressure Effects in the Layered Organic Superconductor  $\alpha\text{-(BEDT-TTF)}_2\text{TIHg(SCN)}_4$**   
Luzia Höhle, Masterarbeit, März 2016.
5. **Broadband-Spectroscopy of Magnetic Materials at Low Temperatures**  
Philip Louis, Masterarbeit, Technical University of Munich, März 2016.
6. **Circuit Nano-electromechanics, Transmon Qubits, Nano-strings and Resonators**  
Daniel Schwienbacher, Masterarbeit, Technical University of Munich, Mai 2016.
7. **Fluctuations and Superconductivity in  $\text{Ba}_{0.78}\text{K}_{0.22}\text{Fe}_2\text{As}_2$**   
Ramez Hosseinian Ahangharnejhad, Masterarbeit, Technical University of Munich, August 2016.
8. **Laser ARPES Investigation of the Semi-Metallic Transition Metal Dichalcogenides  $\text{WTe}_2$  and  $\text{MoTe}_2$**   
Irène Cucchi, Masterarbeit, TU München, Juli 2016.
9. **Investigation of Spin Hall Magnetoresistance in Erbium Iron Garnet/Platinum Systems**  
Hiroto Sakimura, Masterarbeit, Technical University of Munich, Oktober 2016.
10. **Noncommutation and Finite-time Correlations with Propagating Quantum Microwave States**  
Patrick Yard, Masterarbeit, Technical University of Munich, November 2016.
11. **Shubnikov-de Haas Effect and Magnetic Breakdown in the Layered Organic Superconductor  $\kappa\text{-(BEDT-TTF)}_2\text{Cu(NCS)}_2$**   
Sergej Fust, Masterarbeit, Technical University of Munich, November 2016.
12. **Spin Transport in Magnetic Nanostructures**  
Tobias Wimmer, Masterarbeit, Technical University of Munich, November 2016.
13. **Characterization of Hysteretic Flux-driven Josephson Parametric Amplifier**  
Martin Betzenbichler, Masterarbeit, Technical University of Munich, Oktober 2016.

### Completed Bachelor Theses:

14. **Aufbau eines Messstabs für winkelaufgelöste Magnetotransportmessungen**  
Claudio De Rose, Bachelorarbeit, Technical University of Munich (2016).
15. **Towards a Compact 3D Quantum Memory**  
Daniel Repp, Bachelorarbeit, Technical University of Munich (2016).
16. **Magnetic Quantum Oscillations in the Organic Antiferromagnetic Superconductor  $\kappa\text{-(BETS)}_2\text{FeBr}_4$**

Florian Kollmannsberger, Bachelorarbeit, Technical University of Munich (2016).

17. **Spin Hall Magnetoresistance in Pt|ErFeO<sub>3</sub>-Hybrid Structures**  
Daniel Singh, Bachelorarbeit, Technical University of Munich (2016).

**Ongoing Master Theses:**

18. **Characterization of a single photon**  
Le anh Tuan, Masterarbeit, Technical University of Munich, since January 2016.
19. **Magnetic Fluctuations and Superconductivity in FeSe**  
Merlin Mitschek, Masterarbeit, Technical University of Munich, since April 2016.
20. **Defining Manufacturing Conditions for an Electrochemical Sensor**  
Sebastian Meier, Masterarbeit, Technical University of Munich, since April 2016.
21. **Thin Film Fabrication for Spin Caloritronic Experiments**  
Johanna Fischer, Masterarbeit, Technical University of Munich, since October 2016.
22. **Tunneling Spectroscopy in Conductive Ferromagnets**  
Michaela Schleuder, Masterarbeit, Technical University of Munich, since October 2016.
23. **High-field Magnetoresistance Probing the Electronic State of an Organic Superconductor in the Vicinity of the Mott-Insulating Transition**  
Sebastian Oberbauer, Masterarbeit, Technical University of Munich, since October 2016.
24. **Thin Film Samples for Spin Caloritronics**  
Sarah Gelder, Masterarbeit, Technical University of Munich, since October 2016.
25. **Magnon-Phonon Interaction in Magnetoelastic Surface Acoustic Wave Transducers**  
Clemens Mühlenhoff, Masterarbeit, Technical University of Munich, since October 2016.
26. **Magnetization Dynamics and Damping at mK Temperatures**  
Lukas Liensberger, Masterarbeit, Technical University of Munich, since October 2016.
27. **Quantum simulations of many-body systems with superconducting devices**  
Christian Alexander Besson, Masterarbeit, Technical University of Munich, since October 2016.
28. **Pure spin currents in metals and insulators**  
Saki Matsuura, Masterarbeit, Technical University of Munich, since October 2016.
29. **Study of Twin Boundaries in YBa<sub>2</sub>Cu<sub>3</sub>O<sub>6+x</sub> Using Tip-enhanced Raman Scattering (TERS)**  
Jan-Robin Scholz, Masterarbeit, Technical University of Munich, since October 2016.
30. **Remote State Preparation with Quantum Microwaves**  
Behdad Ghaffari, Masterarbeit, Technical University of Munich, since November 2016.

## Research Projects

A large number of our research projects are benefiting from the collaboration with external groups in coordinated research projects, as well as from individual collaborations, exchange programs and visitors. Most collaborations are based on joint projects, which are funded by different research organizations (see list below). A considerable number of collaborations also exists with universities, other research institutions and industry without direct financial support.

### A. German Research Foundation: Excellence Initiative

#### Cluster of Excellence “Nanosystems Initiative Munich”

1. Research Area I: *Quantum Nanophysics*  
F. Deppe, S.T.B. Gönnerwein, R. Gross, H. Huebl, A. Marx
2. Research Area II: *Hybrid Nanosystems*  
S.T.B. Gönnerwein, R. Gross, H. Huebl

### B. German Research Foundation: Collaborative Research Centers

#### Transregional Collaborative Research Center TRR 80: “From Electronic Correlations to Functionality”

1. Project A2: *Spatially and Momentum Resolved Raman Studies of Correlated Systems*  
R. Hackl

### C. German Research Foundation: Priority Programs

1. Pulsed Electron Paramagnetic Resonance at Millikelvin Temperatures  
within the DFG Priority Program 1601 *New frontiers in sensitivity for EPR spectroscopy: from biological cells to nano materials*  
H. Huebl (Az. HU 1896/2-1)
2. Spin-dependent thermo-galvanic effects: experiment  
within the DFG Priority Program 1538 *Spin-Caloric Transport – SpinCAT*  
R. Gross (Az. GR 1132/18-2)
3. Spin-dependent thermo-galvanic effects: experiment  
within the DFG Priority Program 1538 *Spin-Caloric Transport – SpinCAT*  
S.T.B. Gönnerwein, R. Gross (Az. GO 944/4-1, GO 944/4-2)
4. Project: *Raman study of electron dynamics and phase transitions in iron-pnictide compounds*  
within the DFG Priority Program 1458 *“High-Temperature Superconductivity in Iron-Pnictides”*  
R. Hackl, R. Gross, B. Büchner, D. Johrendt, C. Honerkamp (Az. HA 2071/7-1, HA 2071/7-2)

### D. German Research Foundation: Research Projects

1. Project: *Correlated Quantum Microwaves: Continuous-Variables for Remote State Preparation and Quantum Illumination*  
K.G. Fedorov (Az. FE 1564/1-1)



2. Project: *Exotic Superconductivity in Strongly Anisotropic Correlated Organic Metals in the Vicinity of Insulating Phases*  
M. Kartsovnik, W. Biberacher, R. Gross (Az. KA 1652/4-1)
3. Project: *Interaction Between Spin, Lattice, and Charge in Correlated Metals without Inversion Center*  
R. Hackl, R. Gross (Az. HA 2071/8-1)

## E. European Union

1. EU Collaborative Project (call identifier H2020-FETOPEN-1-2016-2017), project title *Magnetomechanical Platforms for Quantum Experiments and Quantum Enabled Sensing Technologies – MaQSens*  
H. Huebl, R. Gross, Grant Agreement No. 736943  
partners: several European Universities and research facilities.
2. EU Collaborative Project (call identifier FP7-ICT-2011-C), project title *Quantum Propagating Microwaves in Strongly Coupled Environments – PROMISCE*  
F. Deppe, A. Marx, R. Gross, Grant Agreement no. 284566  
partners: several European Universities and research institutions.

## F. Free State of Bavaria

1. International PhD Programme of Excellence *Exploring Quantum Matter (ExQM)* within the Elite Network of Bavaria, Project No. K-NW-2013-231  
R. Gross, A. Marx, F. Deppe, K. Fedorov  
Partners: jointly with 12 quantum physics research groups at the TU Munich, the LMU Munich, and the Max Planck Institute of Quantum Optics.

## G. Max Planck Society

1. International Max Planck Research School for *Quantum Science and Technology (IMPRS-QST)*, Spokesperson: Prof. Dr. J. Ignacio Cirac  
R. Gross, A. Marx, F. Deppe, K. Fedorov  
with several partners from the Max Planck Institute of Quantum Optics, the Ludwig-Maximilians-Universität Munich and the Technical University of Munich.

## H. Bavaria California Technology Center (BaCaTeC)

1. Project: *Nematic Order and New Phases in Quantum Materials*  
R. Hackl,  
partners: Profs. Thomas Devereaux, Steve Kivelson, and Sri Raghu (Stanford University)

## I. German Academic Exchange Service

1. Project-based Personnel Exchange Programme (PPP) with Serbia (project 56267076: Fe-based superconductors), collaboration with the Institute of Physics, University of Belgrade (Dr. Z.V. Popovic).  
R. Hackl
2. Project-based Personnel Exchange Programme (PPP) with India (project 57085749: Spin Current Generation and Detection Using FMI/NM Hybrids), collaboration with the IIT Madras, Chennai (Prof. Dr. M. S. Ramachandra Rao).  
R. Gross

## J. Scientific Instrumentation

1. UHV Sputtering System for Superconducting and Magnetic Materials  
R. Gross, DFG-GZ: INST 95-1333-1 FUGG
2. Critical Point Dryer Leica EM CPD 300  
BMBF project Q.com, FKZ: 16KISo110 4515.1545.4556
3. Laser Writer SPS – 4 PICO  
BMBF project Q.com, FKZ: 16KISo110 4515.1545.4556



## Conferences, Workshops, Public Outreach

The Walther-Meißner-Institute has organized/co-organized several conferences, workshops and symposia in 2016. It also was participating in several public outreach events aiming at making science accessible to the public.

### A. 27. Edgar Lüscher Seminar 2016 (20 – 26 February 2016, Klosters, Switzerland)

Rudolf Gross organized a symposium on *Nanomechanics* at the 27. Edgar-Lüscher Seminar together with Joachim Mayer from RWTH Aachen. The symposium was addressing modern aspects of nanomechanical systems, ranging from fracture and flow on a nanoscale to the nonclassical behavior of nanomechanical systems. The talks included Cynthia Volkert (University of Göttingen, Watching things fail: In-situ Electron Microscopy of Fracture and Flow), Hans Hübl (WMI, Nanomechanics – Sensing Vibes and Playing Tunes) and Ralf Riedinger (University of Vienna, Nonclassical correlations between single photons and phonons from a mechanical oscillator).

### B. Spring Meeting of the Condensed Matter Section of DPG (06 – 11 March 2016, Regensburg, Germany)

In 2016, members of the Walther-Meißner-Institute have orga-



nized a Symposium and Focus Session at the Spring Meeting of the Condensed Matter Section of the German Physical Society.

#### Symposium on “Quantum Signatures in Magnetism” (Wednesday, 09 March 2016, 15:00 – 17:45h)

The Symposium was organized by Hans Hübl, Sebastian Gönnerwein and Rudolf Gross of WMI to bring together experts from different but overlapping fields of magnetization dynamics, superconducting quantum circuits, quantum metrology in semiconductors, and in a broader sense quantum technology based solid-state spectroscopy. It was a joint symposium of the Magnetism Division (MA), the Low Temperature Physics Division (TT), the Semiconductor Physics Division (HL), and the Surface Science Division (O) of DPG and aimed to provide an overview of the recent exciting developments.

Magnetism is a quantum phenomenon. Nevertheless, most studies investigate large samples containing many spins, such that the magnetic properties can be described and understood in terms of classical physics. Of particular current interest are magnetization dynamics viz. magnetization relaxation and damping, since the dynamical properties of magnets are key for the fast magnetic switching employed in a manifold of applications. Magnetization dynamics are typically studied using magnetic resonance techniques. The advent of quantum information technologies based on superconducting circuits has triggered a revolution in magnetic resonance spectroscopy. Single photon viz. single spin sensitivity, and the possibility to probe magnetization dynamics employing tailored quantum states, offer a completely new toolbox for modern experiments addressing the quantum properties of magnets.

### Focus Session on “High Temperature Superconductivity in Hydrides” (Thursday, 10 March 2016, 09:30 – 12:45h)

The Focus Session was organized by Rudi Hackl of WMI to discuss recent results from experimental and theoretical studies on high temperature superconductivity in hydrides. The Focus Session was addressing this fascinating topics in six invited talks of leading international experts.

The recent discovery of superconductivity at a transition temperature as high as 203 K in H<sub>3</sub>S was a big surprise although it was predicted theoretically. While unstable at ambient conditions H<sub>3</sub>S is a result of the dissociation of H<sub>2</sub>S for an applied pressure in excess of 100 GPa in accordance with structure predictions. The transition temperature can be estimated with high accuracy by Density Functional Theory for superconductors.

### C. International Workshop “Iron-Based Superconductors” (September 13 – 16, 2016, Munich Residence, Germany)

Almost 100 scientists from three continents met in the Munich residence for the final conference of the DFG Priority Program “High-Temperature Superconductivity in Iron Pnictides” (SPP 1458). The International Workshop “Iron-Based Superconductors” (IBS2016) was jointly organized by Rudi Hackl (WMI), Bernd Büchner (IFW-Dresden) and Dirk Johrendt (TUM).



Iron-based superconductors with high transition temperatures were not only unexpected when discovered in 2008 but turned out to be interesting model systems for studying unconventional Cooper pairing in close proximity to competing phases. Apparently they are another class of superconductors in which electron-phonon interaction does not play a dominant role. The presentations and discussions comprised systematic studies of a broad spectrum of materials and new approaches to materials engineering which may pave the way for future compounds. Examples were superconductivity above 200 K in fairly conventional H<sub>3</sub>S and above 100 K in thin films of FeSe on SrTiO<sub>3</sub>, where several pairing mechanisms may cooperate.

The 24 invited lectures demonstrated that superconductivity is a multidisciplinary field in these days which includes new types of charge and spin order, a broad variety of interaction channels, materials science and applications. The six-years period of the DFG Priority



Program 1458 lead to a plethora of unexpected insights and was very productive. It is our ambition to bring some of the new ideas to fruition.

#### D. Course 3 on “Physics and Electronics in Everyday Life” of the Ferienakademie (18 – 30 September 2016, Sarntal, Italy)



As in the previous years, WMI co-organized the course on “Physics and Electronics in Everyday Life” of the Ferienakademie. The Ferienakademie is jointly organized by the Technical University of Munich, the University of Erlangen/Nuremberg, and the University of Stuttgart to motivate and foster highly talented students. It takes place annually at Sarntal in the Italian Alps. The course was held by Rudolf Gross (WMI) together with

Prof. Dr. Gert Denninger (University of Stuttgart), and Prof. Dr. Vojislav Krstic (University of Erlangen-Nuremberg) as visiting lecturer.

Within the course 3 on “Physics and Electronics in Everyday Life” of Ferienakademie the students prepare presentations on physical phenomena and problems which play an important role in our everyday-life, but usually are poorly understood. Besides the seminars talks there are intensive discussions with the professors and members of other courses. A particular

emphasis of course 3 of Ferienakademie is put on hands-on experiments. They aim at providing students an in-depth insight into physical phenomena by performing experiments by themselves. WMI contributes with a variety of experiments on superconductivity, magnetism and low temperature properties of solids. A relaxing and inspiring atmosphere is provided by a varied supporting program (mountain hiking, excursions to Bozen, table tennis and



chess tournament, Törgelen, etc.). Moreover, within the Ferienakademie the students have the opportunity to meet leaders from industry, politics and science.

### E. Day of Open House 2016 (22 October 2016, Research Campus Garching, Germany)

The Walther-Meißner-Institute contributed to the *Open House Event 2016* (Tag der offenen Tür) on the Research Campus Garching by an attractive program for everybody interested in science. In talks and demonstration experiments, an insight into current research projects in the fields of superconductivity, low temperature research, and nanotechnology was given. In addition, the WMI facilities for thin film technology and single crystal growth could be visited to get an impression of state-of-the-art materials technology. Furthermore, visitors were informed on latest developments in the field of quantum science & technology. In one of the low temperature laboratories they could get insight into the experimental study of superconducting qubits and quantum circuits, in particular on light-matter interaction and coherent quantum evolution. WMI also offered hourly talks on the topics *On the Way to Quantum Computers* (Rudolf Gross) and *Superconductivity and Superfluidity* (Dietrich Einzel) which were completely overcrowded.



Particularly fascinating for visitors are demonstration experiments on low temperature phenomena. Therefore, WMI has made a considerable effort to set up high quality demonstration experiments on the Meißner effect in superconductors (superconducting levitation) and the fountain effect in superfluid  $^4\text{He}$ . For kids and pupils the superconducting racetrack of WMI and the large number of fascinating hands-on experiments with liquid nitrogen are always highly attractive. They can experience that low temperature physics is a lot of fun.



## Cooperations

Other collaborations without direct project funding involve:

- Stanford University, Stanford, USA (T.P. Devereaux, M. Greven, Z.-X. Shen, I. Fisher, B. Moritz, H.N. Ruiz, C. Platt)
- Universidad del País Vasco and Ikerbasque Foundation, Bilbao, Spain (E. Solano, M. Sanz, L. Lamata)
- Instituto de Física Fundamental, CSIC, Madrid, Spain (J.J. Garcia-Ripoll)
- Central Research Institute of the Electric Power Industry, Tokyo, Japan (Dr. S. Ono, Dr. Y. Ando)
- Green Innovation Research Laboratories, NEC Corporation, Japan (Y. Nakamura, J.S. Tsai, K. Inomata, T. Yamamoto)
- University of Tohoku, Sendai, Japan (G.E.W. Bauer, E. Saitoh, J. Barker)
- Japan Science and Technology Agency, Sendai, Japan (H. Adachi, S. Maekawa)
- University of Tokyo, Tokyo, Japan (Y. Nakamura)
- European Synchrotron Radiation Facility (ESRF), Grenoble (H. Müller, F. Wilhelm, K. Ollefs)
- Lund University, Lund, Sweden (D. Mannix)
- Materials Science Research Centre, IIT Madras, India (M.S. Ramachandra Rao, J. Mukherjee)
- Solid State Chemistry Unit, Indian Institute of Science, Bagalore, Indian (D.D. Sarma)
- ETH-Zurich, Switzerland (A. Wallraff, L. Degiorgi, R. Monnier, Dr. M. Lavagnini)
- University of Geneva, Geneva, Switzerland (I. Maggio-Aprile)
- Chalmers University of Technology Gothenburg, Sweden (P. Delsing, G. Wendin)
- University of Alabama, MINT Center, Tuscaloosa, USA (A. Gupta)
- Helsinki University of Technology, Materials Physics Laboratory, Finland (T. Heikkilä)
- Delft University of Technology, Kavli Institute of NanoScience, Delft, The Netherlands (T.M. Klapwijk, G.E.W. Bauer)
- B. Verkin Institute for Low Temperature Research and Engineering, Kharkov, Ukraine (V.G. Peschansky)
- Landau Institute for Theoretical Physics, Chernogolovka, Russia (P. Grigoriev)
- University of Oxford, Clarendon Laboratory, England (A. Karenowska)
- Russian Academy of Sciences, Chernogolovka, Russia (N. Kushch, A. Palnichenko)
- High Magnetic Field Laboratory, Dresden (E. Kampert, J. Wosnitza)
- High-Magnetic-Field Laboratory, Grenoble, France (I. Sheikin)
- High Magnetic Field Laboratory, Toulouse (C. Proust, D. Vignolles)
- National High Magnetic Field Laboratory, Tallahassee, USA (J. Brooks)
- IFW Dresden, Germany (B. Büchner, J. Fink, S.V. Borisenko, M. Knupfer, A. Thomas)
- Max-Planck-Institut für Festkörperforschung, Stuttgart (B. Keimer, L. Boeri)
- University of Tübingen, Germany (R. Kleiner, D. Kölle)
- University of Würzburg, Germany (W. Hanke, F. Assaad, C. Honerkamp, M. Potthoff)
- University of Augsburg, Germany (P. Hänggi, A. Wixforth, A. Kampf, A. Loidl, J. Deisenhofer, V. Tsurkan)
- University of Hamburg, Germany (G. Meier, W. Wurth)

- University of Leipzig, Germany (J. Haase)
- University of Ulm, Abt. Halbleiterphysik, Germany (W. Limmer, M. Abdi)
- RWTH Aachen, Germany (G. Güntherodt, B. Beschoten)
- Ernst-Moritz-Arndt Universität Greifswald, Germany (M. Münzenberg)
- Martin-Luther-Universität Halle, Germany (G. Woltersdorf)
- Universität Regensburg, Institut für Experimentelle und Angewandte Physik, Germany (Ch. Back)
- Universität Bielefeld, Germany (G. Reiss, A. Thomas, T. Kuschel)
- Freie Universität Berlin, Berlin, Germany (R. Di Candia)
- University of British Columbia, Vancouver, Canada (D. Bonn, A. Damascelli)
- TU München, Physics Department, Germany (P. Böni, Ch. Pfeleiderer, F.C. Simmel, Jean Come Lanfranchi, P. Müller-Buschbaum, M. Abdi)
- TU München, Walter Schottky Institut, Germany (G. Abstreiter, M. Stutzmann, J. Finley, M. Brandt, A. Holleitner, U. Wurstbauer)
- TU München, Lehrstuhl für Technische Elektronik (M. Becherer)
- LMU München, Physics Department, Germany (J. von Delft, E. Frey, J. Rädler, S. Ludwig)
- LMU München, Chemistry Department, Germany (H. Ebert, D. Ködderitzsch)
- Universidad de Zaragoza, Departamento de Física de la Materia Condensada, Spain (L. Morellon, J.M. de Teresa, D. Zueco)
- EPFL Lausanne, Switzerland (T. Kippenberg, H. Ronnov)
- University of New South Wales, Sydney, Australia (M. Simmons, A. Morello)
- McMaster University, Hamilton, Canada (J.P. Carbotte)
- Technische Universität Graz, Austria (E. Schachinger)
- Universität Konstanz (A. Leitenstorfer, E. Weig, J. Demsar, A. Pashkin)
- BMW Group, Munich, Germany (J. Schnagl, W. Stadlbauer, G. Steinhoff)
- Siemens AG, CT MM 2, Munich, Germany (R. Matz, W. Metzger)
- Attocube, Munich, Germany (K. Karrai, D. Andres, E. Hoffmann)
- THEVA Dünnschichttechnik, Ismaning, Germany (W. Prusseit)
- Johannes-Kepler-Universität Linz, Institut für Halbleiter- und Festkörperphysik, Austria (A. Ney)
- Jülich Centre for Neutron Science JCNS, Garching, Germany (S. Pütter)
- Université de Toulouse, Laboratoire de Physique Théorique, Toulouse, France (R. Ramazashvili)
- Lawrence Berkeley National Laboratory, Berkeley, USA (A. F. Kemper)
- University of Belgrade, Belgrade, Serbia (Z. Popovic, N. Lazarevic, D. U. Ralevic, R. Gajic)
- University of Aveiro, Portugal (N. A. Sobolev)
- Macquarie University, MQ Research Centre for Quantum Science and Technology, Australia (J. Twamley)
- Instituto de Ciencia de Materiales de Sevilla, Spain (J. Poyato, J.L. Perez-Rodriguez)
- Hungarian Academy of Sciences, Research Institute for Solid State Physics and Optics, Budapest, Hungary (K. Kamaras, I. Tüttö, J. Balogh)
- University of Rome "La Sapienza", Rome, Italy (S. Caprara, C. Di Castro, M. Grilli)

- 
- Hungarian Academy of Sciences, Budapest University of Technology and Economics, Budapest, Hungary (A. Viroztek, A. Zawadowski, G. Mihály)
  - Goethe University, Frankfurt, Germany (S. Winter)
  - National Institute of Standards and Technology, Boulder, USA (H. Nembach, J. Shaw, T.J. Silva)
  - University of Manitoba, Winnipeg, Canada (C.-M. Hu)
  - Kyoto University, Japan (M. Shiraishi)
  - Technische Universität Braunschweig, Germany (D. Menzel, S. Süllo)
  - University of Vienna, Austria (M. Aspelmeyer)
  - Heriot Watt University, Edinburgh, Scotland (M. Hartmann)
  - Universidad Nacional de Colombia, Colombia (O. Moran)
  - University of Birmingham, UK (E.M. Forgan)
  - Fachbereich Physik, Universität Osnabrück, Osnabrück, Germany (J. Wollschläger)
  - Technische Universität Dresden, Germany (S.T.B. Gönnenwein)
  - Fritz Haber Institut Berlin, Germany (T. Seifert, T. Kampfrath)
  - Universität des Saarlandes, Saarbrücken (F.K. Wilhelm-Mauch)
  - University of Groningen, The Netherlands (T. Palstra, M. Mostovoy, A. Aqeel)
  - Innovent Technologieentwicklung Jena, Germany (C. Dubs, O. Surzhenko)



## Stays abroad

Extended visits of members of the Walther-Meißner-Institute at foreign research laboratories:

1. **Mark Kartsovnik**  
Institute of Solid State Physics, Russian Academy of Sciences, Chernogolovka, Russia  
25. 05. - 05. 06. 2016
2. **Matthias Althammer**  
IIT Madras, Chennai, India  
16. 11. - 28. 11. 2016
3. **Rudolf Hackl**  
Institute of Physics, University of Belgrade, Serbia  
14. 11. - 26. 11. 2016
4. **Rudolf Hackl**  
Stanford Institute of Materials and Energy Sciences (SIMES), Stanford Linear Accelerator Center (SLAC), Stanford, USA  
23. 09. - 26. 09. 2016, 11. 10. - 14. 10. 2016
5. **Jan Goetz**  
Massachusetts Institute of Technology, Boston, USA  
06. 12. - 11. 12. 2016
6. **Mathias Weiler**  
National Institute of Standards and Technology, Boulder, CO, USA  
01 08. - 02. 09. 2016

## Conference Talks and Seminar Lectures

### Matthias Althammer

1. **Pure spin currents in ferromagnetic insulator/normal metal hybrids**  
Invited Talk, IIT Madras, India  
24. 11. 2016
2. **Spin Hall Magnetoresistance**  
Seminar Talk, Universität Konstanz, Germany  
09. 12. 2016

### Frank Deppe

1. **Displacement of propagating squeezed microwave states**  
Invited Talk, ScaleQIT International Conference 2016, Delft, The Netherlands  
27. - 29. 01. 2016
2. **Ultrastrong coupling with superconducting flux qubits**  
Invited Talk, Kavli Royal Society International Centre, Chicheley Hall, United Kingdom  
02. - 03. 03. 2016
3. **Ultrastrong coupling and beyond in superconducting circuits**  
Invited Talk, International Workshop on Ultra-Strong Light-Matter Interactions, Bilbao, Spain  
19. - 21. 09. 2016
4. **Continuous-variable propagating quantum microwaves**  
Munich Quantum Symposium, Garching, Germany  
27. - 28. 10. 2016

### Andreas Erb

1. **Single crystal growth of various oxide materials for basic research and applications**  
Invited Talk, French-German Workshop on Oxide, Dielectric and Laser Crystals, IKZ Berlin, Germany  
15. - 16. 09. 2016
2. **Single crystal growth of various oxide materials for basic research and applications**  
2nd Workshop Floating Zone Technique, IFW Dresden, Germany  
06. 04. 2016

### Kirill Fedorov

1. **Displacement of squeezed propagating microwave states**  
Spring Meeting of the American Physical Society (APS), Baltimore, USA  
14. - 18. 03. 2016
2. **Spin-boson model with engineered reservoirs**  
Spring Meeting of the American Physical Society (APS), Baltimore, USA  
14. - 18. 03. 2016
3. **Displacement of squeezed propagating microwave states**  
Spring Meeting of the DPG, Regensburg, Germany  
06. - 11. 03. 2016
4. **Quantum computing and communication with continuous microwaves**  
Solid State Colloquium, Physik-Department, Technische Universität München, Garching, Germany  
02. 06. 2016
5. **Finite-time correlations of balanced two-mode squeezing microwave states**  
Invited Talk, Kryoelektronische Bauelemente 2016, Freyburg, Germany  
09. - 11. 10. 2016

### Kathrin Ganzhorn

1. **Magnon transport in non-local structures**

Invited Talk, Workshop "Spins, waves and interactions", Greifswald, Germany

31. 08. - 02. 09. 2016

### Stephan Geprägs

1. **Non-collinear spin structure in compensated rare earth garnets**

Invited Talk, EMFL User Meeting, Toulouse, France

15. 06. 2016

2. **Pure spin currents in magnetic insulator / normal metal heterostructures**

Invited Talk, Nanoforum Linz, Austria

01. 07. 2016

3. **Pure spin currents in magnetic insulator / normal metal heterostructures**

Invited Talk, International Symposium on Metal and Insulator Spintronics, Yokohama, Japan

25. - 27. 11. 2016

### Jan Goetz

1. **Thermal microwave states acting on a superconducting qubit**

Spring Meeting of the DPG, Regensburg, Germany

07. - 09. 03. 2016

### Rudolf Gross

1. **Quantum Technology Based on Nanostructured Superconductors**

R. Gross

Invited Talk, International Conference on Nano Confined Superconductors and their Applications

03. - 07. 09. 2016, Garmisch-Partenkirchen, Germany.

2. **Quantum Computing with Superconducting Circuits**

Ferienakademie of Technical University of Munich, University of Erlangen and University of Stuttgart, Sarntal, Italy

18. - 30. 09. 2016

3. **Superconducting Quantum Circuits**

Invited Talk, Symposium on Modern trends in condensed matter physics, Bad Honnef, Germany

02. 11. 2016

4. **Auf dem Weg zum Quantencomputer**

Day of Open House, Garching Research Campus, Garching, Germany.

22. 10. 2016

### Rudolf Hackl

1. **Spin-driven nematicity and superconductivity in Fe-based compounds**

Invited Talk, 31. Workshop on Novel Materials and Superconductors, BSFZ Obertraun, Austria

08. 02. 2016

2. **Fluctuations and superconductivity in Fe-based compounds**

Invited Talk, International Conference "Quantum in Complex Matter", Ischia, Italy

26. 06. 2016

3. **Light scattering in correlated d- and f-electron systems**

Invited Talk, International Workshop on "Experiment and Theory of the Electronic Structure of Correlated f-Electron Materials", Temple University, Philadelphia, USA

16. 08. 2016

4. **Interactions and competing phases in unconventional superconductors**

Invited Talk, Naval Research Laboratory, Washington D.C., USA

18. 08. 2016

### Hans Hübl

1. **Circuit nano electromechanics**

Seminar Talk, SFB-Kolloquium, Universität Konstanz, Konstanz, Germany

02. 06. 2016

2. **Circuit nano electromechanics**  
Seminar Talk, Technical University of Vienna, Vienna, Austria  
23. 06. 2016
3. **Magneto-Transport**  
Tutorial, Antiferromagnetic Spintronics, Mainz, Germany  
27. 09. 2016
4. **Magnon Mediated Logic Gates, Determination of effective mechanical properties of a double-layer beam by means of a nano-electromechanical transducer**  
Invited Talk, Insulatronix 2016, Spitzbergen, Norway  
27. 05. 2016
5. **Nanomechanics - Sensing Vibes and Playing Tunes**  
Invited Talk, Lüscher Seminar, Klosters, Switzerland  
20. 02. 2016
6. **Resonators, Strings and Transmons**  
Invited Talk, MagQSens Workshop, Innsbruck, Austria  
26. 04. 2016
7. **All Acoustic Manipulation and Probing of Spin Ensembles**  
Invited Talk, SPICE Workshop, Quantum Acoustics, Mainz, Germany  
18. 05. 2016
8. **Broadband magnetic resonance spectroscopy of chiral magnetic insulators**  
Skyrmion Workshop, Technische Universität München, Germany  
25. 07. 2016
9. **Incoherent magnon transport in non-local devices**  
Invited Talk, Spin-Caloritronix 7, Utrecht, The Netherlands  
13. 07. 2016

### Mark Kartsovnik

1. **BETS-based organic conductors as archetypical magnetic/super-conducting nanostructures**  
Invited Talk, International Conference "Superstripes 2016: Quantum in Complex Matter, Superconductivity, Magnetism and Ferroelectricity", Ischia, Italy  
23. - 29. 06. 2016

### Achim Marx

1. **Thermal Microwave Fields meet Superconducting Qubits**  
Invited Talk, Munich Quantum Symposium 2016, Munich, Germany  
27. - 28. 10. 2016
2. **Thermal Microwave Fields meet Superconducting Qubits**  
Kryoelektronische Bauelemente 2016, Freyburg/Unstrut, Germany  
09. - 11. 10. 2016

### Matthias Opel

1. **Tiefe Temperaturen, Supraleitung und Spinelektronik**  
Invited Talk, Humboldt Academy for Science and Engineering, Gymnasium Vatterstetten, Germany  
16. 03. 2016
2. **Proximity Magnetism and Spin-Hall Magnetoresistance Effect in Pt Thin Films**  
Physikalisches Kolloquium, Universität Osnabrück, Osnabrück, Germany  
12. 05. 2016
3. **Static Magnetic Proximity Effects and Spin-Hall Magnetoresistance in Pt/Y<sub>3</sub>Fe<sub>5</sub>O<sub>12</sub> and Y<sub>3</sub>Fe<sub>5</sub>O<sub>12</sub>/Pt Bilayers**  
Invited Talk, Energy, Materials, Nanotechnology Meeting on Spintronics, Las Vegas, USA  
11. 10. 2016

### Mathias Weiler

1. **Spin Currents and Spin Dynamics**  
Universität Bayreuth, Bayreuth, Germany  
07. 06. 2016





## Appointments

### A. Sebastian Gönnerwein was appointed W<sub>3</sub> professor at TU Dresden

Priv.-Doz. Dr. Sebastian T. B. Gönnerwein received an offer for a W<sub>3</sub>-professorship for solid state physics from the Technical University of Dresden. He accepted the offer and moved to the Institute of Solid States Physics of TU Dresden in July 2016. At TU



Dresden he is focussing on the experimental study of multi-functional magnetic heterostructures and devices. His new position is tightly linked to the novel *Center for Transport and Devices of Emergent Materials (CTD)* at Dresden. On the one hand, we are very happy about the promotion of Sebastian Gönnerwein and congratulate him to his new position. On the other hand, we are of course sad about loosing an excellent scientist and a very nice colleague. We hope to see him often at WMI in future and are looking forward to a fruitful collaboration.

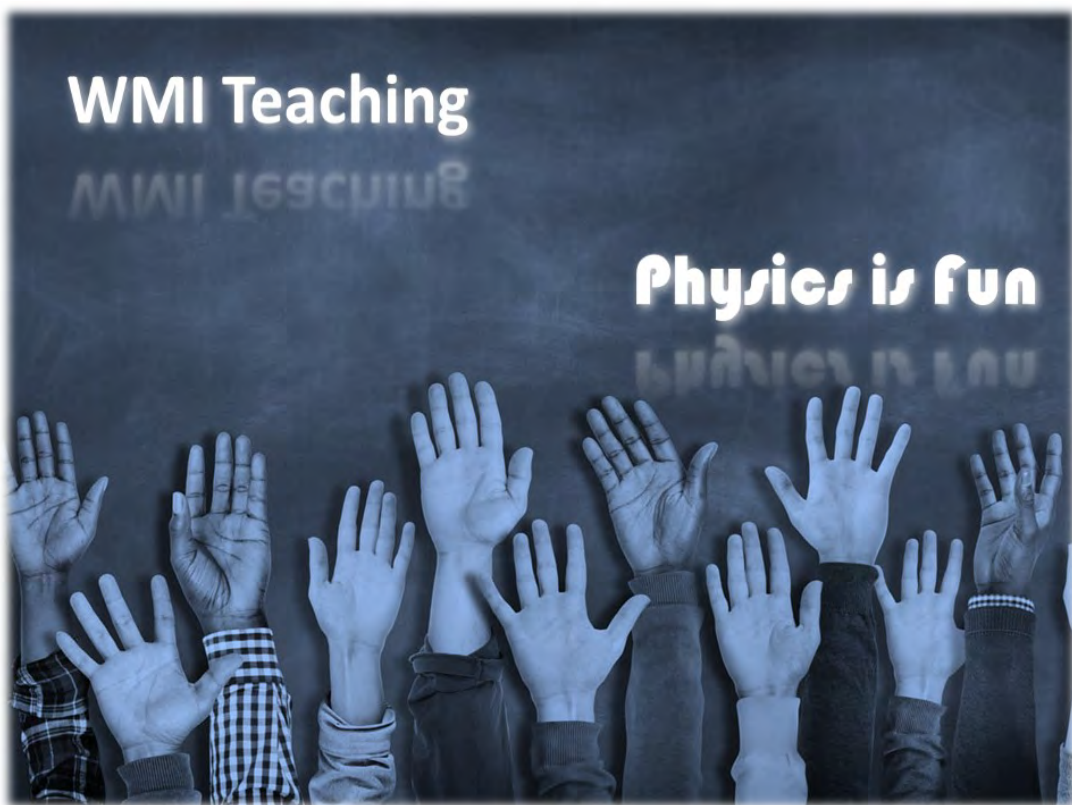
Sebastian Gönnerwein did his PhD in the group of Martin Stutzmann at Walter Schottky Institut of TU Munich on *Two-Dimensional Electron Gases and Ferromagnetic Semiconductors: Materials for Spintronics*. After finishing his PhD in July 2013 with "summa cum laude" he joined the group of Teun Klapwijk at the Kavli Institute of Nano-Science of TU Delft for about two years, supported by a fellowship of the German Research Foundation. At TU Delft, he worked on magnetotransport phenomena in ferromagnetic semiconductors and correlation effects in superconductor/ferromagnet nanostructures. In July 2005, Sebastian Gönnerwein came back to Munich and joined Walther-Meißner-Institute as a research staff member. He started his own junior group at WMI focussing on magnetism and spin electronics, and started the habilitation procedure at TU Munich. In 2010, Sebastian Gönnerwein finish the habilitation process and received the *venia legendi* in experimental physics from TU Munich.

For almost exactly 11 years Sebastian Gönnerwein not only was doing excellent research at WMI, but also setting up several experimental facilities and taking care about administrative tasks as the deputy director of WMI. He did an excellent job in every respect and was one of key players at WMI. In 2008, he received the Arnold-Sommerfeld Award of BAdW for his fundamental work on thin film and nanostructures of superconducting, magnetic and semiconducting materials and their application in novel spintronic devices. In 2015 he received the prestigious "Golden Chalk" (*Goldene Kreide*) for the best lecture of the bachelor course (condensed matter physics I and II). He also was principal investigator within the excellence cluster *Nanosystems Initiative Munich (NIM)* and the DFG Priority Programm 1538 *Spin-Caloric Transport – SpinCAT*. At present, his impressive publication list includes more than 100 publications in refereed journals with more than 3 300 citations (h-index: 32). Sebastian Gönnerwein certainly is an excellent example for the successful fostering of young talents at WMI.

## Membership in Advisory Boards, Committees, etc.

1. **Frank Deppe** is associate member of the Cluster of Excellence *Nanosystems Initiative Munich (NIM)*.
2. **Andreas Erb** is spokesman of the “Arbeitskreis Intermetallische und oxydische Systeme mit Spin- und Ladungskorrelationen” of the *Deutsche Gesellschaft für Kristallzüchtung und Kristallwachstum (DGKK)*.
3. **Sebastian Gönnerwein** is member and principal investigator of the Cluster of Excellence *Nanosystems Initiative Munich (NIM)*.
4. **Rudolf Gross** is member of the Scientific Advisory Board of the Bayerisches Geoinstitut, Bayreuth, Germany.
5. **Rudolf Gross** is member of the Scientific Advisory Board of the Institut de Ciència de Materials de Barcelona, Spain.
6. **Rudolf Gross** is member of the committee for the allocation of Alexander von Humboldt Foundation Research Awards.
7. **Rudolf Gross** is spokesman of the selection committee of the Stern-Gerlach-Medal of the German Physical Society.
8. **Rudolf Gross** is member of the Appointment and Tenure Board of the Technical University of Munich.
9. **Rudolf Gross** is member of the Executive Board of the Cluster of Excellence *Nanosystems Initiative Munich (NIM)* and coordinator of the Research Area 1 on *Quantum Nanosystems*.
10. **Rudolf Gross** is member of the *Munich Quantum Center (MQC)*.
11. **Rudolf Gross** is course leader at the Ferienakademie of the Universities Munich (TU), Stuttgart and Erlangen-Nürnberg since 2005.
12. **Rudolf Hackl** is deputy coordinator of the DFG Priority Program SPP 1458 on *High Temperature Superconductivity in the Iron Pnictides*.
13. **Rudolf Hackl** is member of the evaluation board of the neutron source Heinz Maier-Leibnitz (FRM II).
14. **Hans Hübl** is member and principal investigator of the Cluster of Excellence *Nanosystems Initiative Munich (NIM)*.
15. **Mark Kartsovnik** is member of the Selection Committee of EMFL (European Magnetic Field Laboratories).
16. **Mark Kartsovnik** is member of the International Advisory Committee of the 11<sup>th</sup> International Symposium on Crystalline Organic Metals Superconductors and Ferromagnets (ISCOM 2017).
17. **Matthias Opel** is one of the four elected members of the Speaker Council for the scientists of the Bavarian Academy of Sciences and Humanities.
18. **Matthias Opel** was member of the International Advisory Committee of the EMN (Energy, Materials, Nanotechnology) Meetings, Las Vegas, USA.
19. **Mathias Weiler** is member of the Editorial Review Board of IEEE Magnetics Letters.

# Teaching





## Lectures, Courses and other Teaching Activities

Several members of the Walther-Meißner-Institute give lectures and seminars at the Technical University of Munich.

### Matthias Althammer

- SS 2016
- Seminar: Spin Caloritronics and Spin Pumbing (with H. Hübl, M. Weiler)
  - Seminar: Current Topics in Magneto and Spin Electronics (with M. Brandt, H. Hübl, M. Weiler)
  - Seminar: Advances in Solid-State Physics (with R. Gross, H. Hübl, A. Marx, M. Opel)
- WS 2016/2017
- Magnetismus (Magnetism)
  - Übungen zu Magnetismus (Magnetism, Problem Sessions)
  - Seminar: Spin Caloritronics and Spin Pumping (with H. Huebl, M. Weiler)
  - Seminar: Advances in Solid-State Physics (with R. Gross, H. Hübl, A. Marx, M. Opel)
  - Seminar: Current Topics in Magneto and Spin Electronics (with H. Hübl, M. S. Brandt, M. Weiler)

### Frank Deppe

- WS 2015/2016
- Seminar: Superconducting Quantum Circuits (with R. Gross, A. Marx)
- SS 2016
- Angewandte Supraleitung: Josephson Effekte, supraleitende Elektronik und supraleitende Quantenschaltkreise (Applied Superconductivity: Josephson Effects, Superconducting Electronics and Superconducting Quantum Circuits, with R. Gross)
  - Seminar: Superconducting Quantum Circuits (with R. Gross, A. Marx)
- WS 2016/2017
- Seminar: Superconducting Quantum Circuits (with R. Gross, A. Marx)

### Dietrich Einzel

- WS 2015/2016
- Mathematische Methoden der Physik I (Mathematical Methods of Physics I)
  - Übungen zu Mathematische Methoden der Physik I (Mathematical Methods of Physics I, Problem Sessions)
- SS 2016
- Mathematische Methoden der Physik II (Mathematical Methods of Physics II)
  - Übungen zu Mathematische Methoden der Physik II (Mathematical Methods of Physics II, Problem Sessions)
- WS 2016/2017
- Mathematische Methoden der Physik I (Mathematical Methods of Physics I)
  - Übungen zu Mathematische Methoden der Physik I (Mathematical Methods of Physics I, Problem Sessions)

### Rudolf Gross

- WS 2015/2016
- Physik der Kondensierten Materie I (Condensed Matter Physics I)
  - Übungen zu Physik der Kondensierten Materie I (Condensed Matter Physics I, Problem Sessions, with S. Geprägs)
  - WMI Seminar on Current Topics of Low Temperature Solid-State Physics (with S.T.B. Gönnerwein, R. Hackl, H. Hübl, A. Marx, M. Opel)



- Seminar: Advances in Solid-State Physics (with S.T.B. Gönnerwein, H. Hübl, A. Marx, M. Opel)
  - Seminar: Superconducting Quantum Circuits (with F. Deppe, A. Marx)
  - Festkörperkolloquium (Colloquium on Solid-State Physics, with D. Einzel)
- SS 2016
- Physik der Kondensierten Materie II (Condensed Matter Physics II)
  - Übungen zu Physik der Kondensierten Materie II (Condensed Matter Physics II, Problem Sessions, with S. Geprägs)
  - Angewandte Supraleitung: Josephson Effekte, supraleitende Elektronik und supraleitende Quantenschaltkreise (Applied Superconductivity: Josephson Effects, Superconducting Electronics and Superconducting Quantum Circuits, with F. Deppe)
  - Übungen zu Angewandte Supraleitung: Josephson Effekte, supraleitende Elektronik und supraleitende Quantenschaltkreise (Applied Superconductivity: Josephson Effects, Superconducting Electronics and Superconducting Quantum Circuits, Problem Sessions, with F. Deppe)
  - Seminar: Advances in Solid-State Physics (with S.T.B. Gönnerwein, H. Hübl, A. Marx, M. Opel)
  - WMI Seminar on Current Topics of Low Temperature Solid-State Physics (with S.T.B. Gönnerwein, R. Hackl, H. Hübl, A. Marx, M. Opel)
  - Seminar: Superconducting Quantum Circuits (with F. Deppe, A. Marx)
  - Festkörperkolloquium (Colloquium on Solid-State Physics, with D. Einzel)
  - Ferienakademie: Course 3 “Physics and Electronics in Everyday Life”
- WS 2016/2017
- Physik der Kondensierten Materie I (Condensed Matter Physics I)
  - Übungen zu Physik der Kondensierten Materie I (Condensed Matter Physics I, Problem Sessions, with S. Geprägs)
  - WMI Seminar on Current Topics of Low Temperature Solid-State Physics (with R. Hackl, H. Hübl, A. Marx, M. Opel)
  - Seminar: Advances in Solid-State Physics (with S.T.B. Gönnerwein, H. Hübl, A. Marx, M. Opel)
  - Seminar: Superconducting Quantum Circuits (with F. Deppe, A. Marx)
  - Festkörperkolloquium (Colloquium on Solid-State Physics, with D. Einzel)

### Sebastian T.B. Gönnerwein

- WS 2015/2016
- Seminar: Advances in Solid-State Physics (with R. Gross, H. Hübl, A. Marx, M. Opel)
  - WMI Seminar on Current Topics of Low Temperature Solid State Physics (with R. Gross, R. Hackl, H. Hübl, A. Marx, M. Opel)
  - Seminar: Current Topics in Magneto and Spin Electronics (with M. Brandt, H. Hübl)

### Rudi Hackl

- WS 2015/2016
- WMI Seminar on Current Topics of Low Temperature Solid-State Physics (with R. Gross, S.B.T. Gönnerwein, H. Hübl, A. Marx, M. Opel)
  - Seminar: Advances in Solid-State Physics (with R. Gross, S.T.B. Gönnerwein, A. Marx, M. Opel)
- SS 2016
- WMI Seminar on Current Topics of Low Temperature Solid-State Physics (with R. Gross, H. Hübl, A. Marx, M. Opel)
  - Seminar: Advances in Solid-State Physics (with R. Gross, H. Hübl, A. Marx, M. Opel)
- WS 2016/2017
- WMI Seminar on Current Topics of Low Temperature Solid-State Physics (with R. Gross, H. Hübl, A. Marx, M. Opel)

- Seminar: Advances in Solid-State Physics (with R. Gross, H. Hübl A. Marx, M. Opel)

## Hans Hübl

- WS 2015/2016
- Supraleitung und Tieftemperaturphysik I (Superconductivity and Low Temperature Physics I)
  - Übungen zu Supraleitung und Tieftemperaturphysik I (Superconductivity and Low Temperature Physics I, Problem Sessions)
  - Seminar: Spin Caloritronics and Spin Pumping (with M. Althammer, S. Gönnerwein, M. Weiler)
  - Seminar: Advances in Solid-State Physics (with R. Gross, S.T.B. Gönnerwein, A. Marx, M. Opel)
  - WMI Seminar on Current Topics of Low Temperature Solid State Physics (with R. Gross, S.T.B. Gönnerwein, R. Hackl, A. Marx, M. Opel)
  - Seminar: Current Topics in Magneto and Spin Electronics (with S.T.B. Gönnerwein, M. S. Brandt)
- SS 2016
- Supraleitung und Tieftemperaturphysik II (Superconductivity and Low Temperature Physics II)
  - Übungen zu Supraleitung und Tieftemperaturphysik II (Superconductivity and Low Temperature Physics II, Problem Sessions)
  - Seminar: Spin Caloritronics and Spin Pumping (with M. Althammer, M. Weiler)
  - Seminar: Advances in Solid-State Physics (with R. Gross, A. Marx, M. Opel)
  - WMI Seminar on Current Topics of Low Temperature Solid State Physics (with R. Gross, R. Hackl, A. Marx, M. Opel)
  - Seminar: Current Topics in Magneto and Spin Electronics (with M. S. Brandt)
- WS 2016/2017
- Supraleitung und Tieftemperaturphysik I (Superconductivity and Low Temperature Physics I)
  - Übungen zu Supraleitung und Tieftemperaturphysik I (Superconductivity and Low Temperature Physics I, Problem Sessions)
  - Seminar: Spin Caloritronics and Spin Pumping (with M. Althammer, M. Weiler)
  - Seminar: Advances in Solid-State Physics (with R. Gross, A. Marx, M. Opel)
  - WMI Seminar on Current Topics of Low Temperature Solid State Physics (with R. Gross, R. Hackl, A. Marx, M. Opel)
  - Seminar: Current Topics in Magneto and Spin Electronics (with M. S. Brandt, M. Althammer, M. Weiler, S. Geprägs)

## Mathias Weiler

- WS 2015/2016
- Magnetismus (Magnetism)
  - Übungen zu Magnetismus (Magnetism, Problem Sessions)
  - Seminar: Spin Caloritronics and Spin Pumping (with M. Althammer, S. Gönnerwein, H. Huebl)
  - Seminar: Advances in Solid-State Physics (with R. Gross, S.T.B. Gönnerwein, A. Marx, M. Opel)
  - WMI Seminar on Current Topics of Low Temperature Solid State Physics (with R. Gross, S.T.B. Gönnerwein, R. Hackl, A. Marx, M. Opel)
  - Seminar: Current Topics in Magneto and Spin Electronics (with S.T.B. Gönnerwein, M. S. Brandt)
- SS 2016
- Spin Electronics
  - Übungen zu Spin Electronics (Exercises to Spin Electronics)
  - Seminar: Spin Caloritronics and Spin Pumping (with M. Althammer, H. Huebl)

- Seminar: Advances in Solid-State Physics (with R. Gross, A. Marx, M. Opel)
  - Seminar: Current Topics in Magneto and Spin Electronics (with M. Althammer, H. Hübl, M. S. Brandt)
- WS 2016/2017
- Seminar: Advances in Solid-State Physics (with R. Gross, M. Althammer, F. Deppe, S. Geprägs, H. Hübl, A. Marx, M. Opel)
  - Seminar: Spin Caloritronics and Spin Pumping (with M. Althammer, H. Hübl)
  - Seminar: Current Topics in Magneto and Spin Electronics (with M. Althammer, H. Hübl, M. S. Brandt)

## Seminars and Colloquia

### A. Walther-Meißner-Seminar on Modern Topics in Low Temperature Physics WS 2015/2016, SS 2016 and WS 2016/2017

#### WS 2015/2016:

1. **Thin film B20 Chiral Magnets**  
Priv.-Doz.- Dr. Dirk Menzel, Technische Universität Braunschweig, Germany  
23. 10. 2015
2. **Unidirectional spin hall magnetoresistance in ferromagnet/normal metal bilayers**  
Dr. Can Onur Avci, ETH Zürich, Switzerland  
30. 10. 2015
3. **Silicon quantum processor with robust long-distance qubit couplings**  
Dr. Guilherme Tosi, University of New South Wales, Sydney, Australia  
27. 11. 2015
4. **Towards macroscopic quantum physics with levitated magneto-mechanics**  
Dr. Joshua Slater, Faculty of Physics, University of Vienna, Austria  
04. 12. 2015
5. **Detecting spin-currents generated by a ferrimagnetic insulator**  
Nynke Vliestra, University of Groningen, Groningen, The Netherlands  
18. 12. 2015

#### SS 2016:

6. **Research activities in high frequency technology and measurements techniques at RWTH Aachen**  
Prof. Dr.-Ing. Dirk Heberling, RWTH Aachen, Aachen, Germany  
29. 04. 2016
7. **Levitated Magnets in the Quantum Regime: New Opportunities**  
Prof. Dr. Oriol Romero-Isart, Austrian Academy of Sciences, Innsbruck, Austria  
10. 06. 2016
8. **Electronic, spectroscopic and mechanical properties of thin films and nanostructures**  
Prof. Dr. M.S. Ramachandra Rao, Indian Institute of Technology (IIT) Madras, Chennai, India  
24. 06. 2016
9. **Decoherence in superconducting circuits: TLS and quasiparticles**  
Dr. Michael Marthaler, Karlsruher Institut für Technologie, Karlsruhe, Germany  
08. 07. 2016
10. **Application Trends in Automotive Lighting**  
Dr. Claus Allgeier, OSRAM GmbH, Berlin, Germany  
15. 07. 2016
11. **Reaktorsicherheitsanalysen**  
Dr. Michael Kund, Gesellschaft für Anlagen- und Reaktorsicherheit (GRS), Garching, Germany  
15. 07. 2016
12. **Semi-Quantum Spin Dynamics**  
Prof. Dr. Joe Barker, Tohoku University, Sendai, Japan  
30. 08. 2016
13. **Probing non-integral spin magnons via spin current noise**  
Dr. Akashdeep Kamra, Fachbereich Physik, Universität Konstanz, Germany  
09. 09. 2016

#### WS 2016/2017:

14. **Spin injection and tuneable spin-to-charge conversion at LaAlO<sub>3</sub>/SrTiO<sub>3</sub> oxide interfaces**  
Dr. Hiroshi Naganuma, Unité Mixte de Physique, CNRS, Palaiseau, France  
04. 10. 2016

15. **Integrated optomechanics and linear optics quantum circuits**  
Prof. Dr. Menno Poot, Yale University, New Haven, Connecticut, USA  
19. 10. 2016
16. **Atomic layer deposition for spinelectronic devices**  
Dr. Andy Thomas, IFW Dresden, Germany  
11. 11. 2016
17. **Spin dynamics and transport in complex oxides and heterostructures**  
Prof. Dr. Georg Schmidt, Martin-Luther-Universität Halle-Wittenberg, Halle, Germany  
18. 11. 2016
18. **Models of light-matter interaction. Symmetries and Solutions**  
Dr. Daniel Braak, Institut für Physik, Universität Augsburg, Germany  
19. 12. 2016

## B. Topical Seminar on Advances in Solid State Physics WS 2015/2016, SS 2016 and WS 2016/2017

### WS 2015/2016:

1. **Preliminary discussion and assignment of topics**  
R. Gross, Walther-Meißner-Institut  
13. 10. 2015 and 20. 10. 2015
2. **Ferroelectric tunnel junctions for information storage and processing**  
Rasmus Flaschmann, Technische Universität München  
24. 11. 2015
3. **New perspectives for Rashba spin-orbit coupling**  
Alexander Baklanov, Technische Universität München  
08. 12. 2015
4. **Pressure-induced Mott Transition in an Organic Superconductor with a Finite Doping Level**  
Sebastian Oberbauer, Technische Universität München  
15. 12. 2015
5. **Optically induced coherent transport far above  $T_c$  in underdoped  $\text{YBa}_2\text{Cu}_3\text{O}_{6+\delta}$**   
Jongho Kim, Technische Universität München  
12. 01. 2016
6. **Realization of Microwave Quantum Circuits Using Hybrid Superconducting-Semiconducting Nanowire Josephson Elements**  
Florian Kollmannsberger, Technische Universität München  
19. 01. 2016
7. **New perspectives for Rashba spin orbit coupling**  
Alexander Baklanov, Technische Universität München  
26. 01. 2016

### SS 2016:

8. **Preliminary discussion and assignment of topics**  
R. Gross, Walther-Meißner-Institut  
12. 04. 2016 and 19. 04. 2016
9. **Detection of Defects in Silicon using EDMR**  
Theresa Grünleitner, Technische Universität München  
24. 05. 2016
10. **Magnetoelectric effects in the skyrmion host material  $\text{Cu}_2\text{OSeO}_3$**   
Lukas Liensberger, Technische Universität München  
31. 05. 2016
11. **Fermi surface reconstruction and multiple quantum phase transitions in the antiferromagnet  $\text{CeRhIn}_5$**



Christoph Herb, Technische Universität München  
07. 06. 2016

12. **Electrical switching of an antiferromagnet**  
Marinus Kundinger, Technische Universität München  
14. 06. 2016
13. **Quantum squeezing of motion in a mechanical resonator**  
Yuki Nojiri, Technische Universität München  
28. 06. 2016
14. **Towards Quantum Thermodynamics in Electronic Circuits**  
Julian Bibo, Technische Universität München  
05. 07. 2016

#### **WS 2016/2017:**

15. **Preliminary discussion and assignment of topics**  
R. Gross, Walther-Meißner-Institut  
18. 10. 2016 and 25. 10. 2016
16. **Quasiparticle mass enhancement approaching optimal doping in a high- $T_c$  superconductor**  
Ulrike Zweck, Technische Universität München  
13. 12. 2016
17. **Supeconducting Spintronics**  
Michael Renger, Technische Universität München  
20. 12. 2016
18. **Coherent coupling between a ferromagnetic magnon and a superconducting qubit**  
Min-Xing Xu, Technische Universität München  
10. 01. 2017
19. **Detection of Zeptojoule Microwave Pulses Using Electrothermal Feedback in Proximity-Induced Josephson Junctions**  
Patrick Schnierle, Technische Universität München  
17. 01. 2017

### **C. Topical Seminar: Spin Caloritronics and Spin Pumping SS 2016 and WS 2016/2017**

#### **SS 2016:**

1. **Preliminary discussion and assignment of topics**  
Matthias Althammer, Walther-Meißner-Institut  
14. 04. 2016 and 21. 04. 2016
2. **Antiferromagnetic Spintronics**  
Michaela Schleuder, Technische Universität München  
09. 06. 2016
3. **Pure Spin Currents in erbium iron garnets**  
Hiroto Sakimura, Technische Universität München  
16. 06. 2016
4. **Magnetic field dependence of the magnon spin diffusion length in the magnetic insulator yttrium iron garnet**  
Saki Matsuura, Technische Universität München  
23. 06. 2016
5. **Introduction into Superconducting Spintronics**  
Domenikos Chryssikos, Technische Universität München  
30. 06. 2016
6. **Non-local spin Seebeck effect and magnon mediated magnetoresistance in YIG/Pt hybrids**  
Tobias Wimmer, Technische Universität München  
07. 07. 2016

7. **Introduction to Skyrmions**  
Martin Seltmann, Technische Universität München  
14. 07. 2016

**WS 2016/2017:**

8. **Preliminary discussion and assignment of topics**  
Mathias Weiler, Walther-Meißner-Institut  
20. 10. 2016 and 27. 10. 2016
9. **Direct detection of pure ac spin current by X-ray pump-probe measurements**  
Johannes Gröbmeyer, Technische Universität München  
19. 01. 2017

**D. Topical Seminar on Superconducting Quantum Circuits**  
**WS 2015/2016, SS 2016 and WS 2016/2017**

**WS 2015/2016:**

1. **Preliminary discussion and assignment of topics**  
F. Deppe, A. Marx, R. Gross, Walther-Meißner-Institut  
13. 10. 2015 and 20. 10. 2015
2. **Microwave-Controlled Generation of Shaped Single Photons in Circuit Quantum Electrodynamics**  
Peter Eder, Walther-Meißner-Institut  
03. 11. 2015
3. **Hybrid circuit cavity quantum electrodynamics with a micromechanical resonator**  
Thomas Stolz, Technische Universität München  
17. 11. 2015
4. **Tuneable on-demand single-photon source**  
Jan Goetz, Walther-Meißner-Institut  
01. 12. 2015
5. **A Quantum memory with near-millisecond coherence in circuit QED**  
Lukas Hauertmann, Technische Universität München  
15. 12. 2015
6. **A near-quantum-limited Josephson traveling-wave parametric amplifier**  
Michael Fischer, Walther-Meißner-Institut  
19. 01. 2016
7. **Unconventionally coupled nano-electromechanics**  
Daniel Schwienbacher, Walther-Meißner-Institut  
26. 01. 2016
8. **Microwave-Controlled Generation of Shaped Single Photons in Circuit Quantum Electrodynamics**  
Peter Eder, Walther-Meißner-Institut  
02. 02. 2016

**SS 2016:**

9. **Preliminary discussion and assignment of topics**  
F. Deppe, A. Marx, R. Gross, Walther-Meißner-Institut  
12. 04. 2016 and 19. 04. 2016
10. **Microwave Single Photon Sources**  
Tuan Le Anh, Technische Universität München  
03. 05. 2016
11. **Displacement and Squeezing with continuous variable microwaves**  
Patrick Yard, Technische Universität München

10. 05. 2016
12. **Reaching the quantum limit of sensitivity in electron spin resonance**  
Stefan Appel, Technische Universität München  
24. 05. 2016
  13. **Demonstration quantum error-correction that extends the life-time of quantum information**  
Sebastian Meier, Technische Universität München  
24. 05. 2016
  14. **3D transmon qubit characterization-towards a 3D quantum memory**  
Daniel Repp, Technische Universität München  
31. 05. 2016
  15. **Scalable Quantum Simulation of Molecular Energies**  
Yannick Brunken, Technische Universität München  
07. 06. 2016
  16. **Satisfying the Einstein-Podolsky-Rosen criterion with massive particles**  
Andreas Pöschl, Technische Universität München  
14. 06. 2016
  17. **Large cooperativity and microkelvin cooling with a three-dimensional optomechanical cavity**  
Waldemar Kaiser, Technische Universität München  
21. 06. 2016
  18. **Interaction of Strain and Nuclear Spins in Silicon: Quadrupolar Effects on Ionized Donors**  
Stefan Weber, Technische Universität München  
28. 06. 2016
  19. **Measuring and Suppressing Quantum State Leakage in a Superconducting Qubit**  
Timo Joas, Technische Universität München  
05. 07. 2016
  20. **Digital feedback in SC Quantum Circuits**  
Michael Petrov, Technische Universität München  
12. 07. 2016

#### **WS 2016/2017:**

21. **Preliminary discussion and assignment of topics**  
F. Deppe, A. Marx, R. Gross, Walther-Meißner-Institut  
18. 10. 2016 and 25. 10. 2016

## **E. Solid State Colloquium**

The WMI has organized the Solid-State Colloquium of the Faculty of Physics in WS 2015/2016, SS 2016, and WS 2016/2017. The detailed program can be found on the WMI webpage: <http://www.wmi.badw-muenchen.de/teaching/Seminars/fkkoll.html>.



# Staff







## Staff of the Walther-Meißner-Institute

### Director

Prof. Dr. Rudolf Gross

### Deputy Director

Priv.-Doz. Dr. habil. Hans Hübl

### Technical Director

Dr. Achim Marx

The deputy director, the technical director and the elected representative of the scientific staff (Dr. Matthias Opel) are members of the WMI Executive Committee and support the director in the management of WMI.

### Administration/Secretary's Office

Ludwig Ossiander

Emel Dönertas

### Scientific Staff

Dr. Matthias Althammer

Dr. Frank Deppe

Prof. Dr. Andreas Erb

Dr. Kirill Fedorov

Dr. Stephan Geprägs

Priv.-Doz. Dr. habil. Rudolf Hackl

Dr. Mark Kartsovnik

Dr. Matthias Opel

Dr. Matthias Pernpeintner

Dr. Nynke Vlietstra

Dr. Mathias Weiler

Dipl.-Phys. Andreas Baum

Dipl.-Phys. Thomas Böhm

M. Sc. Alma Dorantes

Dipl.-Phys. Peter Eder

M. Sc. Michael Fischer

M. Sc. Kathrin Ganzhorn

Dipl.-Phys. Jan Goetz

M. Sc. Daniel Jost

M. Sc. Stefan Klingler

Dipl.-Phys. Hannes Maier-Flaig

M. Sc. Stefan Pogorzalek

M. Sc. Philip Schmidt

M. Sc. Daniel Schwienbacher

M. Sc. Stefan Weichselbaumer

M. Sc. Edward Xie

### Technical Staff

Peter Binkert

Thomas Brenninger, M.Sc.

Dieter Guratzsch

Astrid Habel

Karen Helm-Knapp

Dipl.-Ing. (FH) Josef Höss

Sebastian Kammerer

Christoph Kastl

Julius Klaus

Robert Müller

Jan Naundorf

Georg Nitschke

Christian Reichlmeier

Alexander Rössl

Harald Schwaiger

Helmut Thies

Siegfried Wanninger

### Assistants

Sybilla Plöderl

Maria Botta

**Permanent Guests**

Dr. Werner Biberacher

Prof. Dr. B.S. Chandrasekhar

Dr. Kurt Uhlig

Prof. Dr. Dietrich Einzel

## Guest Researchers

1. Dr. Werner Biberacher  
permanent guest
2. Prof. Dr. B.S. Chandrasekhar  
permanent guest
3. Prof. Dr. Dietrich Einzel  
permanent guest
4. Dr. Kurt Uhlig  
permanent guest
5. Dr. Joynarayan Mukherjee, IIT Madras, Chennai, India  
11. 01. - 10. 03. 2016
6. Dr. Joshua Slater, Universität Wien, Austria  
25. 01. - 12. 02. 2016, 14. 03. - 10. 04. 2016, 26. 04. - 30. 05. 2016, 13. 06. - 16. 07. 2016
7. Julen S. Pedernales, Universidad del Pais Vasco, Bilbao, Spain  
25. 01. - 29. 01. 2016
8. Dr. Zhiyong Qui, Institute for Materials Research, Tohoku University, Sendai, Japan  
30. 01. - 06. 02. 2016
9. Diana Geiger, Institut für Festkörperphysik, Technische Universität Wien, Austria  
10. 03. - 24. 03. 2016
10. Masashi Shiraishi and Ryo Oshima, Kyoto University, Japan  
11. 03. - 15. 03. 2016
11. Dr. Oleg Vyaselev, Institute of Solid Physics, Chernogolovka, Russia  
04. 04. - 16. 05. 2016
12. Dr. Nedad Lazarevic, University of Belgrade, Belgrade, Serbia  
14. 04. - 28. 04. 2016, 12. 09. - 17. 09. 2016
13. Prof. Maja Scepanovic, University of Belgrade, Belgrade, Serbia  
14. 04. - 19. 04. 2016
14. Prof. Mirjana Grujic-Brojcin, University of Belgrade, Belgrade, Serbia  
14. 04. - 19. 04. 2016
15. Dr. Steve Winter, Goethe-Universität, Frankfurt, Germany  
19. 04. - 21. 04. 2016
16. Urtzi Las Heras, Universidad del Pais Vasco, Bilbao, Spain  
12. 06. - 19. 06. 2016
17. Prof. Dr. M.S. Ramachandra Rao, Materials Science Research Centre, IIT Madras, Chennai, India  
18. 06. - 30. 06. 2016
18. Dr. Nynke Vlietstra, University of Groningen, The Netherlands  
07. 07. - 15. 07. 2016
19. Prof. Dr. I. Tüttö, Research Institute for Solid State Physics and Optics, Hungarian Academy of Sciences Budapest, Budapest, Hungary  
23. 07. - 31. 07. 2016
20. Prof. V. Marchenkov, Institute of Metal Physics, Yekaterinburg, Russia  
18. 08. - 21. 08. 2016
21. Prof. Dr. Joseph Barker, Tohoku University, Sendai, Japan  
24. 08. - 31. 08. 2016
22. Zahra Inanloo Maranloo, Sharif University Teheran, Teheran, Iran  
03. 09. - 28. 11. 2016

23. Dr. Akashdeep Kamra, University of Konstanz, Germany  
06. 09. - 11. 09. 2016
24. Prof. Valentin Peschansky, B.I. Verkin Institute, Kharkov, Ukraine  
21. 09. - 28. 09. 2016
25. Yuri Aperecido Opata, University of Denmark, Denmark  
17. 10. - 27. 11. 2016
26. Prof. Zoran Popovic, University of Belgrade, Belgrade, Serbia  
10. 12. - 18. 12. 2016
27. Prof. Vladimir Zverev, Institute of Solid Physics, Chernogolovka, Russia  
15. 12. - 24. 12. 2016

## Scientific Advisory Board

According to the statutes of the Bavarian Academy of Sciences and Humanities (BAdW) the Scientific Advisory Board evaluates the quality of the scientific work of Walther-Meißner-Institute (WMI) and gives advice to its Executive Committee to provide scientific quality assurance. The Scientific Advisory Board regularly reports to the Research Committee of BAdW.

The members of the Scientific Advisory Board include members of BAdW with appropriate scientific background, representatives of the two Munich universities (TUM and LMU), as well as leading national and international scientists. They are appointed by the Section III "Naturwissenschaften, Mathematik, Technikwissenschaften" of BAdW for five years. The director of WMI is a consultive member of the WMI Scientific Advisory Board. The Scientific Advisory Board is headed by a chairperson and deputy chairperson. They are elected by the Section III "Naturwissenschaften, Mathematik, Technikwissenschaften" of BAdW for five years at the suggestion of the members of the WMI Scientific Advisory Board. The chairperson of the Scientific Advisory Board must be a member of BAdW.

The present members of the WMI Scientific Advisory Board are:

- **Vollhardt, Dieter**, chairman (BAdW, University of Augsburg)
- **Abstreiter, Gerhard**, deputy chairman (BAdW, Technical University of Munich)
  
- **Bloch, Immanuel** (LMU Munich and Max-Planck-Institute of Quantum Optics)
- **Bühler-Paschen, Silke** (Technical University of Vienna)
- **Finley, Jonathan** (Technical University of Munich)
- **Gross, Rudolf**, consultive member (BAdW, Technical University of Munich)
- **Hänsch, Theodor** (BAdW, LMU Munich and Max-Planck-Institute of Quantum Optics)
- **Schwoerer, Markus** (BAdW, University of Bayreuth)
- **Wallraff, Andreas** (ETH Zurich)
- **Weiss, Dieter** (University of Regensburg)
- **Zinth, Wolfgang** (BAdW, LMU Munich)



## Executive Committee

Walther-Meißner-Institute is headed by the scientific director who is responsible for the development and implementation of the research program. He holds a full professor position at one of the Munich universities (TUM or LMU). He is appointed in a joint process of the respective university and BAdW. The director is supported by the deputy director, the technical director and an elected representative of the scientific staff. They are appointed by the Section III "Naturwissenschaften, Mathematik, Technikwissenschaften" of BAdW for five years at the suggestion of the members of the WMI Scientific Advisory Board.

The present members of the WMI Executive Committee are:

- **Gross, Rudolf**, director
- **Hübl, Hans**, deputy director
- **Marx, Achim**, technical director
- **Opel, Matthias**, representative of the scientific staff





**Contact:**

Walther-Meißner-Institut  
Bayerische Akademie der Wissenschaften  
Walther-Meißner-Str. 8  
D - 85748 Garching  
GERMANY

Phone: +49 – (0)89 289 14201  
Fax: +49 – (0)89 289 14206  
E-mail: Sekretariat@wmi.badw.de

**[www.wmi.badw.de](http://www.wmi.badw.de)**

**Published by:**



Walther-Meißner-Institut  
Walther-Meißner-Str. 8, D - 85748 Garching  
December 2016